NASA Technical Paper 1316

Wind-Tunnel Investigation at Supersonic Speeds of a Canard-Controlled Missile With Fixed and Free-Rolling Tail Fins

A. B. Blair, Jr.

SEPTEMBER 1978

NASA

NASA Technical Paper 1316

Wind-Tunnel Investigation at Supersonic Speeds of a Canard-Controlled Missile With Fixed and Free-Rolling Tail Fins

A. B. Blair, Jr.
Langley Research Center
Hampton, Virginia

NASA
National Aeronautics
and Space Administration

**Scientific and Technical
Information Office**

1978

SUMMARY

A wind-tunnel investigation was made at free-stream Mach numbers from 1.70 to 2.86 to determine the effects of fixed and free-rolling tail-fin afterbodies on the static longitudinal and lateral aerodynamic characteristics of a cruciform canard-controlled missile model. The effect of small canard roll- and yaw-control deflections was also investigated.

The results indicate that the fixed and free-rolling tail configurations have about the same lift-curve slope and longitudinal stability level at low angles of attack. For the free-rolling tail configuration, the canards provide conventional roll control with no roll-control reversal at low angles of attack. The free-rolling tail configuration reduced induced roll due to model roll angle and canard yaw control.

INTRODUCTION

It is well documented that missile configurations which utilize forward surfaces to provide control experience the problem of induced rolling moments at supersonic Mach numbers. One approach to the solution of this problem, which is described in reference 1, uses a free-rolling tail-fin afterbody on a canard-controlled missile model to reduce induced rolling moments.

The idea of using free-rolling tail fins is not new. From 1950 to 1960, the NASA and its predecessor, NACA, investigated a number of roll-control devices in free flight as part of their aerodynamic control research program for missiles and airplanes. For some of these tests, a free-rolling tail-fin assembly was used on the missile airframes, not only to stabilize the models longitudinally but also to eliminate unwanted, induced rolling moments that were generated by the various roll controls under investigation (e.g., ref. 2). In many cases, the free-rolling tails were on nonmaneuvering missile systems (e.g., boost-glide trajectories at low angles of attack). More recently (1960 to 1973), the U.S. Navy has conducted research on bomb-shaped bodies (free-fall stores) with free-rolling tail fins (refs. 3 and 4) as a means of reducing dispersion and of increasing accuracy by eliminating the effect of flow asymmetries over the tail fins.

The present investigation was conducted to provide some insight into the effectiveness of the free-rolling tail concept for the reduction or elimination of large induced rolling moments that are generally experienced by maneuvering canard-controlled missile configurations at supersonic speeds. In an effort to reduce or eliminate these induced rolling moments, an experimental wind-tunnel investigation has been made to determine the effect of a free-rolling (no fin cant) cruciform tail on the stability and control characteristics of a canard-controlled missile. The results of a similar test conducted by the U.S. Navy with canted free-rolling tail fins can be found in reference 5. The rolling tail concept also offers the potential of enabling the canards to provide some

measure of roll control, either increased roll-damping or roll-attitude control at low angles of attack. There is a growing need to give canard-controlled missile configurations more simplicity and modular flexibility. The free-rolling tail concept may satisfy these requirements by allowing a missile configuration to have a single control system utilizing a cruciform canard control system for pitch, yaw, and roll control.

The tests were conducted in the Langley Unitary Plan wind tunnel at Mach numbers from 1.70 to 2.86. The nominal angle-of-attack range was -3° to 25° at model (canard) roll angles of 0° to 45° and at a Reynolds number of 6.6×10^6 per meter (2.0×10^6 per foot). Results of these tests include the effects of small roll- and yaw-control deflections of the canards on the longitudinal and lateral aerodynamic characteristics of the model with a fixed and free-rolling tail-fin afterbody.

SYMBOLS

The aerodynamic coefficient data are referred to the body-axis system except for lift and drag which are referred to the stability-axis system. The moment reference was located aft of the model nose at 49.0 percent of the reference body length.

Measurements and calculations were made in the U.S. Customary Units. Measurements are presented in the International System of Units (SI), with the equivalent values given parenthetically in U.S. Customary Units (ref. 6).

A reference area; maximum cross-sectional area of body, 0.003425 m^2 (0.036870 ft^2)

C_A axial-force coefficient, Axial force/qA

$C_{A,b}$ base axial-force coefficient, Base axial force/qA

C_D drag coefficient, Drag/qA

$C_{D,b}$ base drag coefficient, Base drag/qA

C_L lift coefficient, Lift/qA

C_{L_α} lift-curve slope, per degree

C_l rolling-moment coefficient, Rolling moment/qAd

C_m pitching-moment coefficient, Pitching moment/qAl

C_N normal-force coefficient, Normal force/qA

C_n yawing-moment coefficient, Yawing moment/qAd

C_Y side-force coefficient, Side force/qA

d	reference diameter, 6.604 cm (2.600 in.)
l	reference body length, 99.060 cm (39.000 in.)
M	Mach number
q	free-stream dynamic pressure, N/m^2 (psfa)
α	angle of attack, deg
δ_{roll}	differential deflections of two canards (canards 2 and 4, shown in sketch (a)) for roll control; individual canards are deflected indicated amount; negative to provide counterclockwise rotation when viewed from rear, deg
δ_{yaw}	yaw-control deflection of two canards (canards 1 and 3, shown in sketch (a)); positive for leading edge right when viewed from rear, deg
ϕ_c	model roll angle; positive clockwise when viewed from rear (for $\phi_c = 0^o$, canards are in vertical and horizontal planes), deg
$\dot{\phi}_{tail}$	roll rate of tail-fin afterbody; positive clockwise when viewed from rear, rpm
$\partial C_m/\partial C_L$	static longitudinal stability parameter

Canards

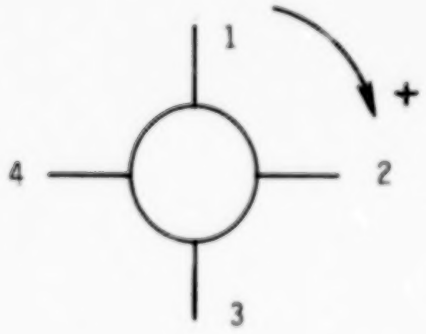

$\phi_c = 0^o$

Rear view

Sketch (a)

APPARATUS AND TESTS

Wind Tunnel

The investigation was conducted in the low Mach number test section of the Langley Unitary Plan wind tunnel, which is a variable-pressure, continuous-flow facility. The test section is approximately 2.13 m (7 ft) long and 1.22 m (4 ft) square. The nozzle leading to the test section is of the asymmetric sliding-block type, which permits a continuous variation in Mach number from about 1.5 to 2.9. (See ref. 7.)

Model

Dimensional details of the model are shown in figure 1(a) and a model photograph is shown in figure 2. The model was a cruciform missile configuration that consisted of a cylindrical body with canards, aft tail fins, and a tangent ogive nose of fineness ratio 3.0. The complete model body had a fineness ratio of 15. The canards and tail fins had slab cross sections with beveled leading and trailing edges. In order for the model to have a free-rolling tail-fin assembly, the tail-fin afterbody was mounted on a set of low-friction ball bearings and was free to rotate through 360° (lock screw out). For the fixed-tail configuration (lock screw in), the tail fins were locked in line with the canards. For both the fixed and free-rolling tail configurations, the canards were deflected to provide roll control and yaw control. The tail fins were not deflected (zero cant angle) and the tail-fin assembly had no braking system.

Test Conditions

Tests were performed at the following tunnel conditions:

Mach number	Stagnation temperature		Stagnation pressure		Reynolds number	
	K	°F	kPa	psfa	per meter	per foot
1.70	339	150	56.4	1178	6.6×10^6	2.0×10^6
2.16	339	150	68.5	1430	6.6	2.0
2.36	339	150	75.7	1580	6.6	2.0
2.86	339	150	98.4	2056	6.6	2.0

The dewpoint temperature measured at stagnation pressure was maintained below 239 K (-30° F) to assure negligible condensation effects. All tests were performed with boundary-layer transition strips measured streamwise on both sides of the canards and tail fins and located 3.05 cm (1.20 in.) aft of the body nose and 1.02 cm (0.40 in.) aft of the leading edges. The transition strips were approximately 0.157 cm wide (0.062 in.) and were composed of No. 50 sand grains sprinkled in acrylic plastic. (See ref. 8.)

The primary method for controlling tail-fin rotational speed was by limiting the model angle of attack. In the early stages of this test program, tail-fin rotational speed was nominally limited to 200 rpm as a safety precaution; however, this limit was extended to 500 rpm as more confidence was gained. In order to satisfy these limits, only small canard deflections were made.

Measurements

Aerodynamic forces and moments on the model were measured by means of a six-component electrical strain-gage balance which was housed within the model. The balance was attached to a sting which was, in turn, rigidly fastened to the model support system. Balance-chamber pressure (base pressure) was measured by means of a single static-pressure orifice located in the vicinity of the balance. One light-emitting diode with a photo-transistor receiver pick-up mounted on the sting was used in conjunction with a color-coded ring at the base of the model to record tail-fin afterbody revolutions. The accuracy of this recording system was ±20 rpm. No attempt was made to measure the afterbody torque that was produced by the internal ball-bearing friction, viscous-layer skin friction, or aerodynamic damping.

Corrections

The angles of attack have been corrected for deflection of the balance and sting due to aerodynamic loads. In addition, angles of attack have been corrected for tunnel-flow misalignment. The drag and axial-force coefficient data have been adjusted to free-stream static pressure acting over the model base. Typical measured values of base axial-force and drag coefficients are presented in figure 3.

PRESENTATION OF RESULTS

DISCUSSION

Longitudinal Aerodynamic Characteristics

The longitudinal aerodynamic characteristics of the model with zero control deflection are presented in figures 4 and 5 for $\phi_c = 0^o$ and 45°, respectively. In general, at low angles of attack ($\alpha \leq 4^o$), both the fixed and free-rolling tail configurations have about the same lift-curve slope C_{L_α} and stability level $\partial C_m/\partial C_L$. At the higher angles of attack for $\phi_c = 0^o$, the free-rolling tail configuration has more nonlinear pitching-moment coefficient characteristics with a slight pitch-up tendency and, in general, less restoring moment than the fixed-tail configuration. These aerodynamic differences between the two configurations for the $\phi_c = 45^o$ case (fig. 5) are less pronounced, with the pitching-moment curves becoming more nearly linear with increases in Mach number for the free-rolling tail configuration. However, the fixed-tail configuration now exhibits the pitch-up tendency that characterized the free-rolling tail configuration at $\phi_c = 0^o$. This pitch-up trend is typical for a missile with cruciform tail fins in the ×-position ($\phi_c = 45^o$) at supersonic speeds. Flow-field effects, in conjunction with adverse panel-to-panel interference between the windward and leeward tail-fin surfaces, result in a small overall reduction in tail lift capability. This loss of lift for the fixed-tail configuration ($\phi_c = 45^o$) can be seen in the lift-coefficient curves presented in figure 5 and for the free-rolling tail configuration at $\phi_c = 0^o$ in figure 4. Visual observation has shown that for $\phi_c = 0^o$, the free-rolling tail fins are generally interdigitated to the canards (×-position) when rotation stops and are therefore in a similar flow environment as the fixed-tail case when $\phi_c = 45^o$. This loss in tail lift would account for the pitch-up tendency.

The longitudinal aerodynamic characteristics of the model with a free-rolling tail and with canards on and off are presented in figure 6. Removing the canards results in the expected decrease in lift-curve slope and increase in stability level. The nonlinear pitching moment observed in the data of figure 4, to a lesser extent in figure 5, and also in figure 6 is attributed to small misalignments of the canards which generate asymmetrical flow fields in the region of the tail fins. These effects are more pronounced at the lower angles of attack and are reflected in the magnitudes of the tail-fin rotational speed.

An interesting observation that can be made from the previously presented data, in conjunction with tables I to IV for the free-rolling tail configuration, is the aerodynamic lockup (referred to hereinafter as aero lockup) that occurs at discrete angles of attack for each roll angle and Mach number. Aero lockup occurs when the tail fins essentially stop rotating but oscillate through very small angles. As a result, the tail fins are approximately interdigitated with respect to the canards for $\phi_c = 0^o$.

A possible explanation for the aero-lockup condition is that a vorticity combination in the flow field from the body viscous cross-flow separation and the canard trailing vortex results in a wake geometry that has stabilizing effects (slows or stops tail-fin rotation) on the leeward side in the region of the cruciform tail fins. However, it appears that this stabilizing wake geometry is established only when there are no other significant upstream asymmetric flow disturbances such as those produced by model roll angles and certain canard deflections. In such cases, the stabilizing wake geometry is either eliminated, reduced, or delayed until higher angles of attack are reached. (See tables III and IV.) Generally, with no asymmetric upstream disturbances, the discrete angles of attack for aero lockup fall into a range between approximately 4^o and 9^o.

The results from many vapor-screen investigations of bodies with forward lifting surfaces show that, beginning at about $\alpha = 5^o$, vortices and their corresponding wake geometries are clearly visible on the leeward side of the bodies in the region where tail fins would normally be mounted (e.g., see ref. 9). Vapor-screen studies of the test model were not made during the current investigation; however, the methods of reference 10 were used to predict the leeside vortex locations on the test model at $M = 2.16$. The predictions indicate that above $\alpha = 12^o$ at $M = 2.16$, the canard vortices ($\phi_c = 0^o$) do not impinge on the tail fins whereas the body vortices remain in the leeward region of the tail fins. These analytical results indicate that the body vortices may contribute to aero-lockup phenomenon for the test angle-of-attack range of this investigation.

In reference 11, five stages of rolling motion are described for a complete free-rolling cruciform body-tail missile configuration for missile angles of attack from 0^o to 90^o at subsonic Mach numbers. These basic stages are (1) "linear" rolling motion, (2) roll "slow-down," (3) roll "lock-in," (4) roll "break-out," and (5) roll "speed-up." It appears that, in general, the free-rolling tail fins of the present test model exhibit the first three stages of these rolling motions at supersonic Mach numbers. The third stage, roll lock-in, is identical to the aero-lockup term used in this paper. Perhaps if the

test angle of attack of this investigation had been greater, the free-rolling tail fins would have exhibited all five stages of rolling motion of the configuration used in the subsonic tests.

Lateral Aerodynamic Characteristics

The lateral aerodynamic characteristics of the model with zero canard deflection are presented in figures 7 to 9 for $\phi_c = 0^o$, 26.6^o, and 45^o, respectively. In general, the free-rolling tail configuration reduced the induced rolling-moment coefficient at the higher angles of attack. For $\phi_c = 26.6^o$, where typically large induced rolling moments occur, the angle of attack was terminated to stay within the rpm limit. Apparently, the increasing tail-fin rolling rate with angle of attack is proportional to the induced rolling moments generated by the asymmetric flow fields.

The lateral aerodynamic characteristics of the model with free-rolling tail fins and canards on and off are presented in figure 10. This figure is shown primarily to indicate that the basic configuration with zero canard deflection had small canard misalignments that resulted in a positive rolling-moment coefficient for the free-rolling tail with small roll rates (~100 rpm) at low angles of attack. These rolling-moment coefficients are reduced at the lower angles of attack when the basic configuration tail fins are fixed (figs. 7 to 9).

The roll-control characteristics of the model with a fixed and a free-rolling tail are presented in figure 11 ($\phi_c = 0^o$) and figure 12 ($\phi_c = 45^o$). A small negative roll control using canards 2 and 4, with each canard differentially deflected only 0.5^o, was used to satisfy the tail-fin roll-rate limit. For the free-rolling tail configuration at $\phi_c = 0^o$, the canards provide conventional roll control in the low angle-of-attack range since a negative roll control of the horizontal canards produces a negative rolling moment. Therefore, the typical roll-control reversal that is characteristic of a canard-controlled missile at low angles of attack (demonstrated herein by the fixed-tail configuration) is eliminated. At the higher angles of attack where the adverse effect of the vortex wakes generated by the differentially deflected canards has little or no influence on the tail fins, the rolling-moment coefficients of the fixed and free-rolling tail configurations are about the same. (See fig. 12(b).) In addition, the aero lockup is delayed to higher angles of attack where these adverse vortex wakes have cleared the tail fins. (See table III.)

The yaw-control characteristics of the model with a fixed and a free-rolling tail are presented in figure 13. The canards are effective in providing yawing moment, but it is accompanied by large adverse induced rolling moments (fixed-tail configuration) which are typical for canard-controlled missiles. The data show that for limited angles of attack at the low Mach numbers and for the complete angle-of-attack range at $M = 2.86$, the free-rolling tail configuration reduces these induced rolling moments that are generated by the yaw-control deflection of the canards. However, the free-rolling tail configuration has a reduction in yaw-control capability in the low angle-of-attack range which decreases with increases in Mach number. At the higher angles of attack ($\alpha > 12^o$) for $M = 2.86$ only, the free-tail configuration has greater

yaw-control capability than the fixed-tail configuration. Again, the aero lockup is delayed to higher angles of attack. (See table IV.)

CONCLUSIONS

A wind-tunnel investigation was made at free-stream Mach numbers from 1.70 to 2.86 to determine the effects of fixed and free-rolling tail-fin afterbodies on the static longitudinal and lateral aerodynamic characteristics of a cruciform canard-controlled missile model. The effect of small canard roll- and yaw-control deflections was also investigated. The results of the investigation are as follows:

1. The fixed and free-tail configurations have about the same lift-curve slope and longitudinal stability level at low angles of attack.

2. For the free-rolling tail configuration, the canards provide conventional roll control with no roll-control reversal at low angles of attack.

3. The free-rolling tail configuration reduced induced roll due to model roll angle and canard yaw control.

Langley Research Center
National Aeronautics and Space Administration
Hampton, VA 23665
August 9, 1978

REFERENCES

1. Sawyer, Wallace C.; Jackson, Charlie M., Jr.; and Blair, A. B., Jr.: Aerodynamic Technologies for the Next Generation of Missiles. Paper presented at the AIAA/ADPA Tactical Missile Conference (Gaithersburg, Maryland), Apr. 27-28, 1977.

2. Schult, Eugene D.: Free-Flight Measurements of the Rolling Effectiveness and Operating Characteristics of a Bellows-Actuated Split-Flap Aileron on a 60° Delta Wing at Mach Numbers Between 0.8 and 1.8. NACA RM L54H17, 1954.

3. Regan, Frank J.; and Falusi, Mary E.: The Static and Magnus Aerodynamic Characteristics of the M823 Research Store Equipped With Fixed and Freely Spinning Stabilizers. NOLTR 72-291, U.S. Navy, Dec. 1, 1972. (Available from DDC as AD 751 658.)

4. Regan, F. J.; Shannon, J. H. W.; and Tanner, F. J.: The Joint N.O.L./R.A.E./W.R.E. Research Programme on Bomb Dynamics. Part III. A Low-Drag Bomb With Freely Spinning Stabilizers. WRE-Report-904 (WR&D), Australian Def. Sci. Serv., June 1973.

5. Darling, John A.: Elimination of the Induced Roll of a Canard Control Configuration by Use of a Freely Spinning Tail. NOLTR 72-197, U.S. Navy, Aug. 16, 1972.

6. Mechtly, E. A.: The International System of Units - Physical Constants and Conversion Factors (Second Revision). NASA SP-7012, 1973.

7. Schaefer, William T., Jr.: Characteristics of Major Active Wind Tunnels at the Langley Research Center. NASA TM X-1130, 1965.

8. Stallings, Robert L., Jr.; and Lamb, Milton: Effects of Roughness Size on the Position of Boundary-Layer Transition and on the Aerodynamic Characteristics of a 55° Swept Delta Wing at Supersonic Speeds. NASA TP-1027, 1977.

9. Spahr, J. Richard; and Dickey, Robert R.: Wind-Tunnel Investigation of the Vortex Wake and Downwash Field Behind Triangular Wings and Wing-Body Combinations at Supersonic Speeds. NACA RM A53D10, 1953.

10. Dillenius, Marnix F. E.; and Nielsen, Jack N.: Prediction of Aerodynamics of Missiles at High Angles of Attack in Supersonic Flow. NEAR TR 99 (Contract No. N00014-74-C-0050); Nielsen Eng. & Res., Inc., Oct. 1975. (Available from DDC as AD A018 680.)

11. Hardy, Samuel R.: Subsonic Wind Tunnel Tests of a Canard-Control Missile Configuration in Pure Rolling Motion. NSWC/DL TR-3615, U.S. Navy, June 1977. (Available from DDC as AD A044 957.)

TABLE I.- SUMMARY OF TEST DATA FROM FREE-ROLLING TAIL CONFIGURATION WITH ZERO CONTROL DEFLECTION

M	α, deg	ϕ_c, deg	Tail-fin roll rate, rpm[a]	Remarks
			Counterclockwise	
1.70	-1.9	0	115	
	-.8		122	
	0		115	
	1.2		127	
	2.2		97	
	4.4		88	
	6.6		80	
	8.9		0	Stopped rolling
	11.1		0	Aero lockup
	13.5		0	Very small oscillation angle
	↓			
	17.9		0	
1.70	-2.0	26.6	108	
	-.5		133	
	-.1		121	
	1.1		127	
	2.1		116	
	4.5		12	Potated very slowly
	6.6		116	Roll rate apparently increasing with α
1.70	-2.4	45	105	
	-.9		112	
	0		123	
	.9		112	
	2.2		124	
	4.4		0	Stopped rolling
	6.5		0	Very small oscillation angle
	8.8		21	Rotated very slowly
	↓			
	17.8		0	Aero lockup
2.16	-1.2	0	120	
	.1		114	
	1.0		112	
	2.2		110	
	3.3		96	
	5.5		75	
	7.7		0	Stopped rolling; aero lockup
	↓			
	24.7		0	

[a]When viewed from the rear.

TABLE I.- Continued

M	α, deg	ϕ_c, deg	Tail-fin roll rate, rpm[a]	Remarks
			Counterclockwise	
2.16	-1.0	26.4	121	
	-.1		122	
	.9		130	
	2.1		107	
	3.2		96	
	5.4		0	Stopped rolling
	7.5		0	
	7.8		199	Roll rate apparently increasing with α
2.16	-1.4	45	100	
	-.1		104	
	1.0		99	
	2.1		100	
	3.2		87	
	5.4		0	Stopped rolling
	7.5		0	
	9.9		114	Started rolling
	12.0		128	
	14.1		195	Roll rate increasing with α
2.36	-1.5	0	143	
	-.2		129	
	.9		83	
	2.0		78	
	2.9		72	
	5.2		37	
	7.3		27	
	9.6		0	Stopped rolling; aero lockup
	↓			
	23.7		0	Large oscillation angle
2.36	-1.5	26.6	80	
	0		94	
	.9		98	
	2.0		61	
	3.1		0	Stopped rolling
	5.3		0	
	7.4		194	Roll rate apparently increasing with α

[a]When viewed from the rear.

TABLE I.- Continued

M	α, deg	ϕ_c, deg	Tail-fin roll rate, rpm[a]	Remarks
			Counterclockwise	
2.36	-1.0	45	56	
	.3		70	
	1.3		100	
	2.4		56	
	3.5		54	
	5.6		0	Stopped rolling
	7.7		33	Started rolling
	9.9		118	Roll rate increasing with α
	12.0		161	
	14.4		167	
	16.5		122	
	18.7		0	Stopped rolling; aero lockup
	↓			
	23.8		0	
2.86	-2.9	0	23	Low roll rates
	-1.6		71	
	-.5		64	
	.7		62	
	1.8		36	
	3.8		0	Stopped rolling; aero lockup
	↓			
	22.0		0	
2.86	-2.8	26.5	33	
	-1.5		49	
	-.6		51	
	.6		0	Oscillated; 2 or 3 revolutions
	1.8		50	Started rolling
	3.7		0	Stopped rolling
	5.9		0	
	8.0		131	Started rolling
	10.0		0	Stopped rolling
	11.5		230	Roll rate apparently increasing with α

[a]When viewed from the rear.

TABLE I.- Concluded

M	α, deg	ϕ_c, deg	Tail-fin roll rate, rpm[a]	Remarks
			Counterclockwise	
2.86	-2.5	45	27	Low roll rates
	-1.5		51	
	-.5		93	
	.7		50	
	1.7		0	Stopped rolling
	3.9		0	Small oscillation angle
	5.9		0	
	8.1		75	Started rolling
	10.3		120	Steady rolling
	12.6		124	
	14.6		0	Stopped rolling
	17.0		0	
	19.1		0	
	20.2		157	Started rolling

[a]When viewed from the rear.

TABLE II.- SUMMARY OF TEST DATA FROM FREE-ROLLING TAIL CONFIGURATION WITH CANARD OFF

M	α, deg	ϕ_c, deg	Tail-fin roll rate, rpm[a]	Remarks
			Clockwise	
1.70	-2.0	0	54	Very low roll rates
	-.9		37	
	0		39	
	1.0		46	
	2.1		47	
	4.0		31	
	6.0		31	
	8.0		0	Stopped and started to roll
	10.0		0	
	12.1		30	
	14.2		28	
	16.4		26	Aero lockup
2.16	-1.6	0	33	Very low and steady roll rates
	-.9		34	
	-.1		31	
	1.0		47	
	2.0		20	
	3.0		30	
	5.0		23	
	7.0		0	Stopped rolling
	9.1		0	Stopped; started for several revolutions at a very slow rate
	11.3		0	
	13.4		26	Stopped; started; oscillated
	↓			
	23.2		27	Rolled hesitantly and irregularly

[a]When viewed from the rear.

TABLE II.- Concluded

M	α, deg	ϕ_c, deg	Tail-fin roll rate, rpm[a]	Remarks
			Clockwise	
2.36	-1.2	0	74	Low roll rates
	-.3		47	
	.8		86	
	1.8		52	
	2.8		102	
	4.9		88	
	6.9		45	Stopped; started; and oscillated
	9.0		0	Rolled hesitantly and irregularly
	↓			
	23.0		42	
2.86	-2.5	0	39	Low roll rates
	↓			
	5.6		28	
	7.8		0	Stopped rolling
	9.8		0	Oscillated through small angle
	↓			
	21.6		0	

[a]When viewed from the rear.

TABLE III.- SUMMARY OF TEST DATA FROM FREE-ROLLING TAIL CONFIGURATION WITH TWO CANARDS DIFFERENTIALLY DEFLECTED 0.5° EACH FOR NEGATIVE ROLL CONTROL

M	α, deg	ϕ_c, deg	Tail-fin roll rate, rpm[a]	Remarks
			Clockwise	
1.70	-2.2	0	98	
	-1.1		96	
	0		90	
	1.2		100	
	2.4		114	
	4.5		123	
	6.6		131	
	8.9		97	
	11.1		0	Stopped rolling; aero lockup
	↓			
	17.9		0	Small oscillation angle
1.70	-2.3	45	102	
	-1.3		81	
	-.1		83	
	1.3		105	
	2.2		104	
	4.3		128	
	↓			
	10.8		207	Roll rate increasing with α; $\alpha > 11°$; rpm > 500
2.16	-1.2	0	93	
	0		97	
	1.1		109	
	2.2		122	
	3.3		136	
	5.5		154	
	7.6		164	Steady rolling
	↓			
	16.7		138	
	18.9		0	Stopped rolling; aero lockup
	↓			
	24.8		0	

[a]When viewed from the rear.

TABLE III.- Continued

M	α, deg	ϕ_c, deg	Tail-fin roll rate, rpm[a]	Remarks
			Clockwise	
2.16	-1.3	45	82	
	0		84	
	1.0		95	
	2.1		95	
	3.3		104	
	5.4		150	
	7.6		207	Steady rolling
	↓			
	12.0		151	
	14.3		0	Stopped rolling; aero lockup
	↓			
	24.5		0	
2.36	-1.3	0	109	
	-.1		121	
	.8		103	
	2.0		95	
	3.1		147	
	5.2		123	
	7.3		110	
	9.6		0	Stopped rolling; aero lockup
	↓			
	24.4		0	
2.36	-1.0	45	88	
	.4		71	
	1.3		105	
	2.3		93	
	3.4		108	
	5.6		168	
	7.8		178	
	10.0		156	
	12.2		0	Stopped rolling; aero lockup
	↓			
	24.2		0	

[a]When viewed from the rear.

TABLE III.- Concluded

M	α, deg	ϕ_c, deg	Tail-fin roll rate, rpm[a]	Remarks
			Clockwise	
2.86	-2.7	0	51	
	-1.5		67	
	-.4		87	
	.7		104	
	2.1		80	
	3.8		99	
	5.9		123	Steady rolling
	↓			
	14.7		133	
	17.0		0	Stopped rolling; aero lockup
	↓			
	22.6		0	
2.86	-2.6	45	84	Low roll rates
	-1.5		58	
	-.5		65	
	.6		71	
	1.7		73	
	3.8		105	Steady rolling
	↓			
	10.3		42	
	12.5		0	Stopped rolling; aero lockup
	↓			
	22.5		0	

[a]When viewed from the rear.

TABLE IV.- SUMMARY OF TEST DATA FROM FREE-ROLLING TAIL CONFIGURATION WITH VERTICAL CANARDS DEFLECTED 5° FOR POSITIVE YAW CONTROL

M	α, deg	ϕ_c, deg	Tail-fin roll rate, rpm[a]		Remarks
			Clockwise	Counterclockwise	
1.70	-2.2	0	360		
	-1.1		134		
	0			80	Roll direction changed
	1.0			314	Roll rate increasing with α
	2.1			463	Excessive roll rate
2.16	-1.3	0	152		
	0			53	Low roll rate
	1.1			240	
	2.2			430	
	3.3			517	
	6.2			522	Excessive roll rate
2.36	-1.3	0	191		
	-.2			36	Very low roll rate both directions
	.9			187	Roll rate increasing with α
	2.0			360	
	3.0			500	
	6.7			590	Excessive roll rate
2.86	-2.7	0	351		
	-1.5		177		
	-.5		55		
	.6			84	Roll direction changed
	1.7			206	Roll rate increasing with α
	3.9			439	
	5.8			527	
	8.3			507	
	10.3			354	
	12.5			94	
	14.1			0	Stopped rolling; "stable" aero lockup
	↓				
	22.7			0	

[a]When viewed from the rear.

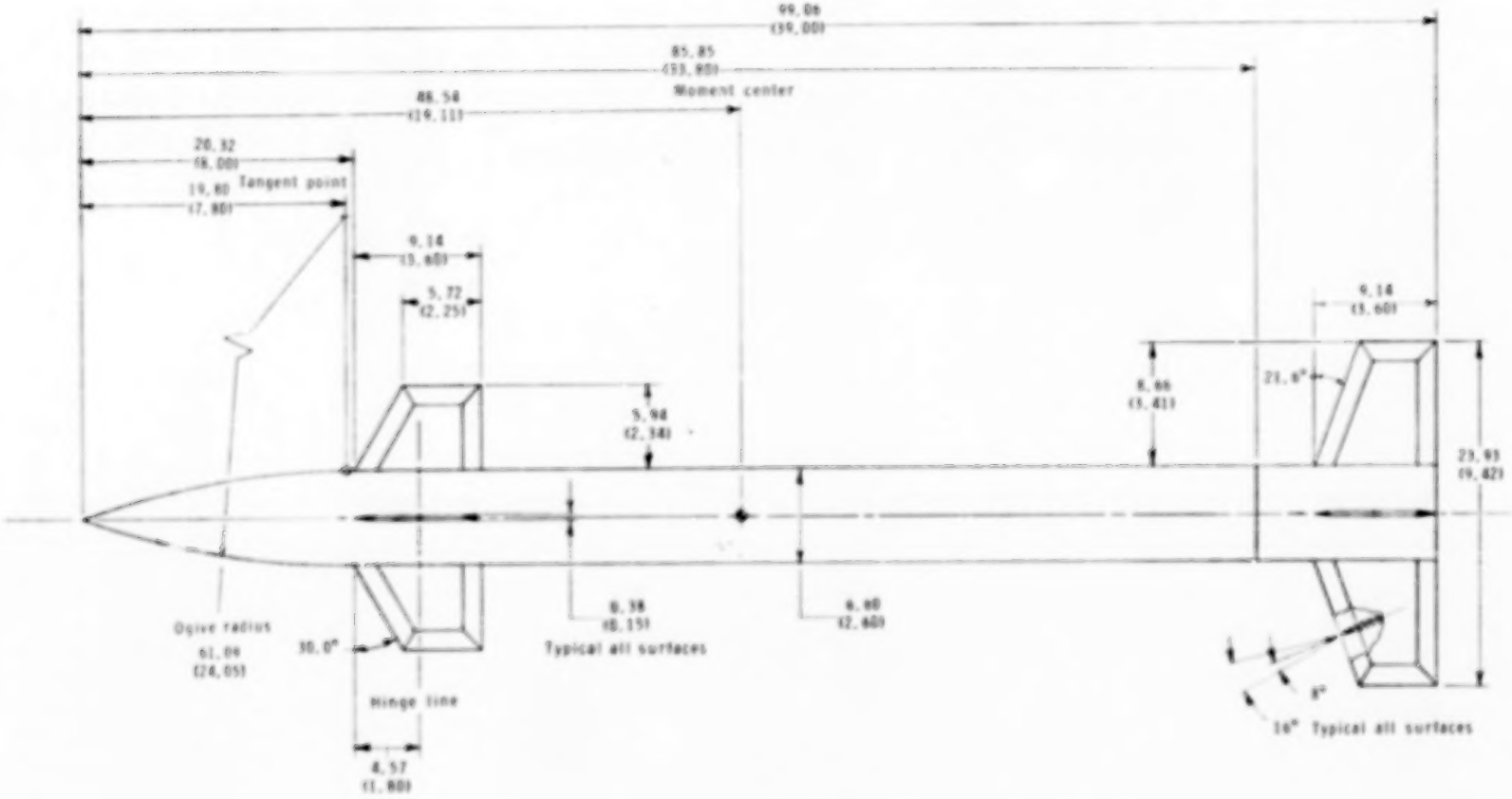

(a) Complete model.

Figure 1.- Model details. All dimensions are in centimeters (inches) unless otherwise indicated.

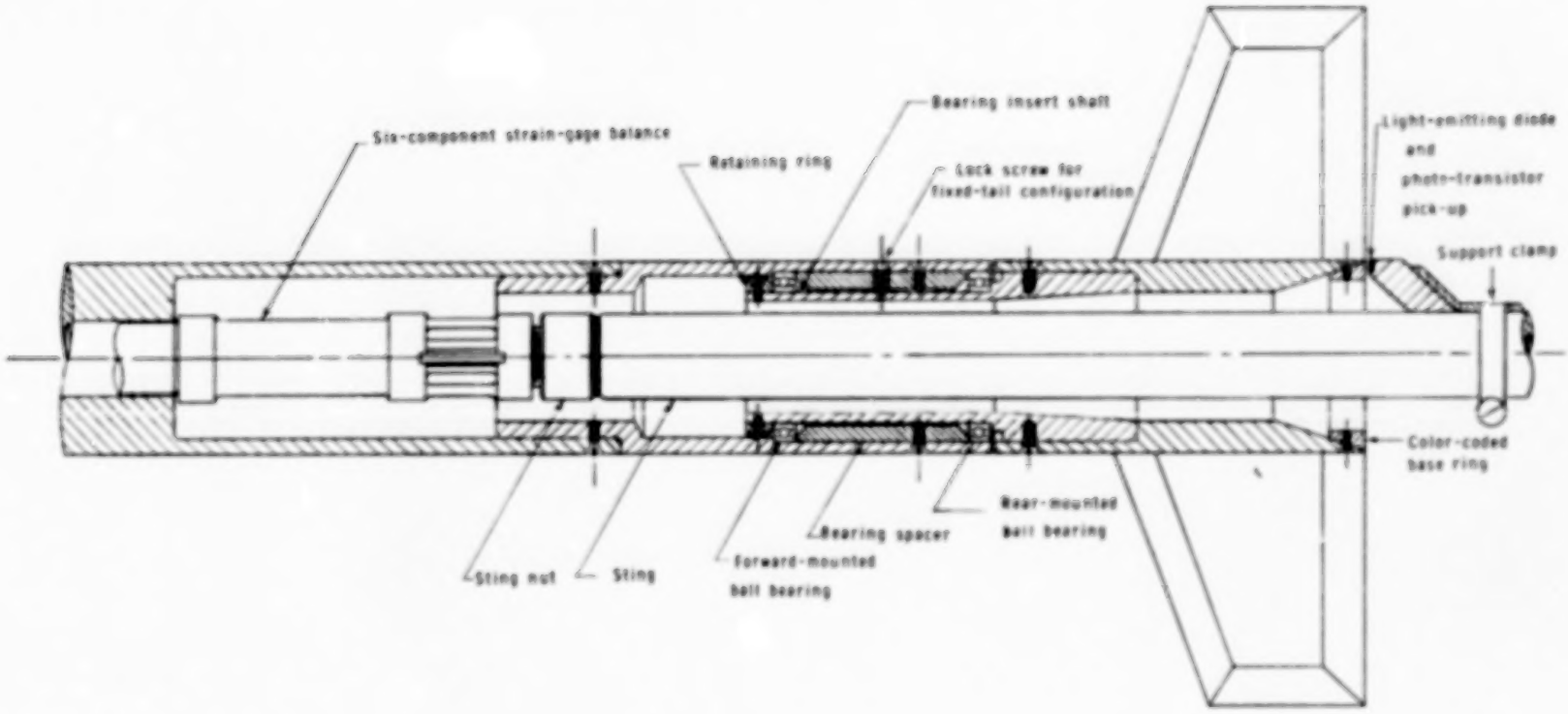

(b) Ball-bearing spindle assembly and sting support.

Figure 1.- Concluded.

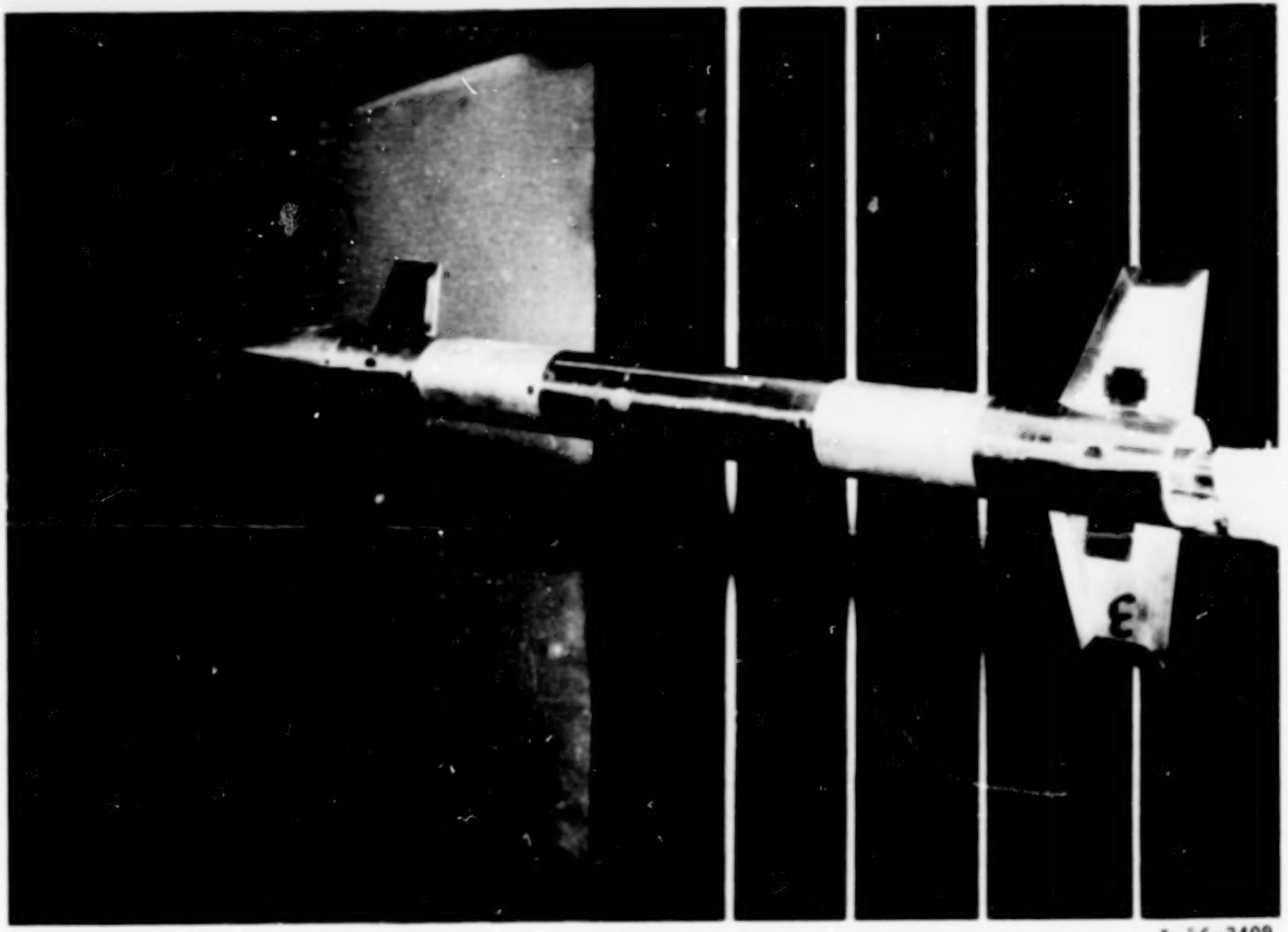

L-76-3409

Figure 2.- Model.

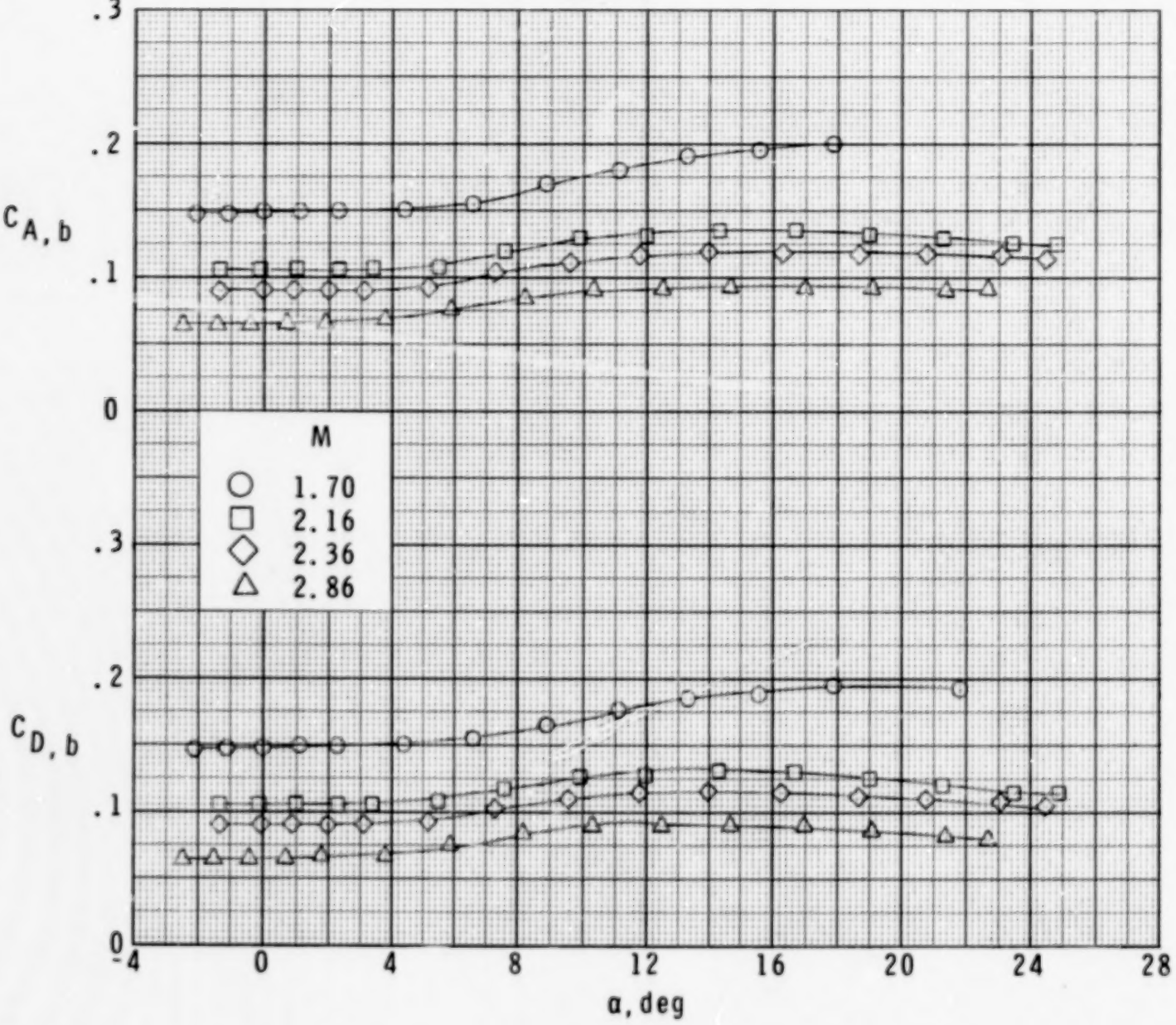

Figure 3.- Typical variation of measured $C_{A,b}$ and $C_{D,b}$ with angle of attack.

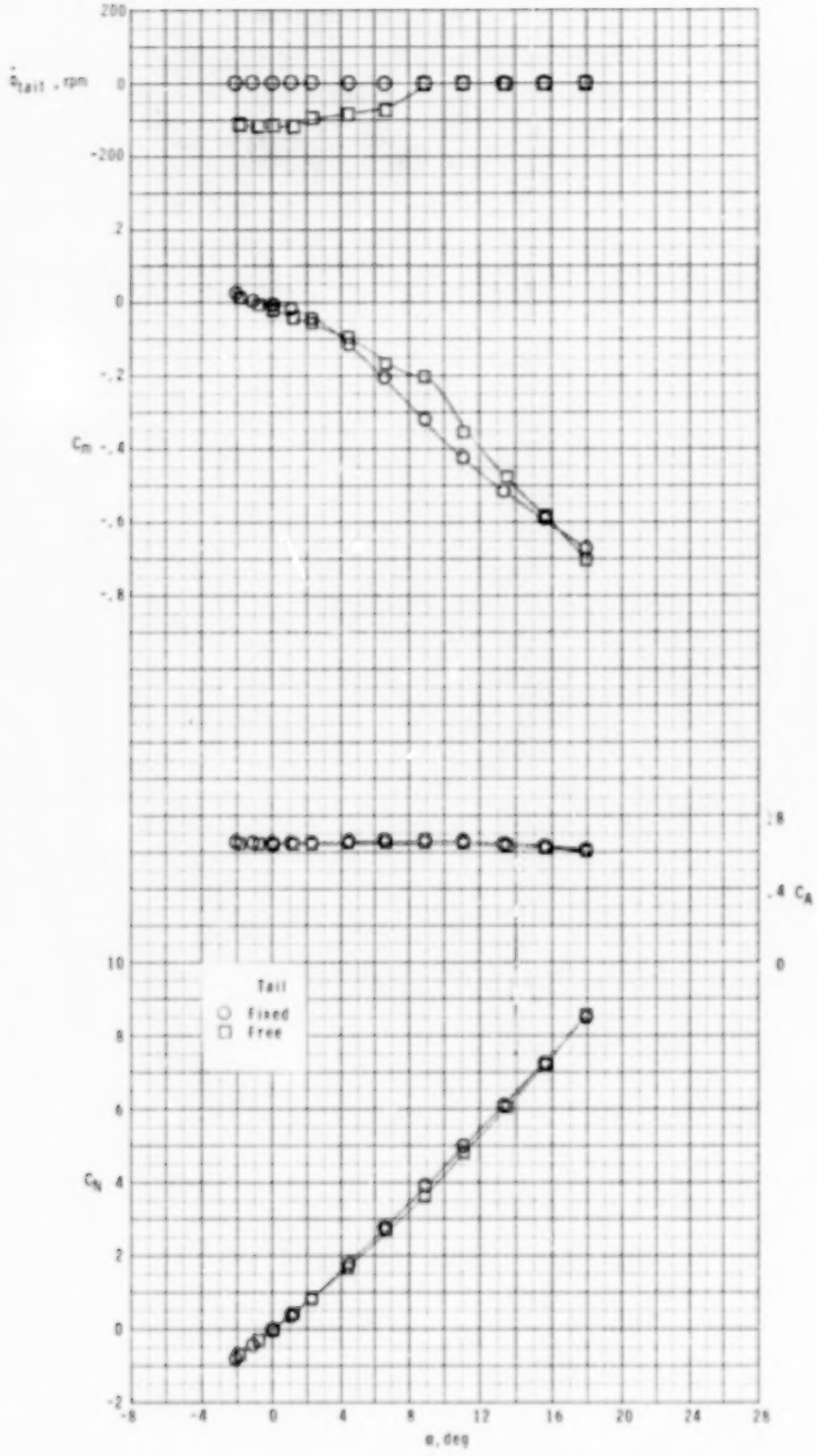

(a) M = 1.70.

Figure 4.- Effect of free-rolling tail on longitudinal aerodynamic characteristics of model with zero control deflection at $\phi_c = 0^o$.

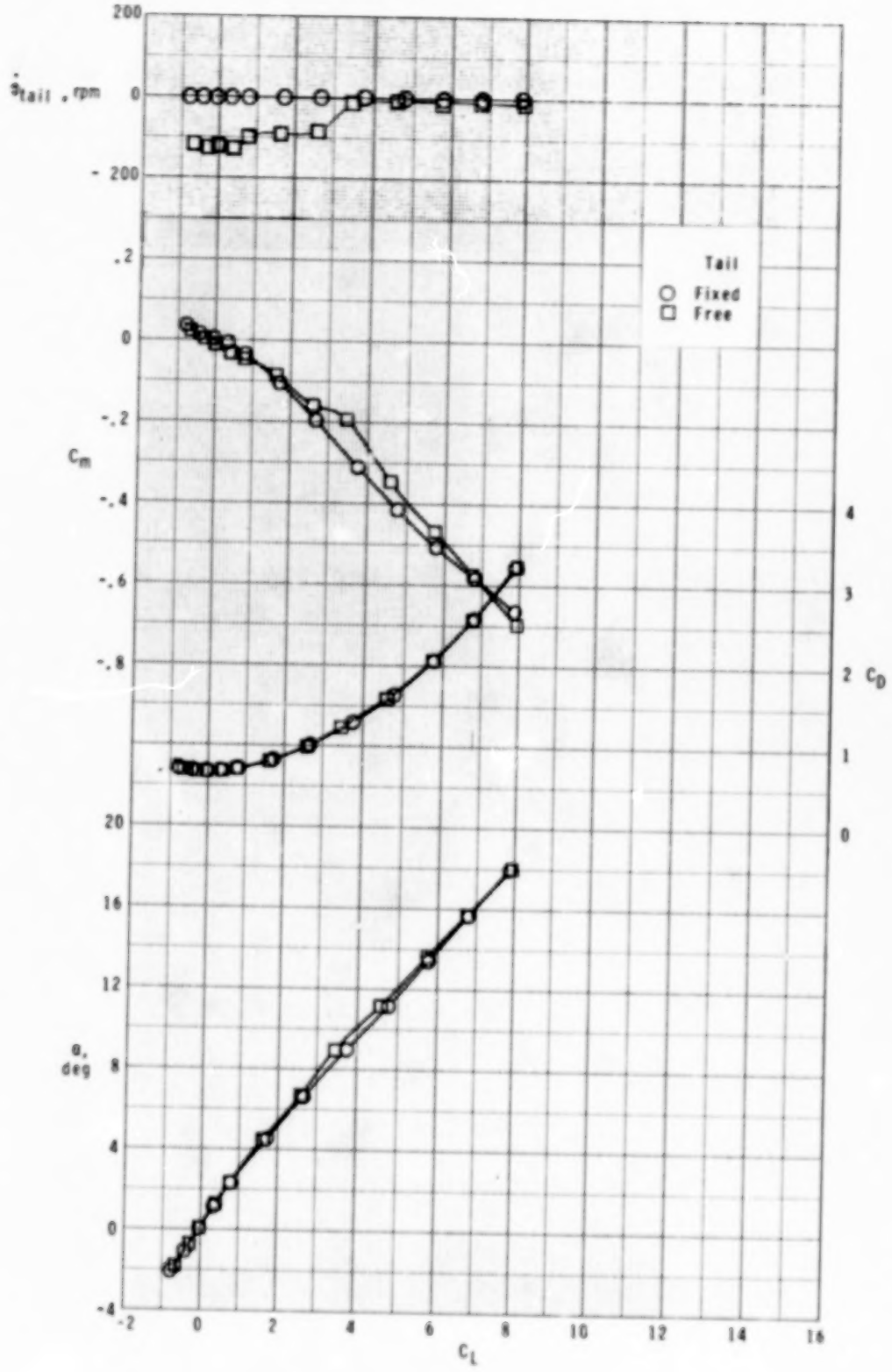

(a) Concluded.

Figure 4.- Continued.

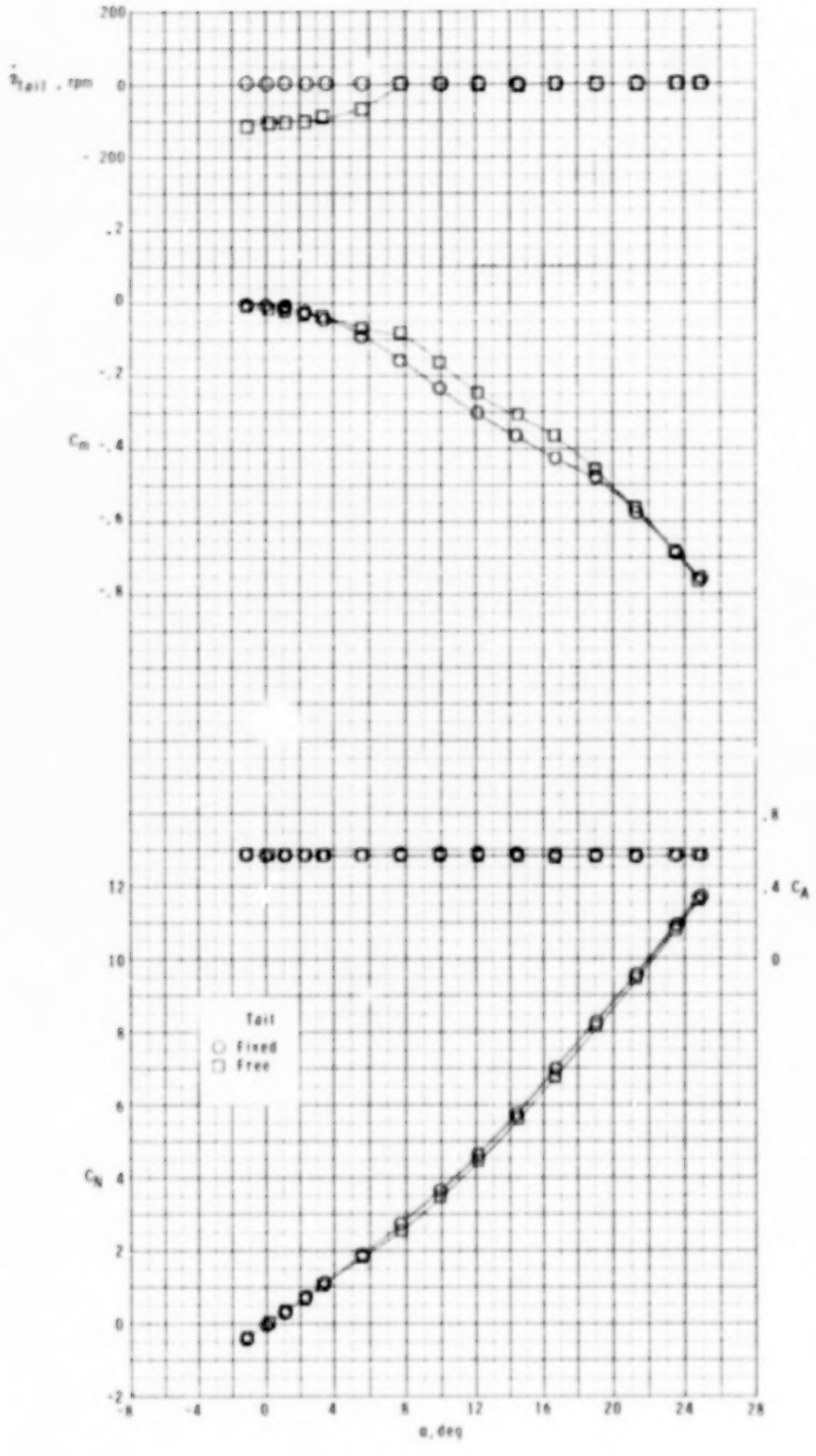

(b) M = 2.16.

Figure 4.- Continued.

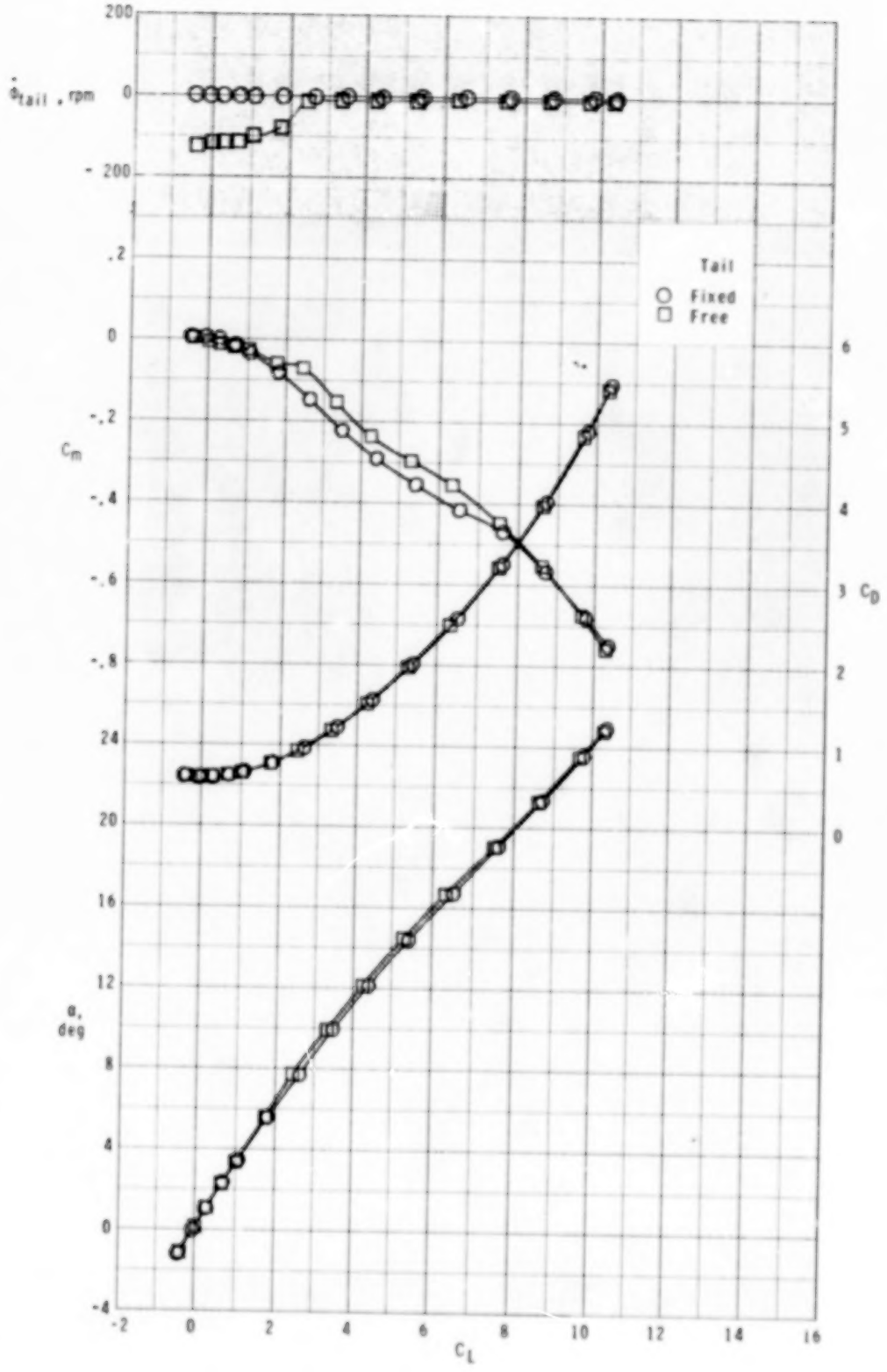

(b) Concluded.

Figure 4.- Continued.

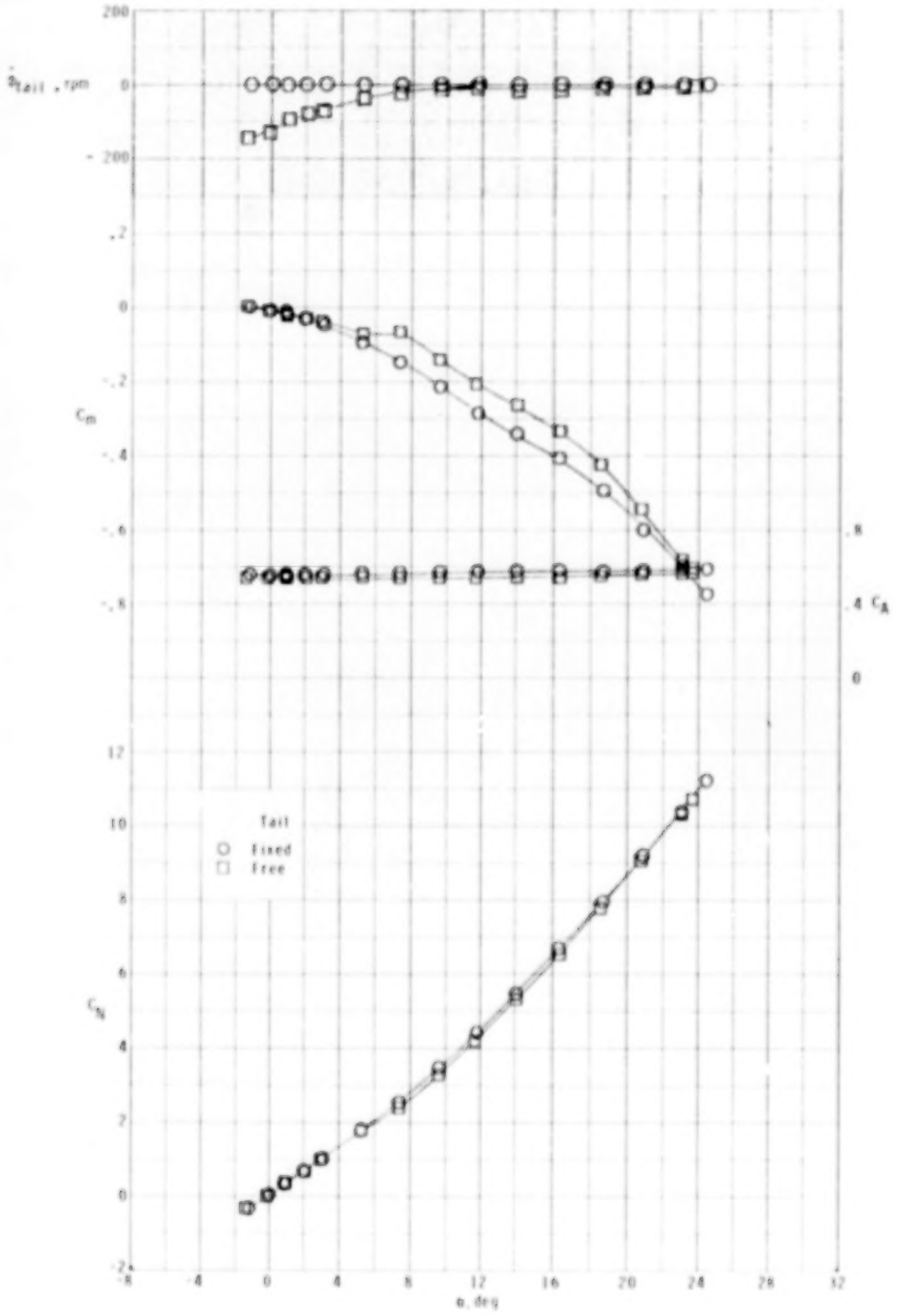

(c) M = 2.36.

Figure 4.- Continued.

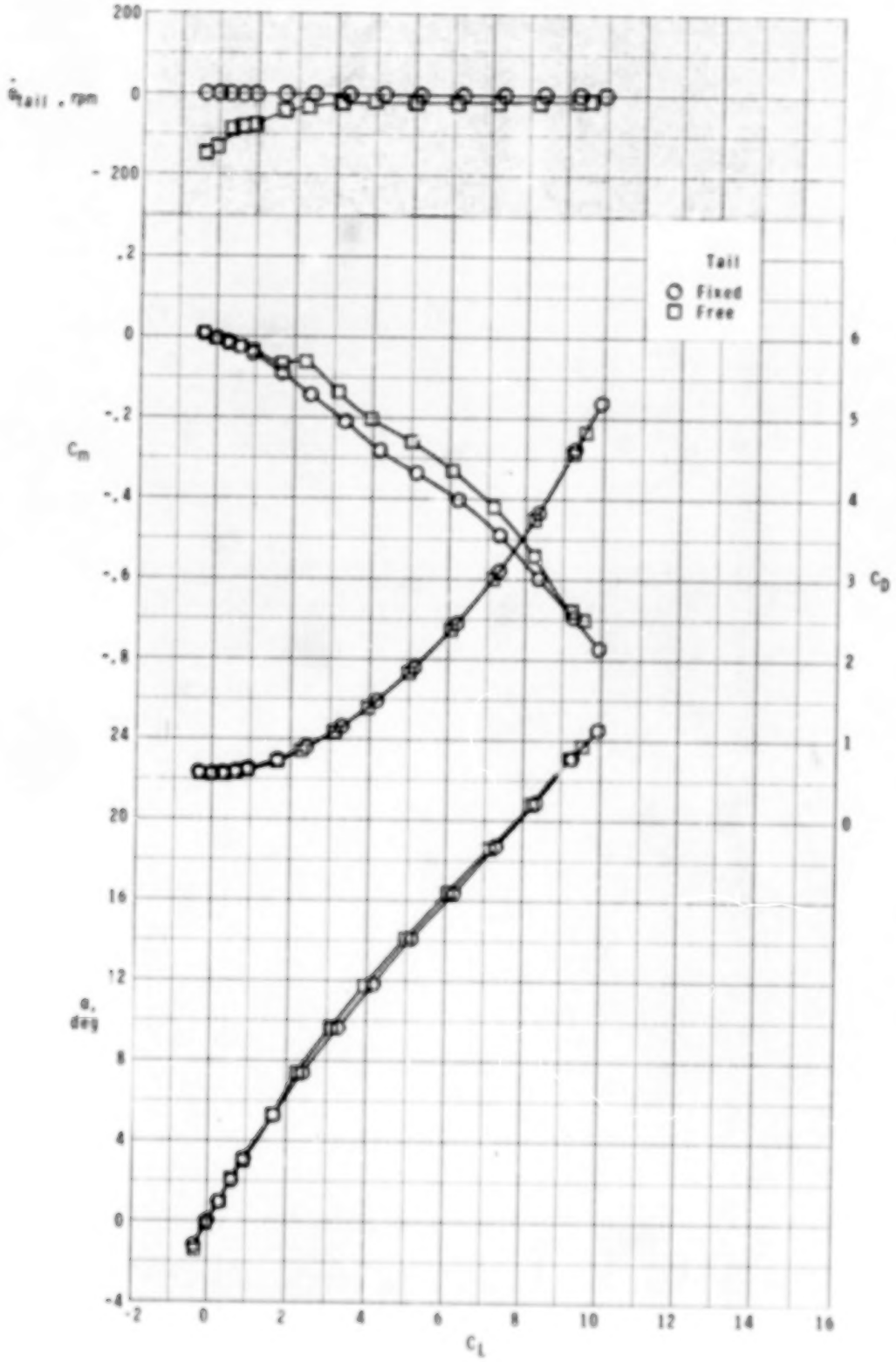

(c) Concluded.

Figure 4.- Continued.

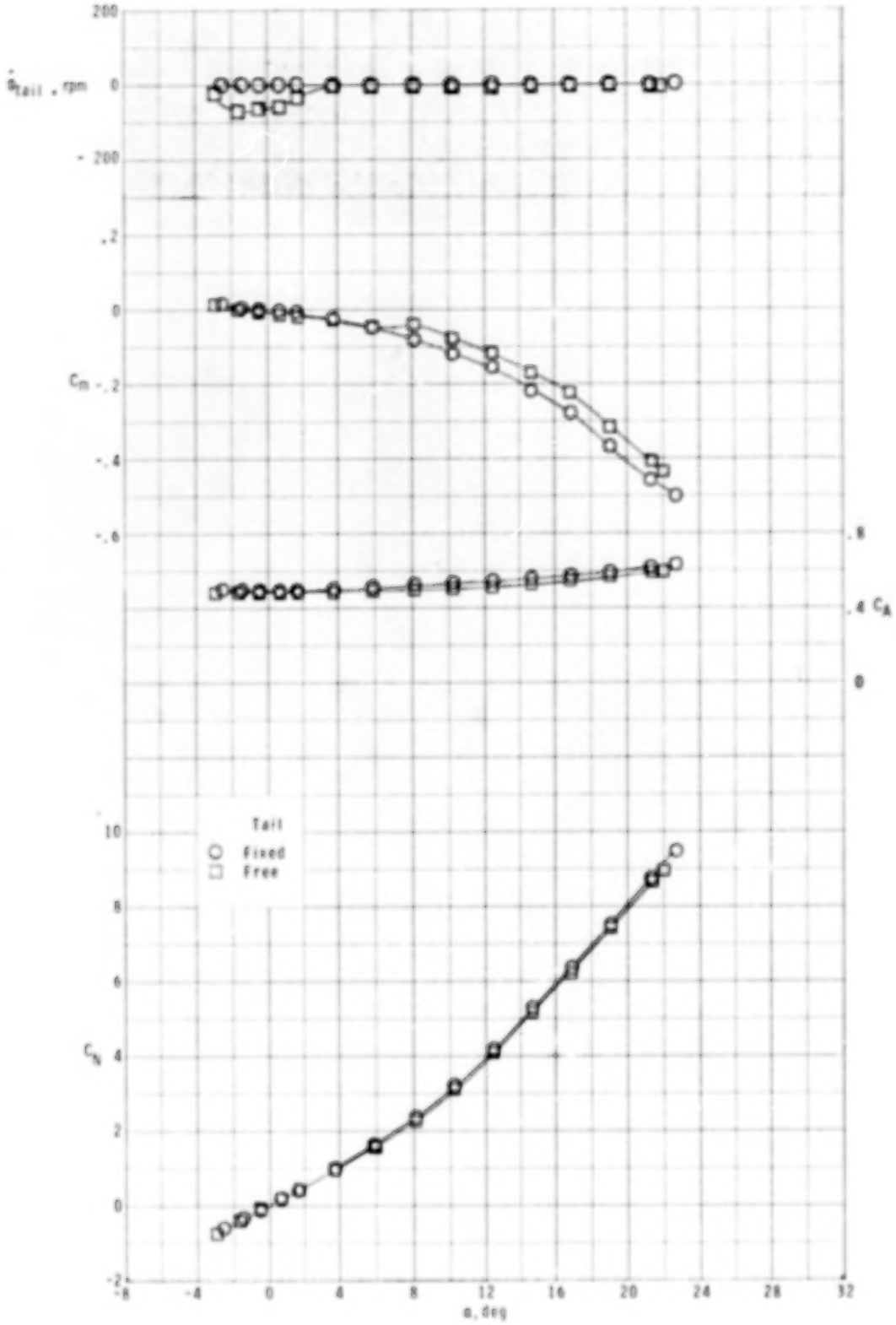

(d) M = 2.86.

Figure 4.- Continued.

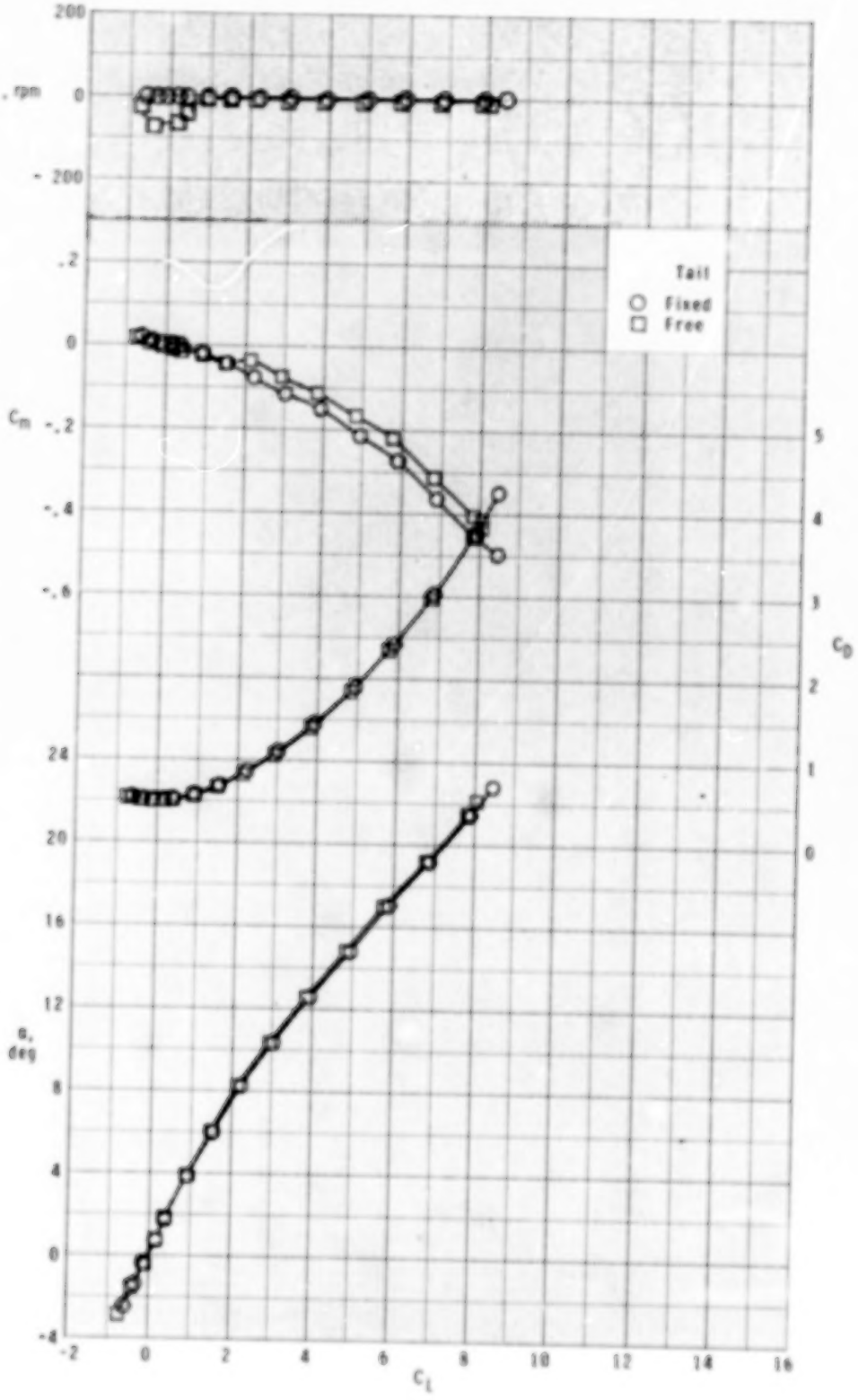

(d) Concluded.

Figure 4.- Concluded.

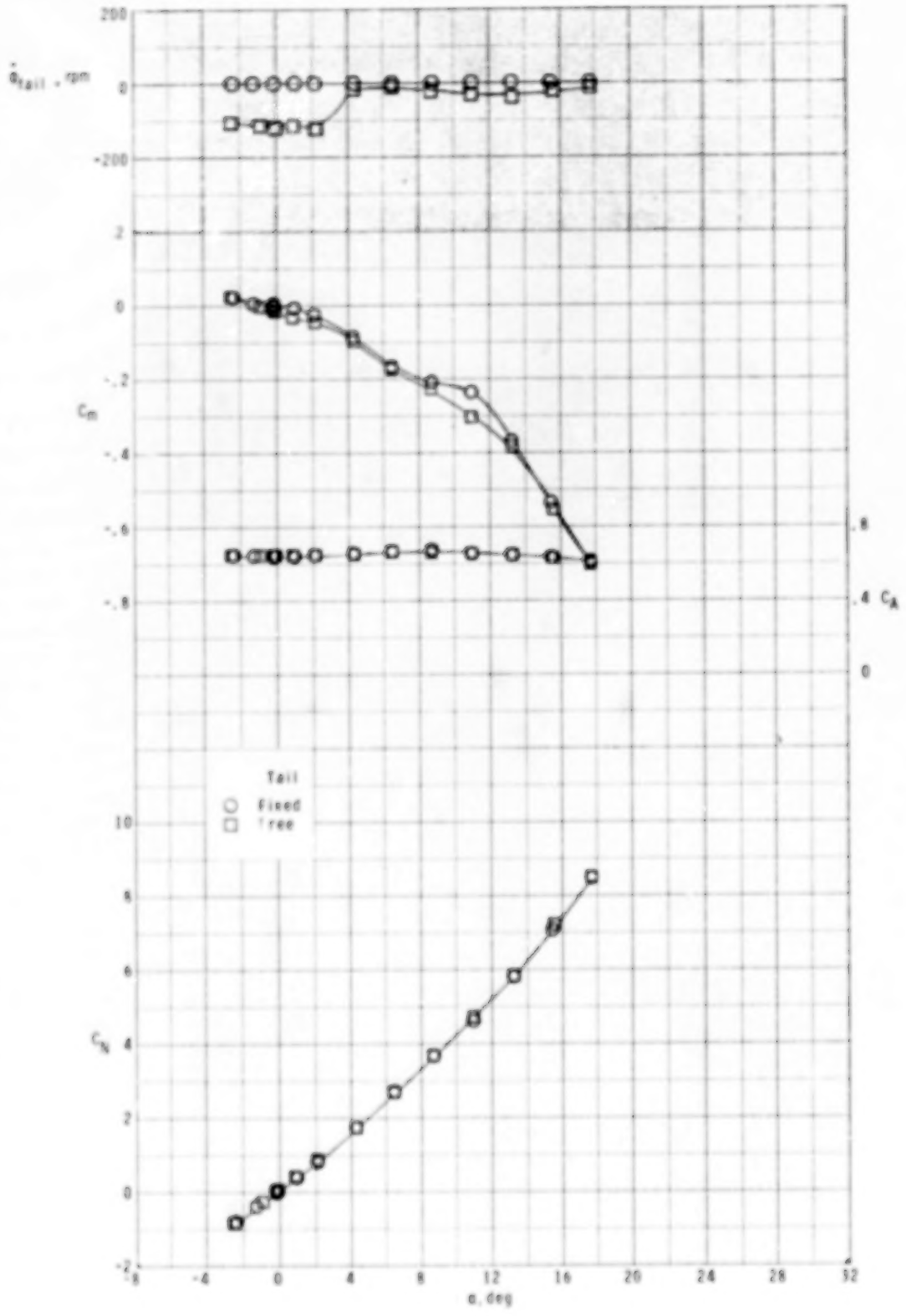

(a) M = 1.70.

Figure 5.- Effect of free-rolling tail on longitudinal aerodynamic characteristics of model with zero control deflection at $\phi_c = 45^o$.

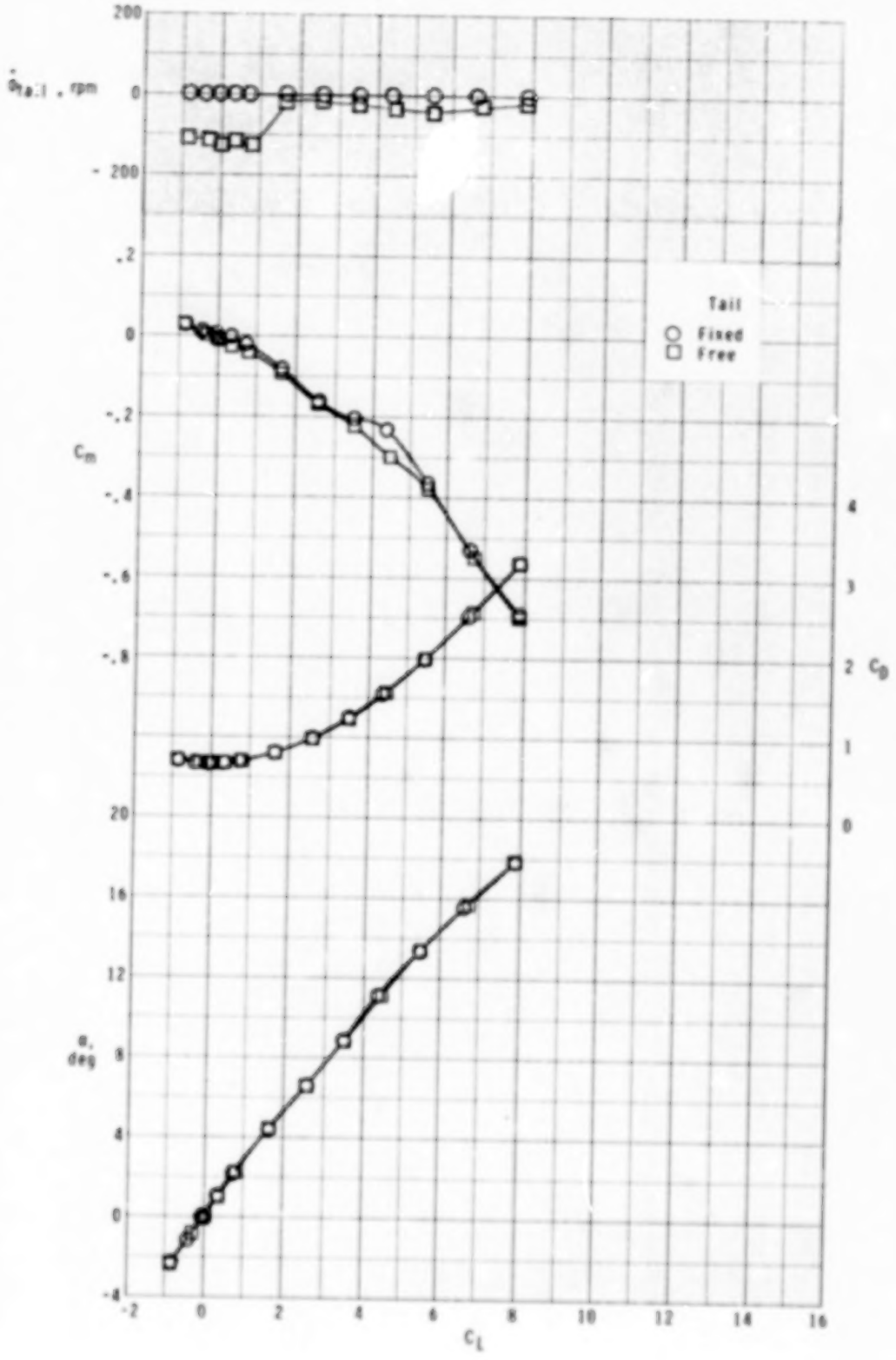

(f' Concluded.

Figure 5.- Continued.

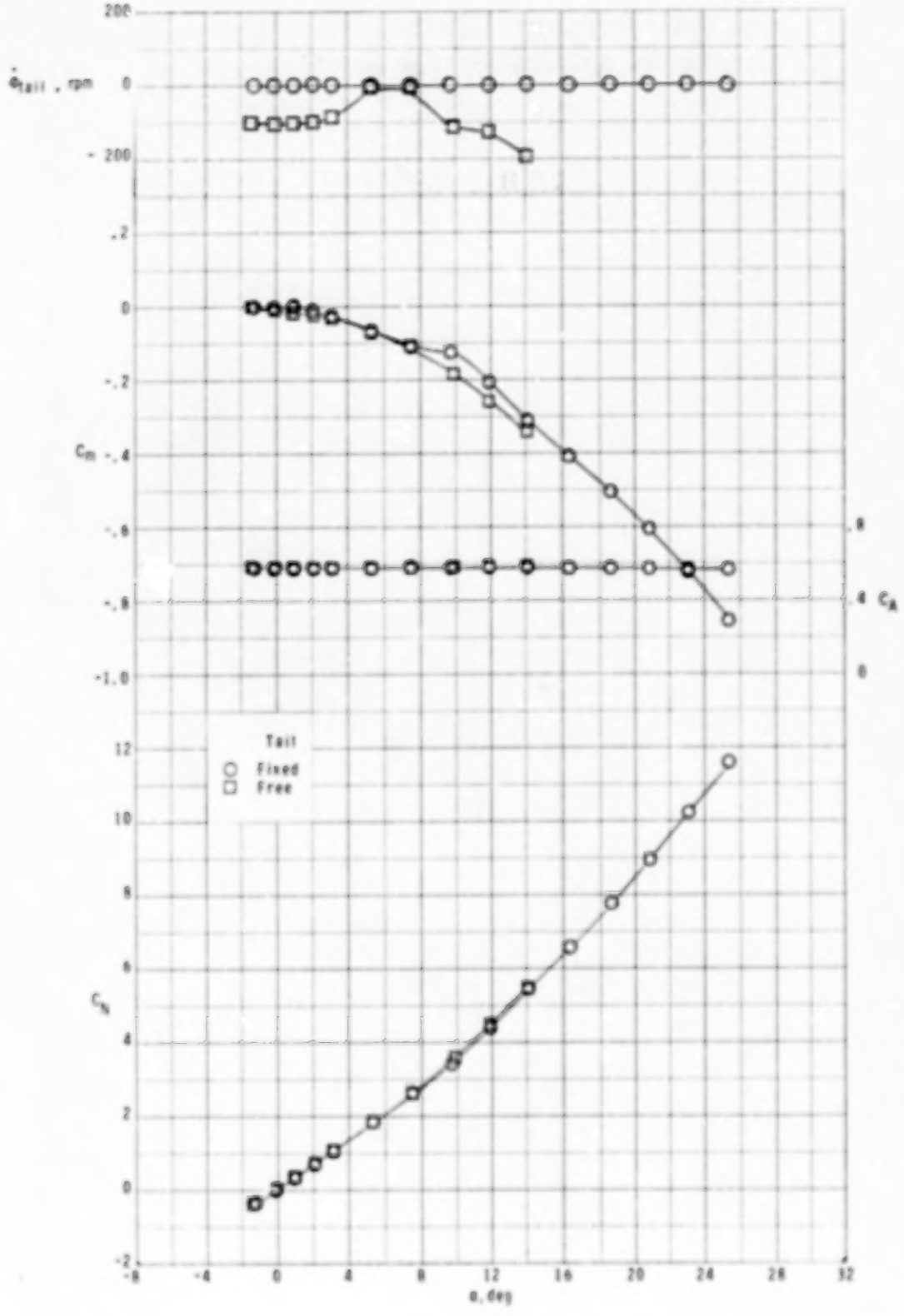

(b) M = 2.16.

Figure 5.- Continued.

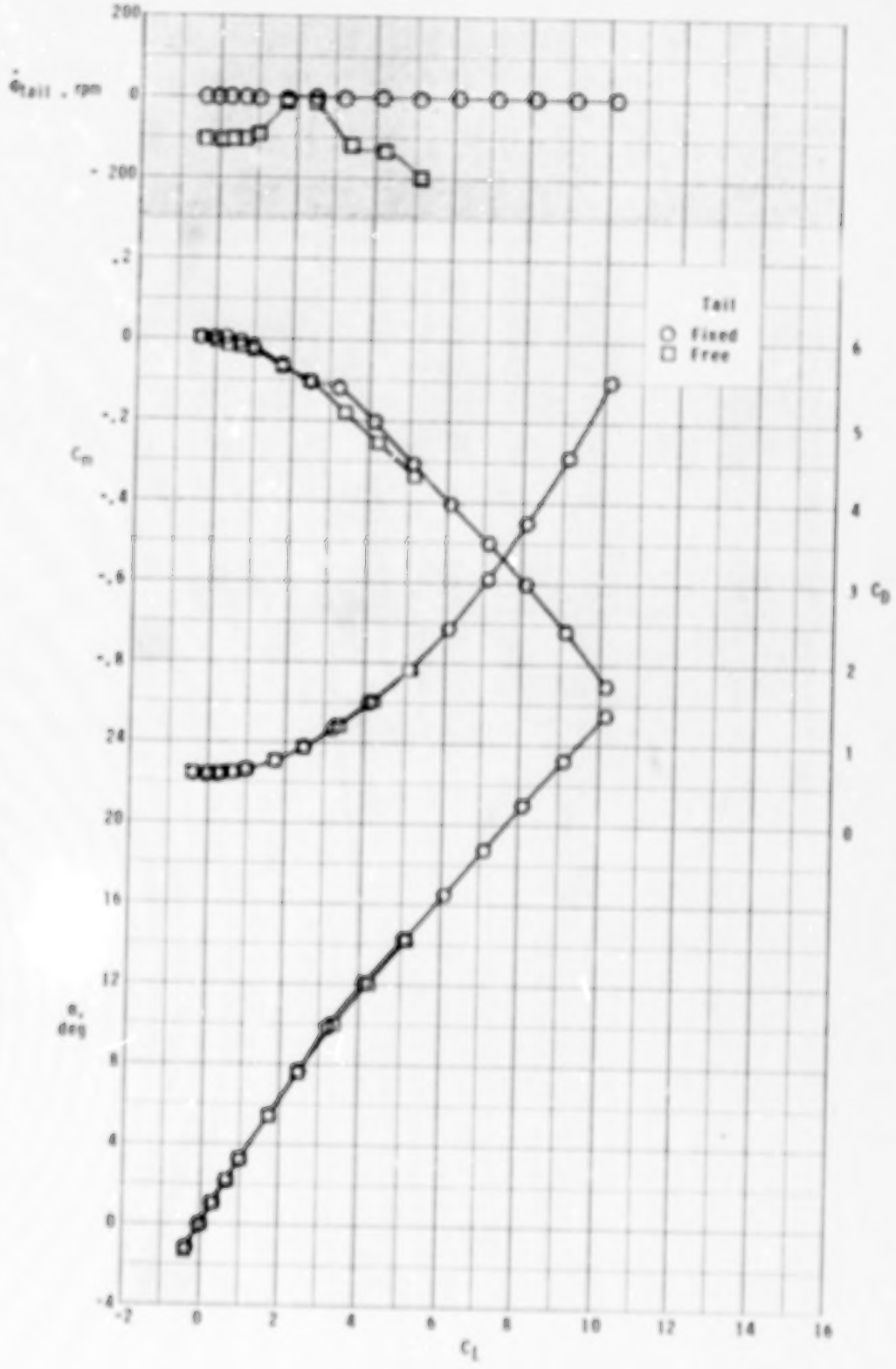

(b) Concluded.

Figure 5.- Continued.

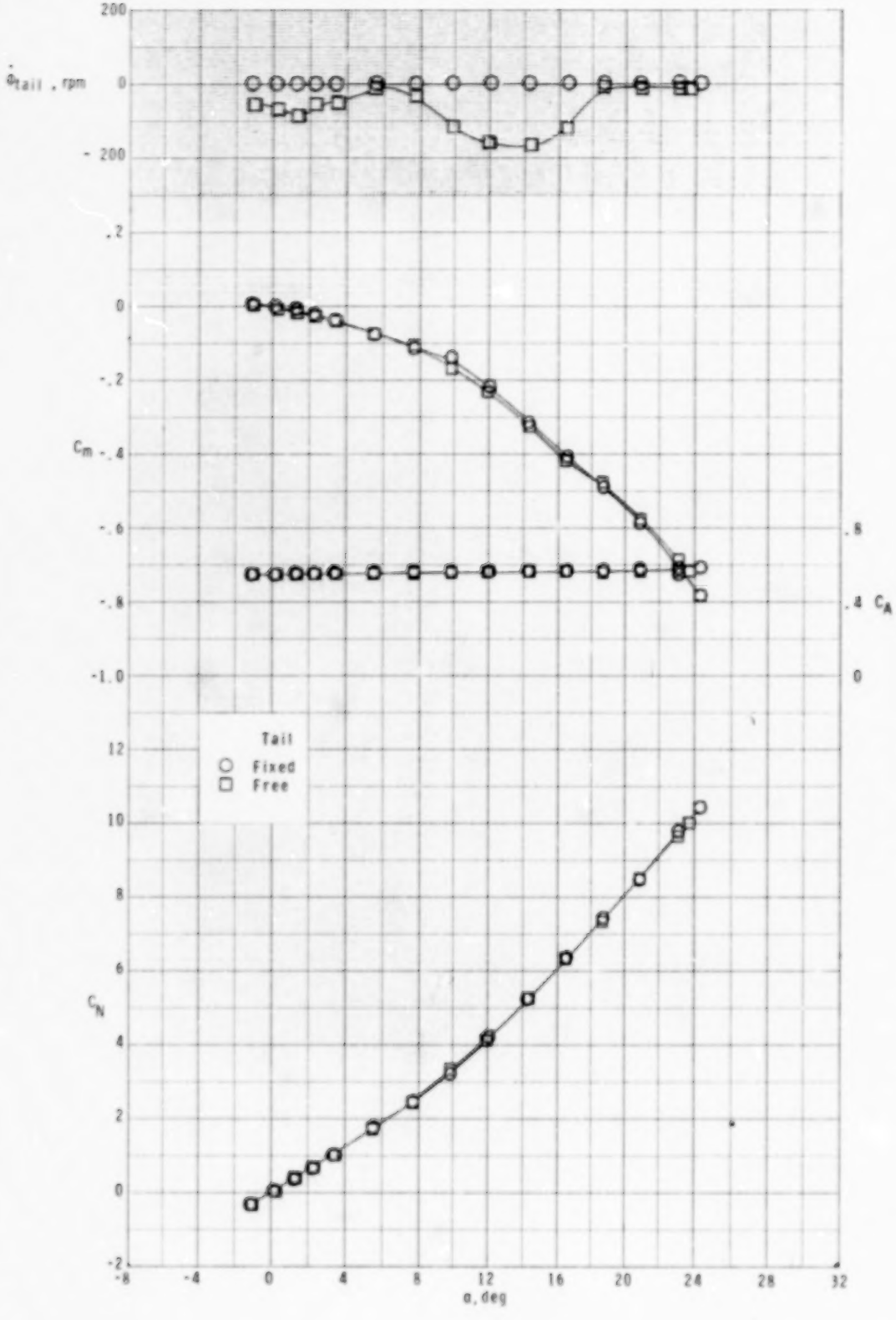

(c) M = 2.36.

Figure 5.- Continued.

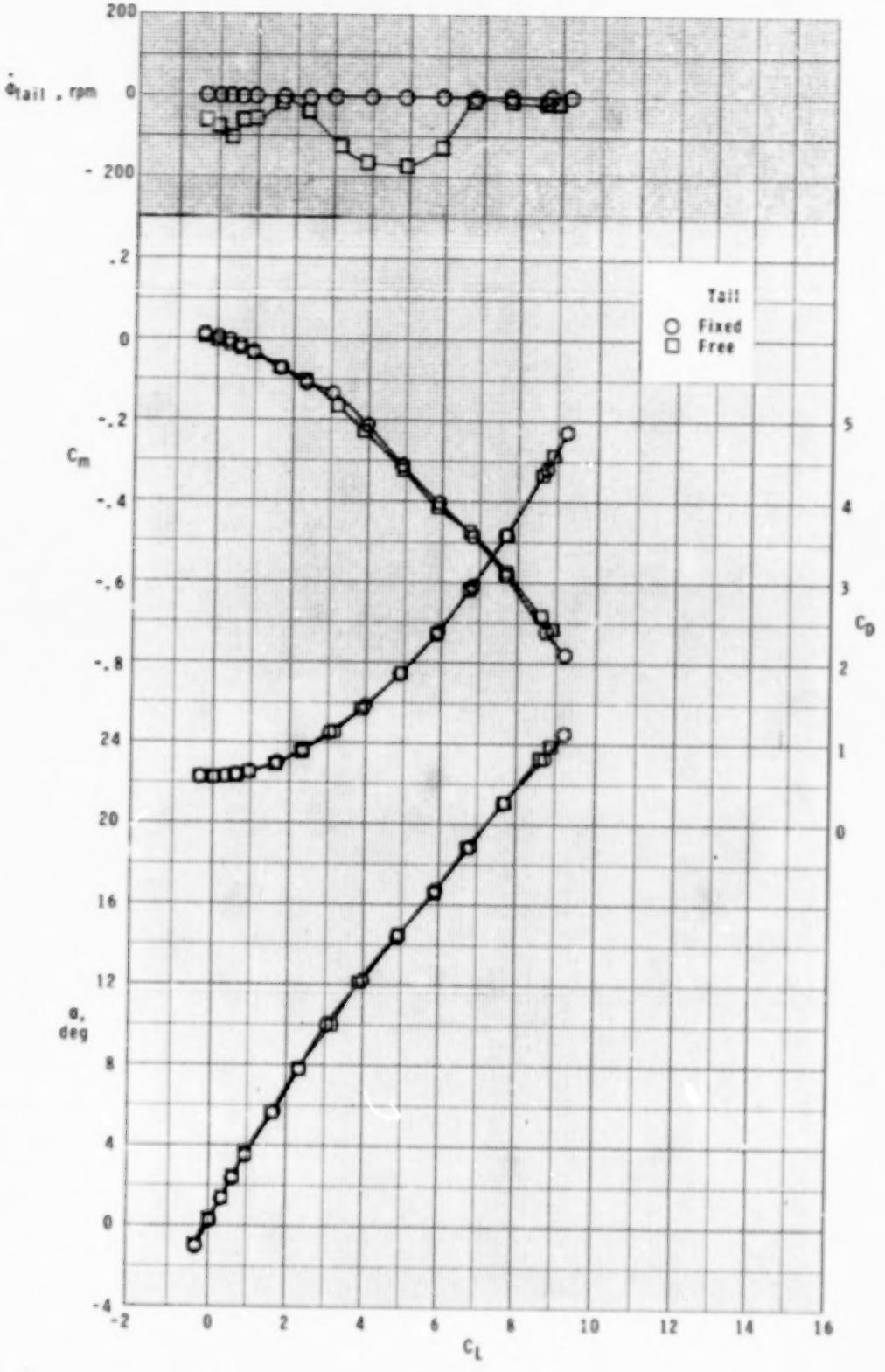

(c) Concluded.

Figure 5.- Continued.

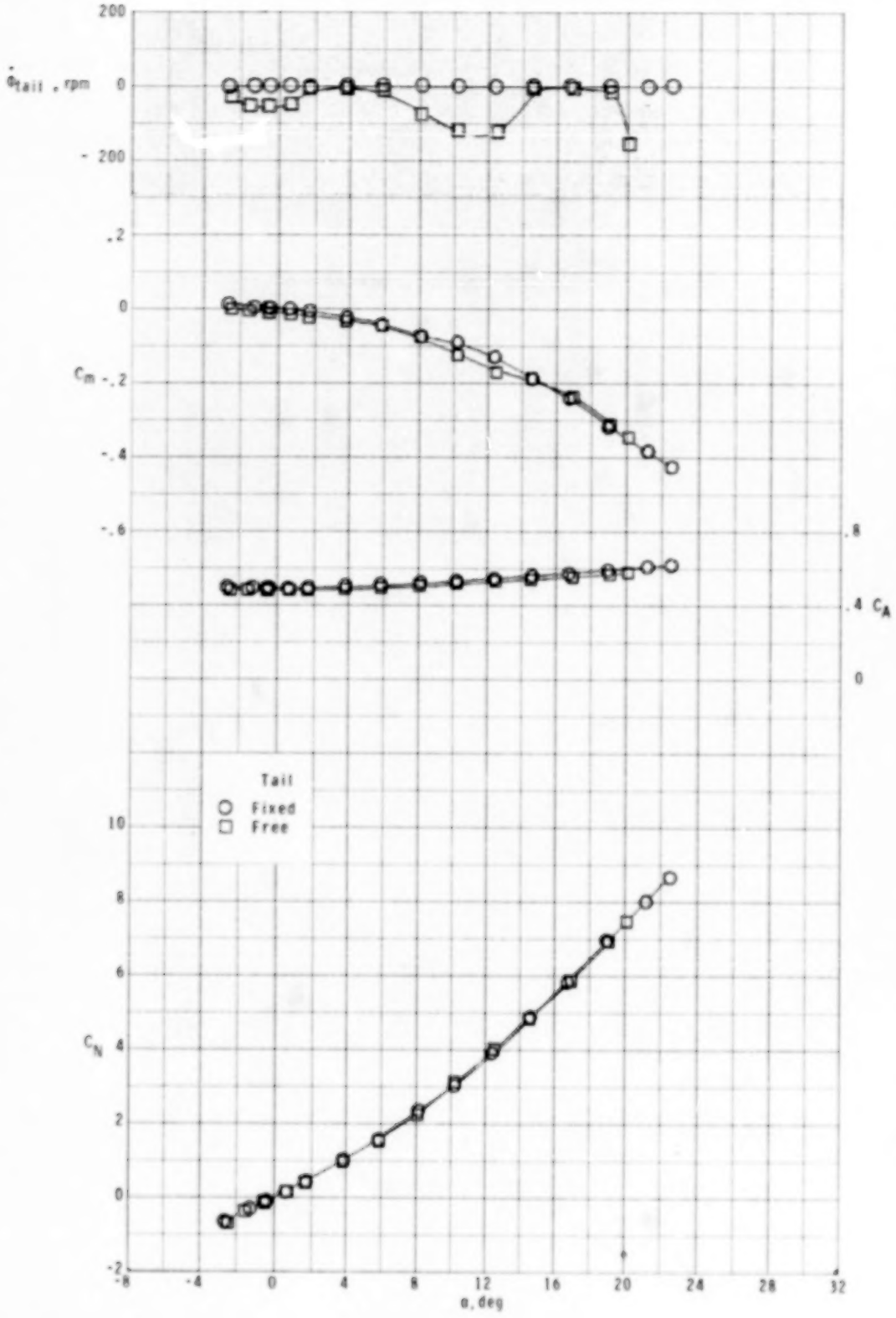

(d) M = 2.86.

Figure 5.- Continued.

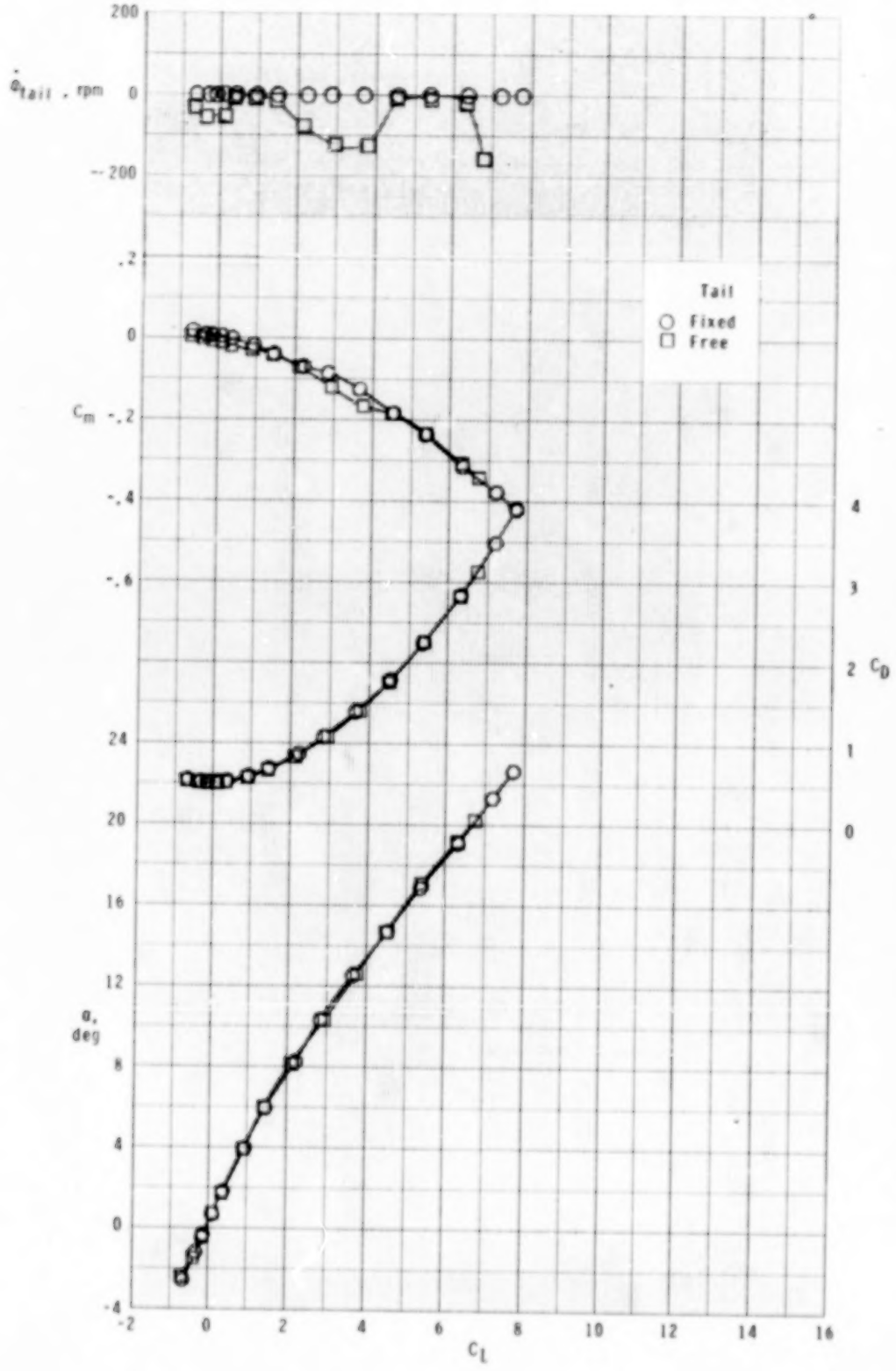

(d) Concluded.

Figure 5.- Concluded.

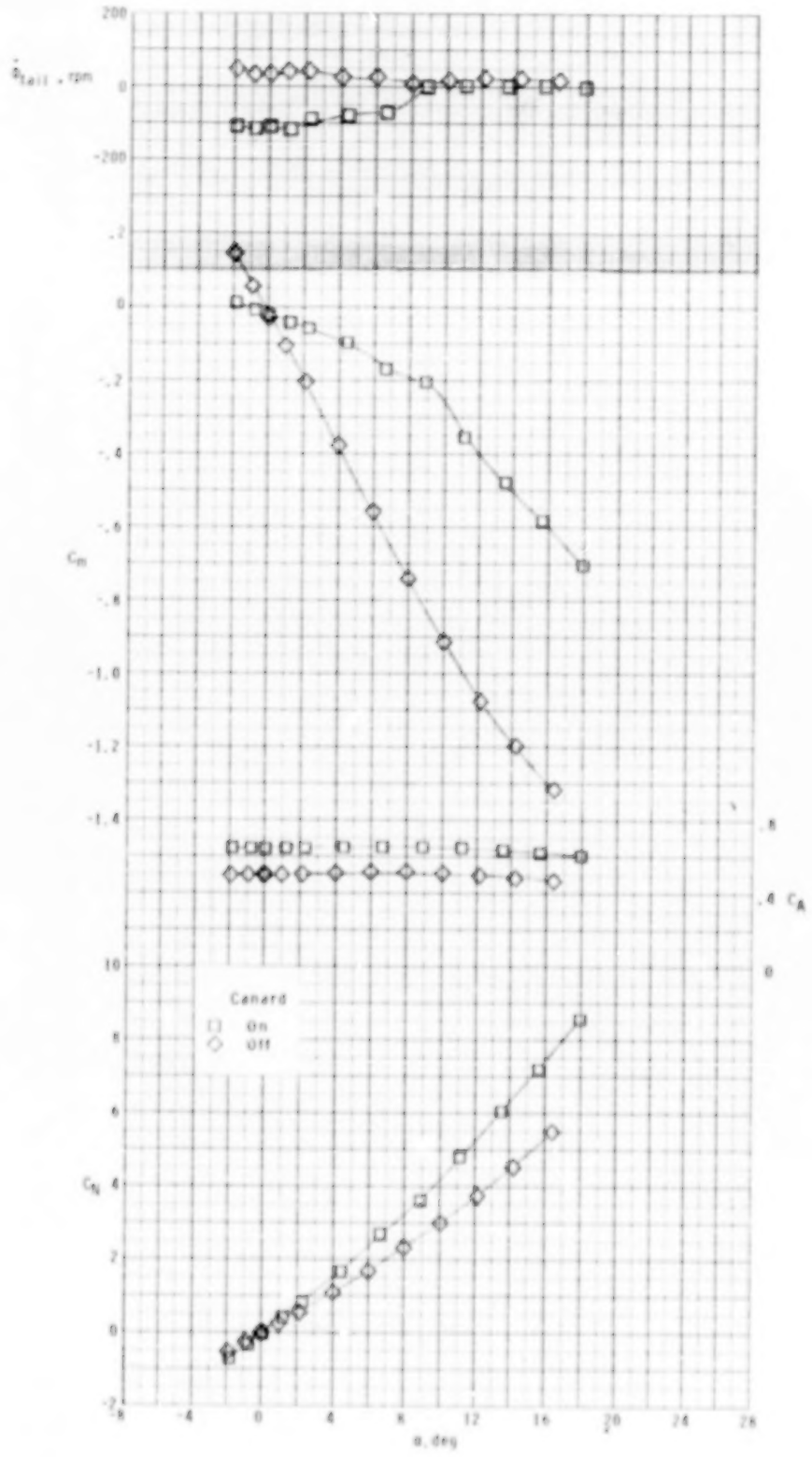

(a) M = 1.70.

Figure 6.- Effect of canards on longitudinal aerodynamic characteristics of model with free-rolling tail at $\phi_c = 0^o$.

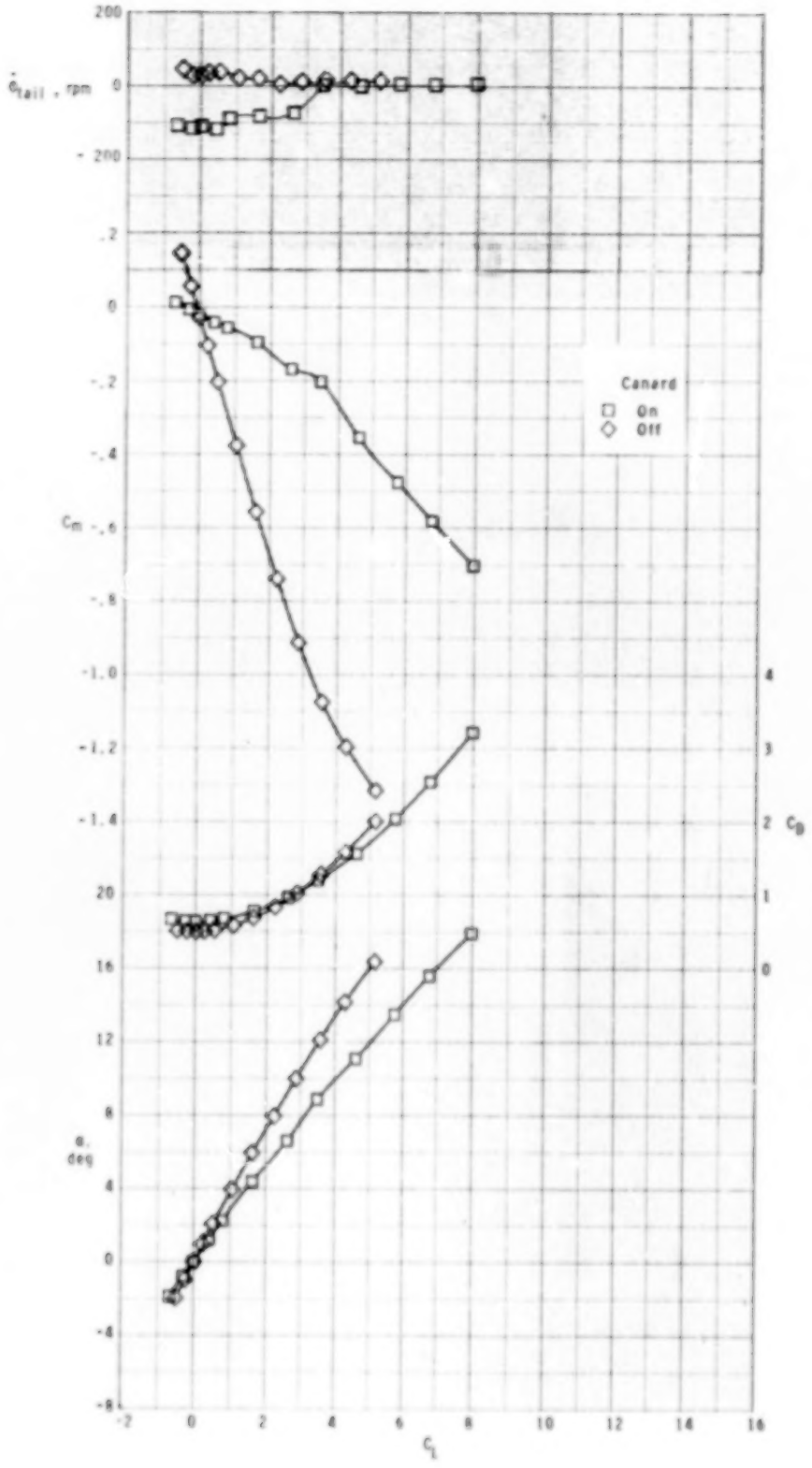

(a) Concluded.

Figure 6.- Continued.

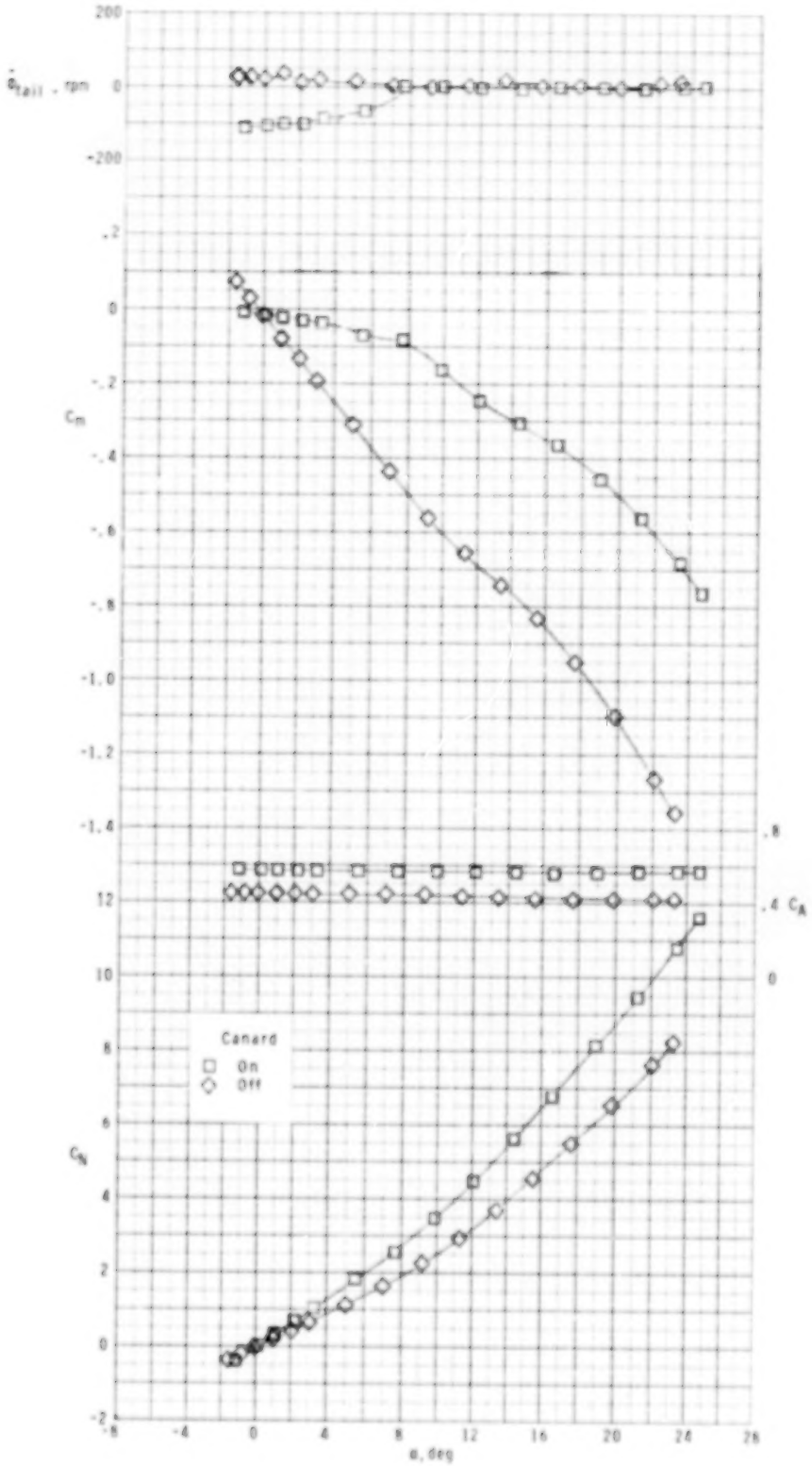

(b) M = 2.16.

Figure 6.- Continued.

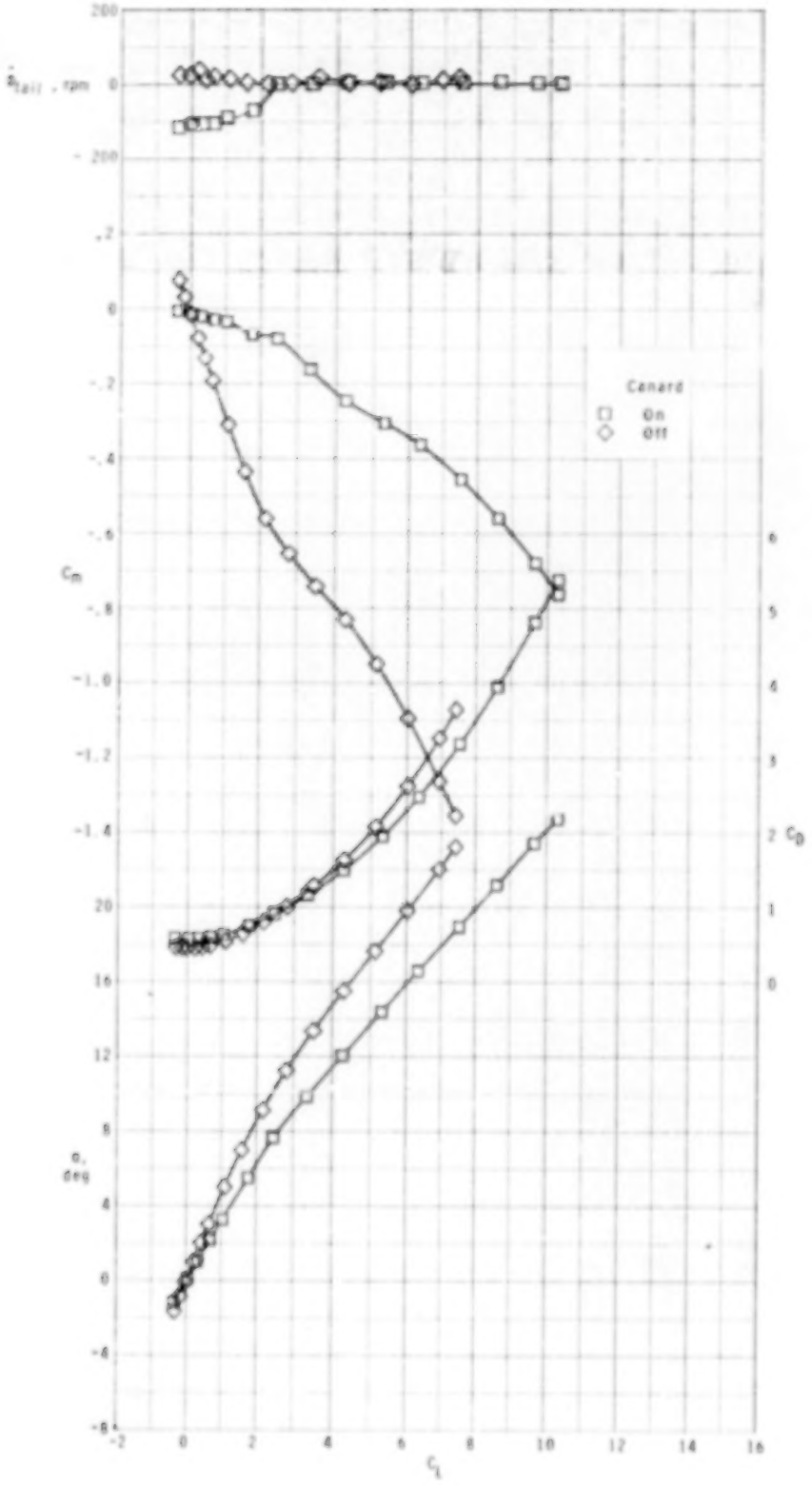

(b) Concluded.

Figure 6.- Continued.

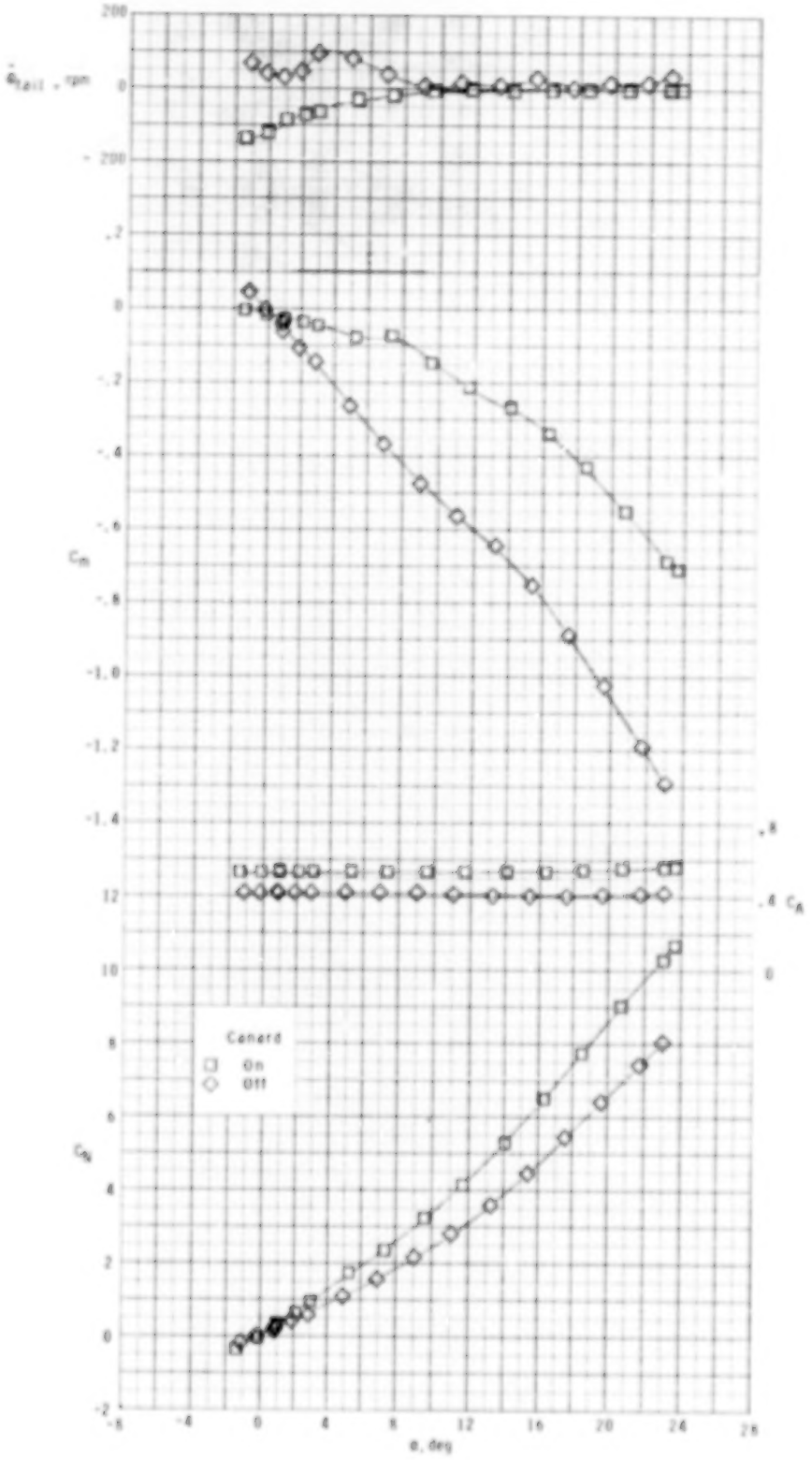

(c) M = 2.36.

Figure 6.- Continued.

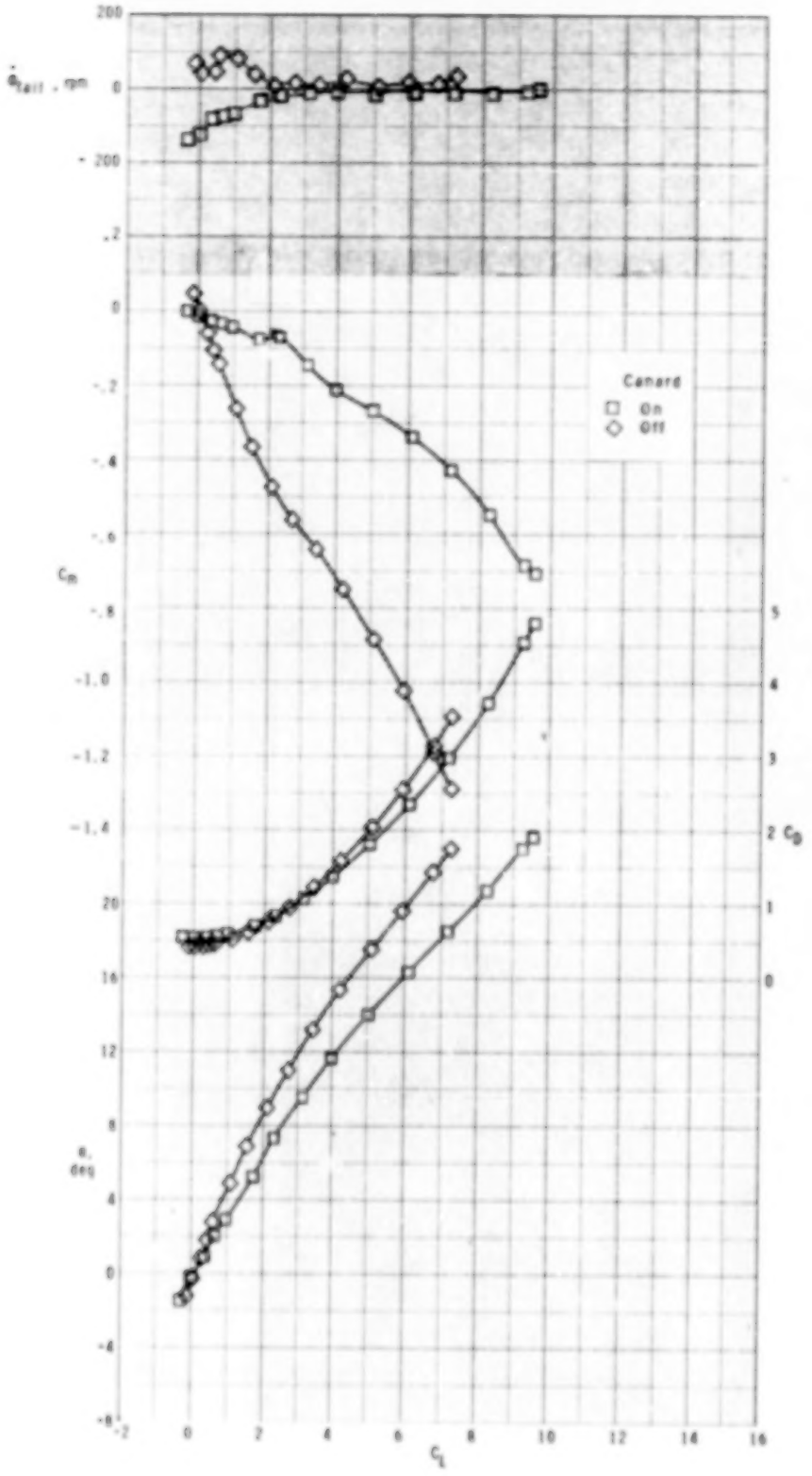

(c) Concluded.

Figure 6.- Continued.

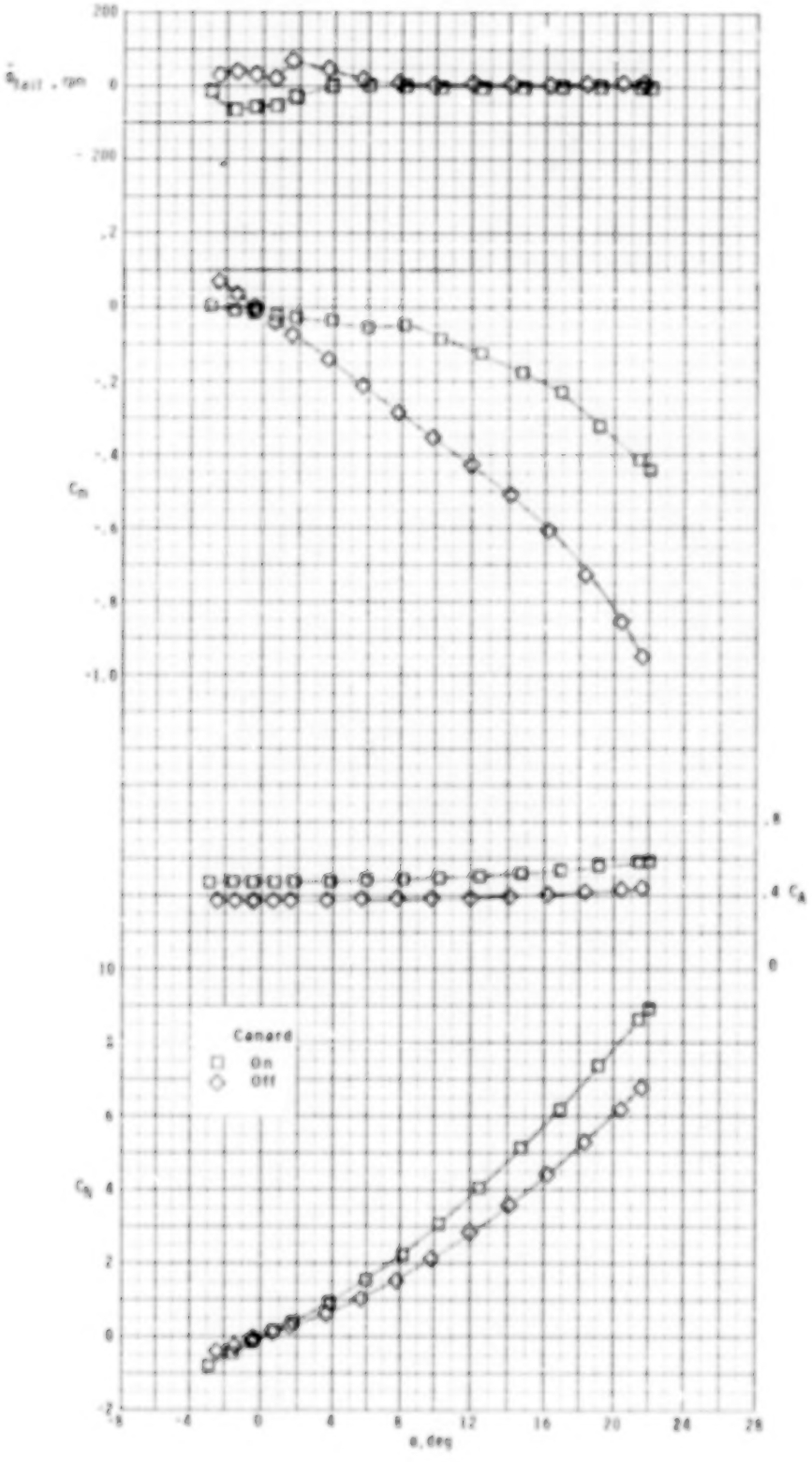

(d) M = 2.86.

Figure 6.- Continued.

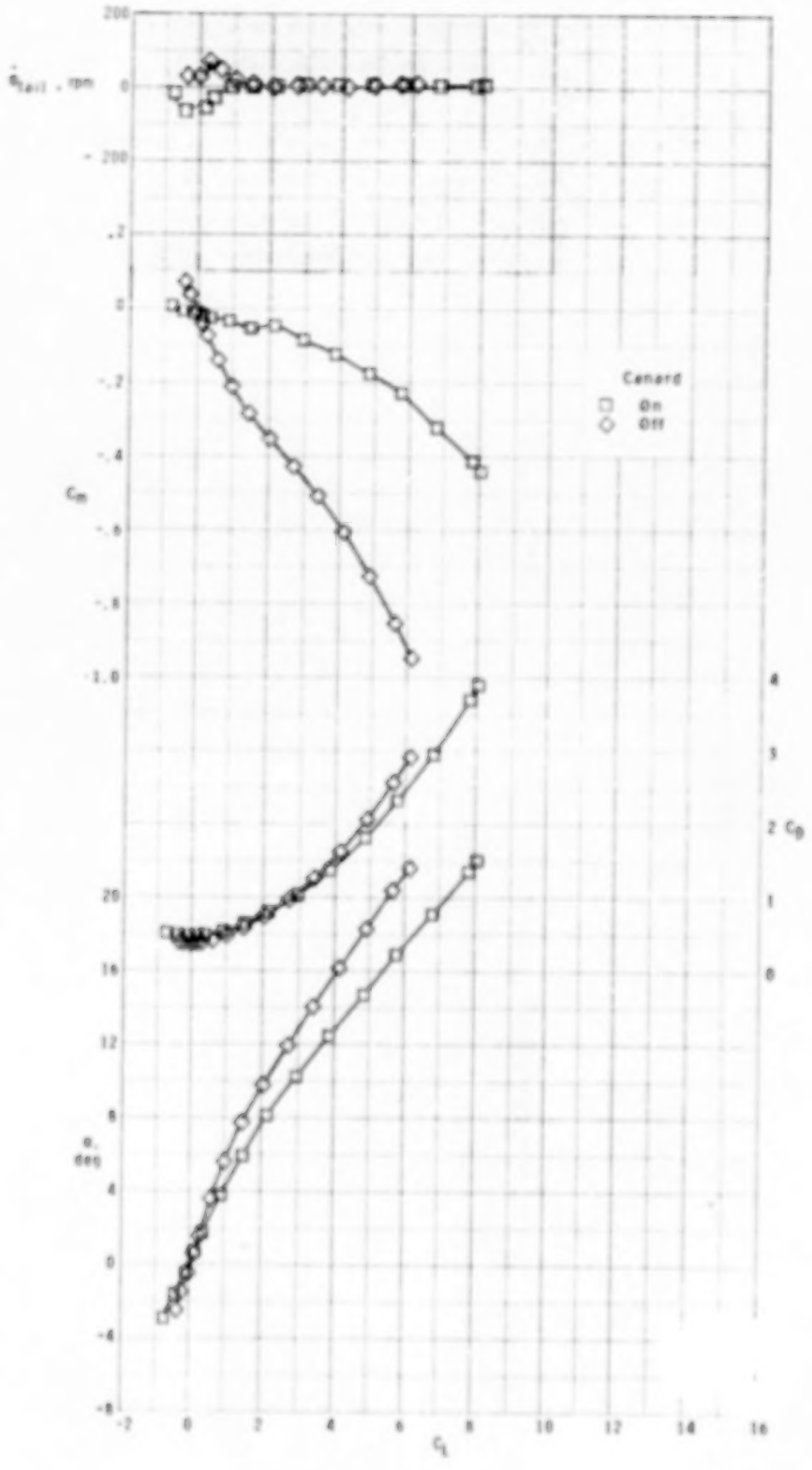

(d) Concluded.

Figure 6.- Concluded.

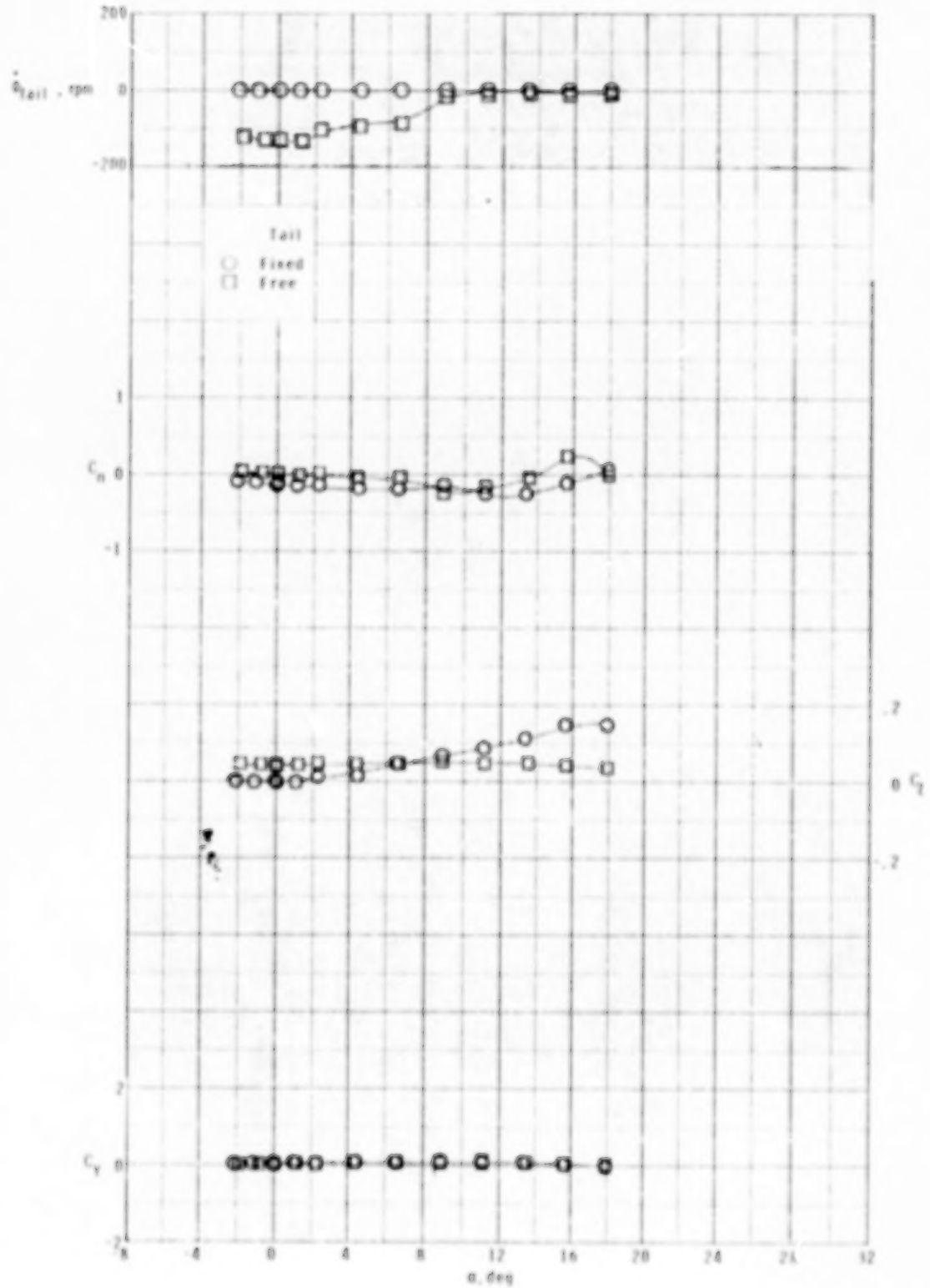

(a) M = 1.70.

Figure 7.- Effect of free-rolling tail on lateral aerodynamic characteristics of model with zero control deflection at $\phi_c = 0^o$.

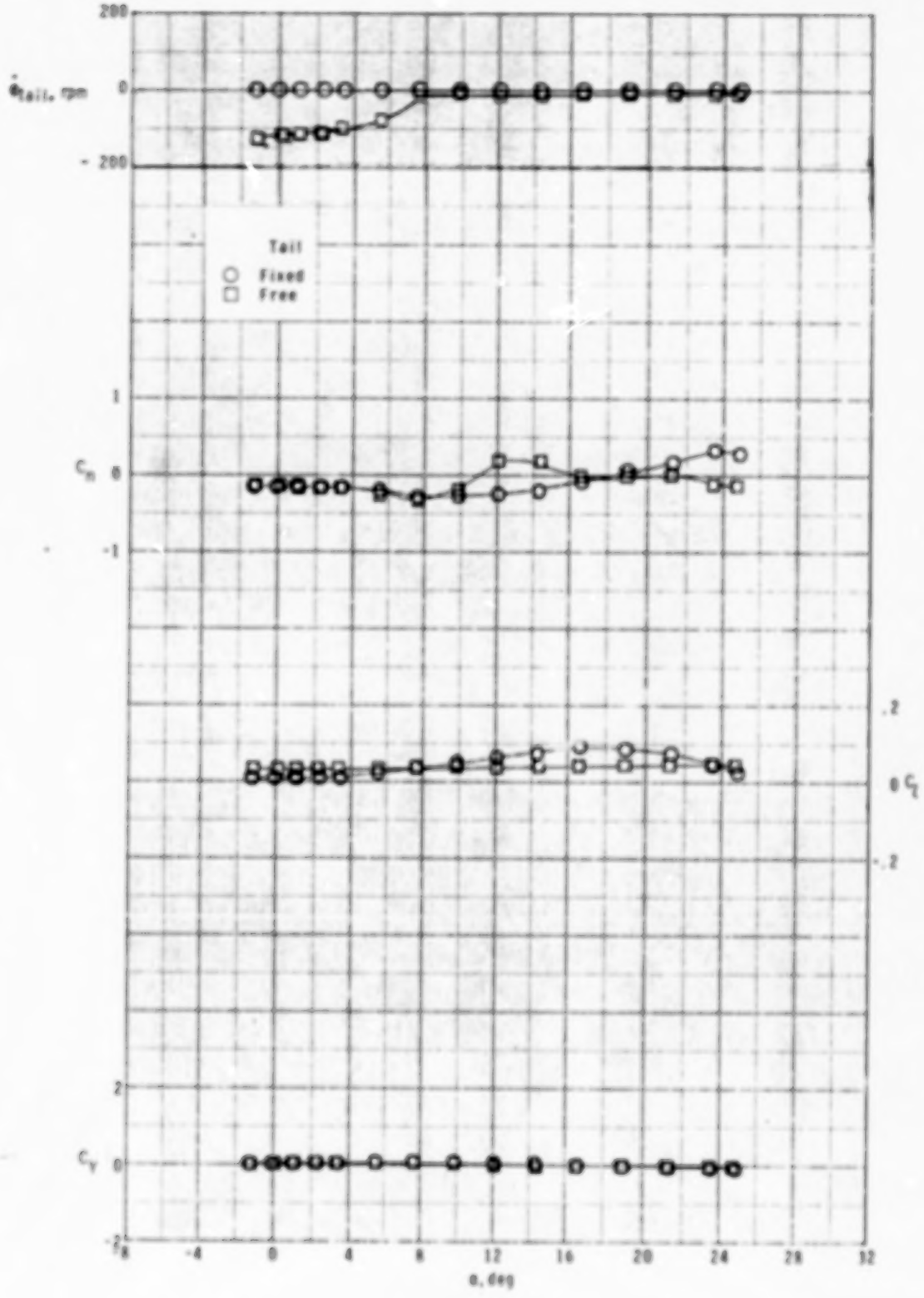

(b) M = 2.16.

Figure 7.- Continued.

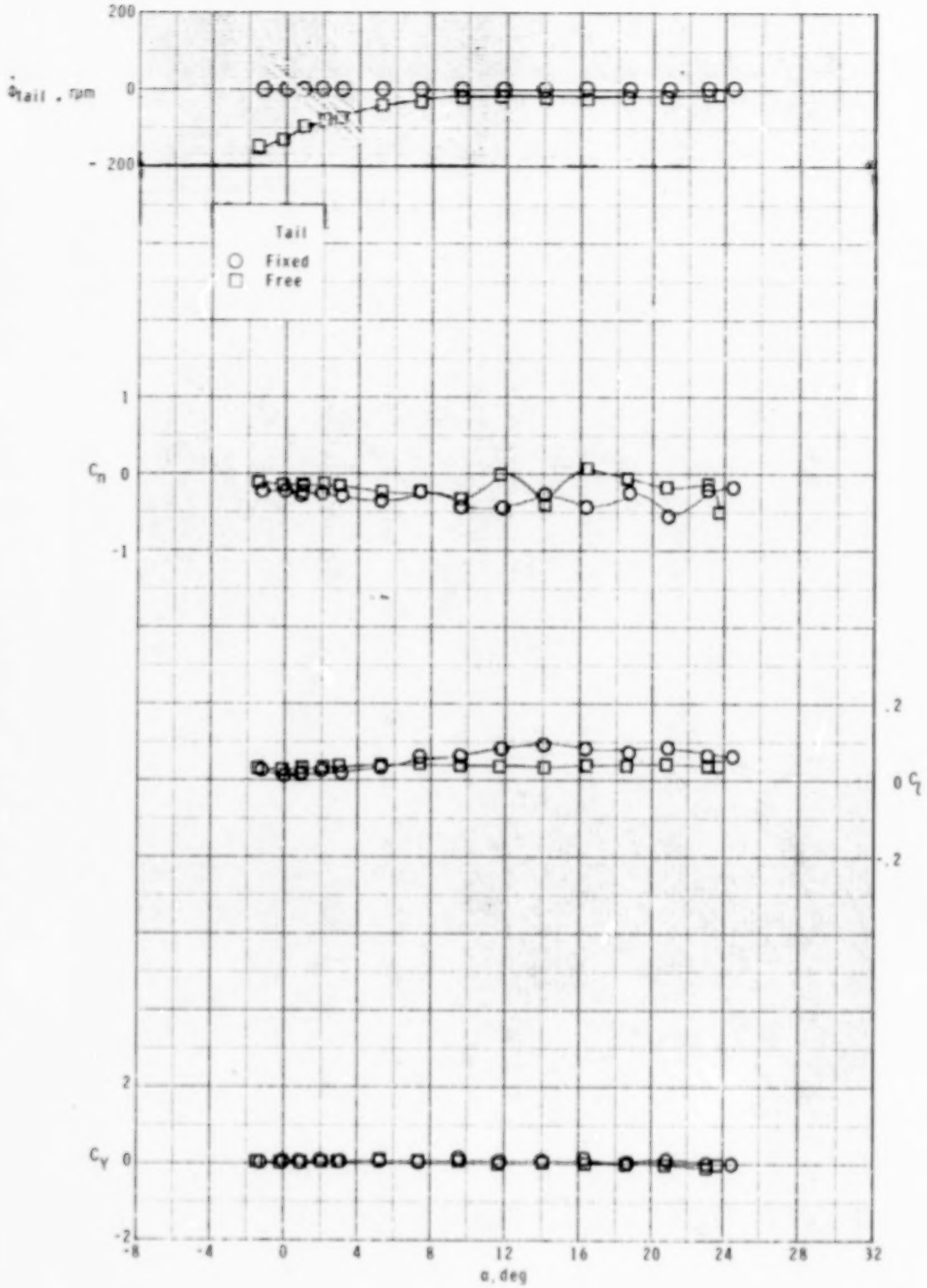

(c) M = 2.36.

Figure 7.- Continued.

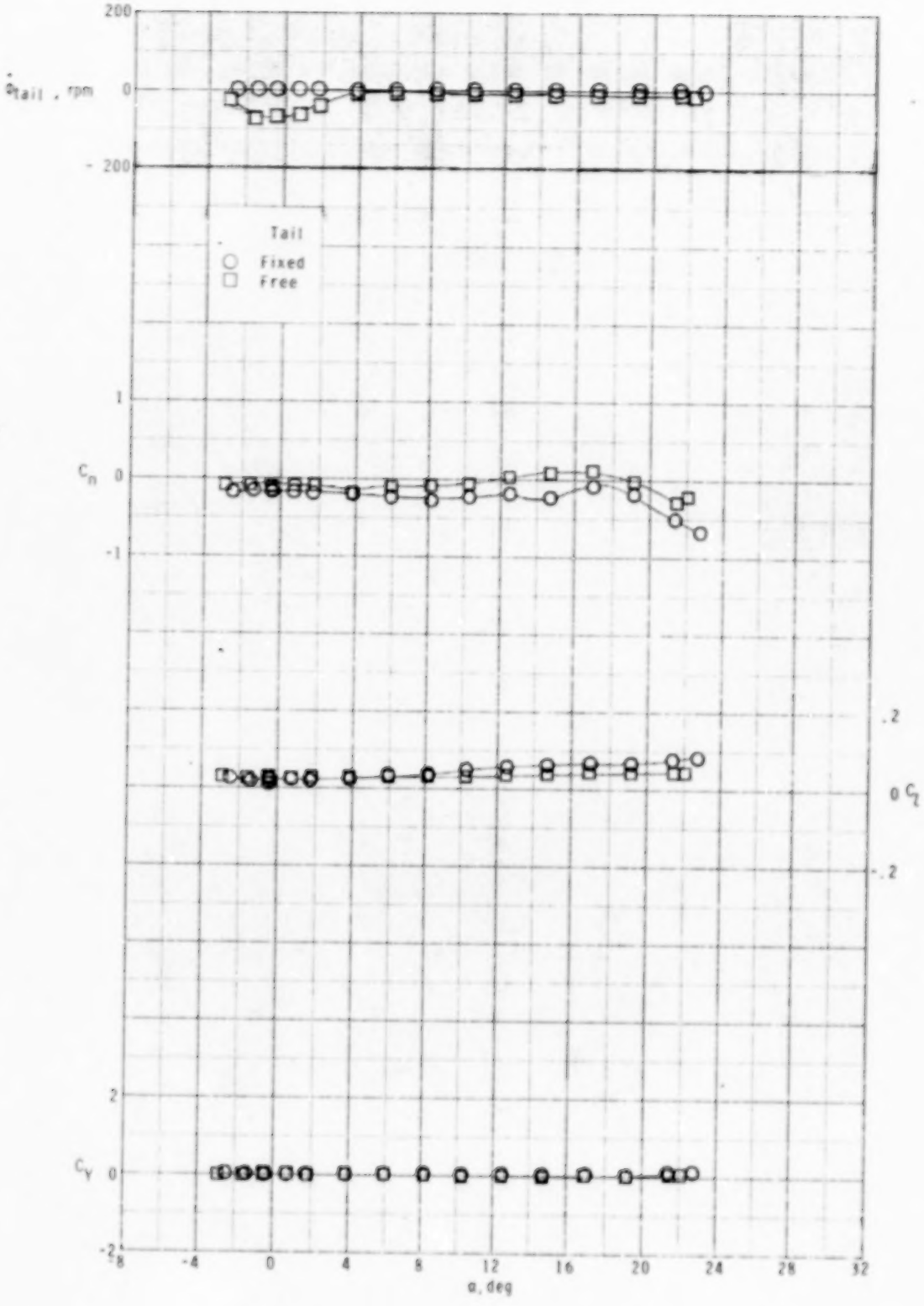

(d) M = 2.86.

Figure 7.- Concluded.

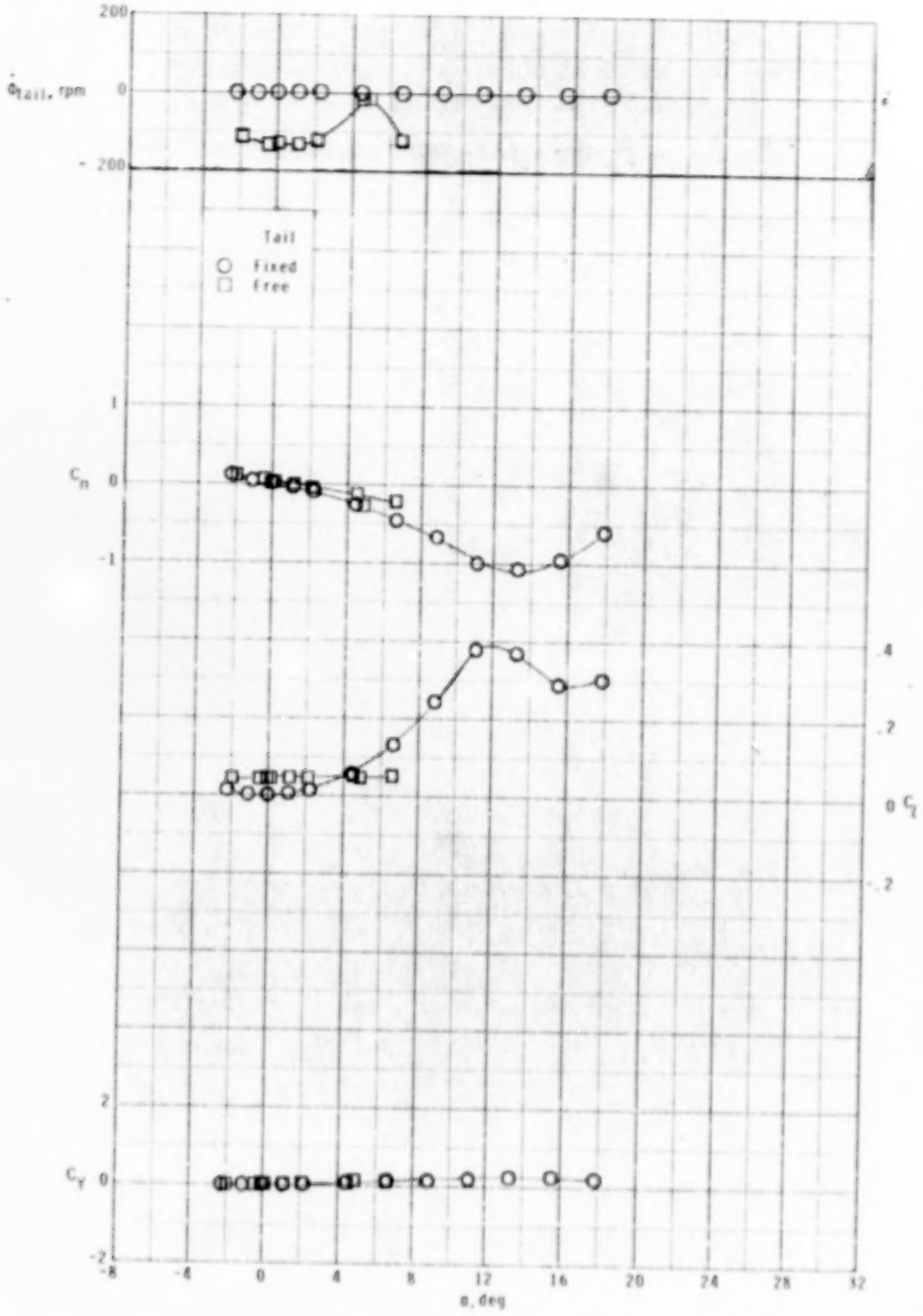

(a) M = 1.70.

Figure 8.- Effect of free-rolling tail on lateral aerodynamic characteristics of model with zero control deflection at $\phi_c = 26.6^\circ$.

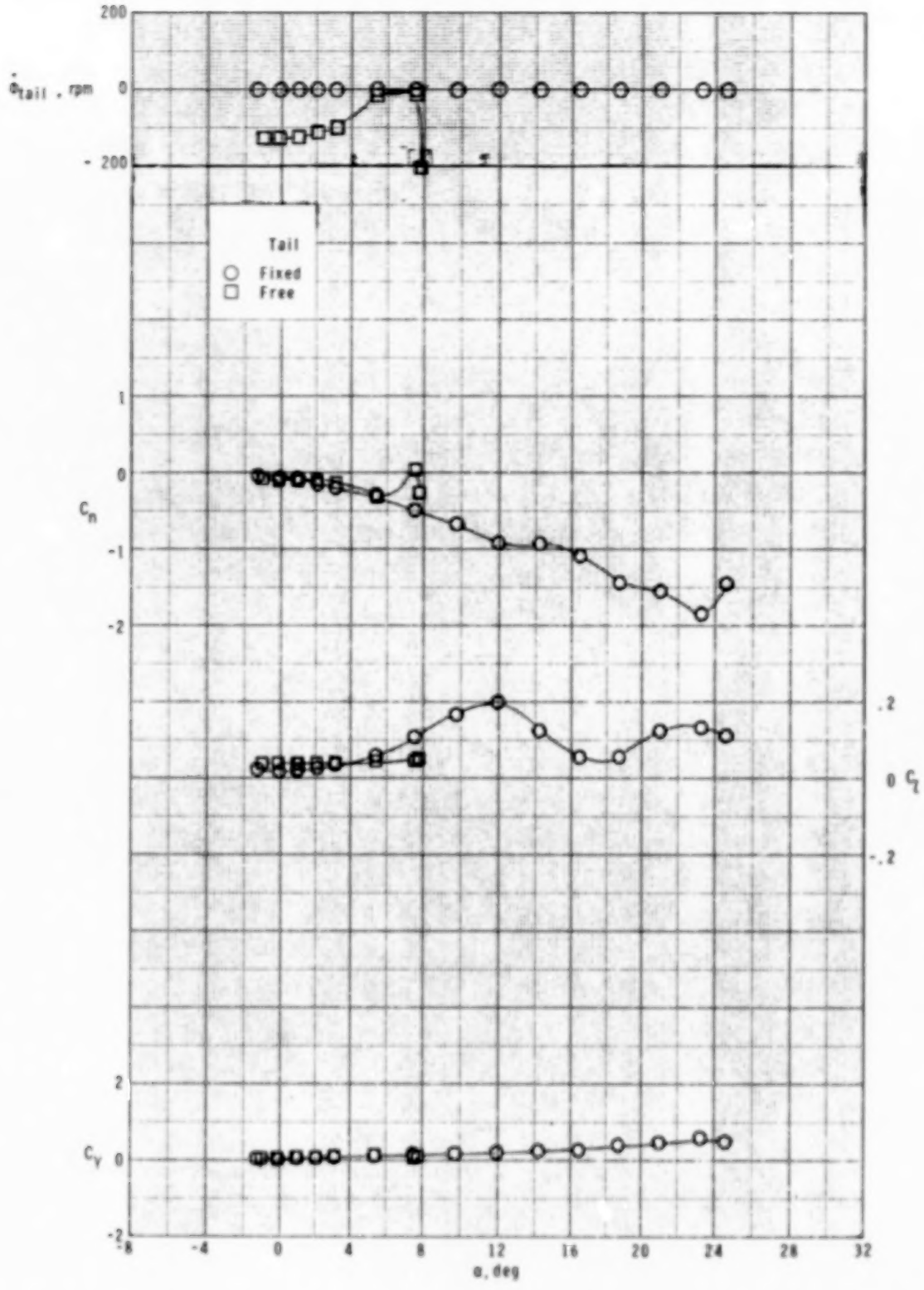

(b) M = 2.16.

Figure 8.- Continued.

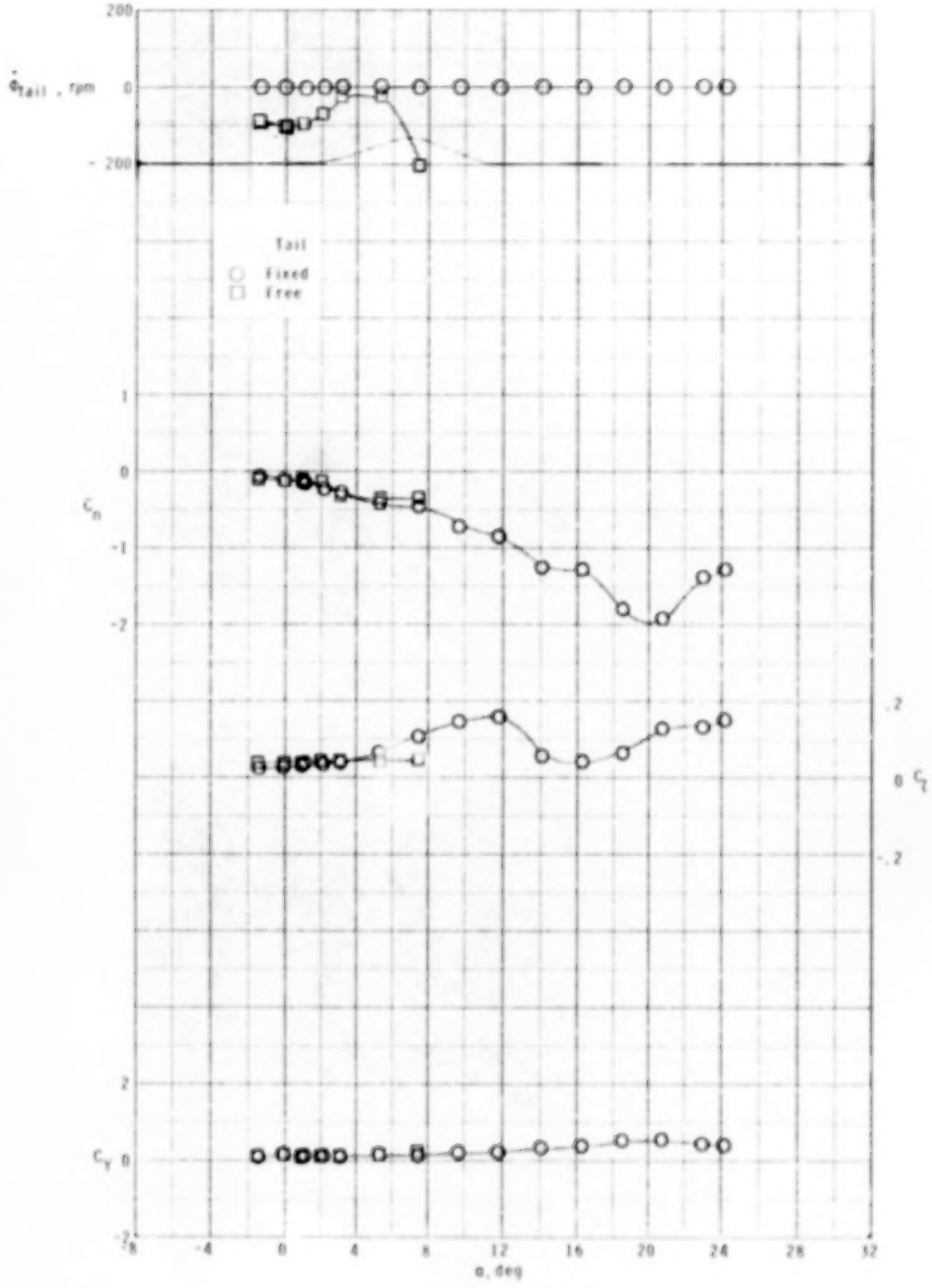

(c) M = 2.36.

Figure 8.- Continued.

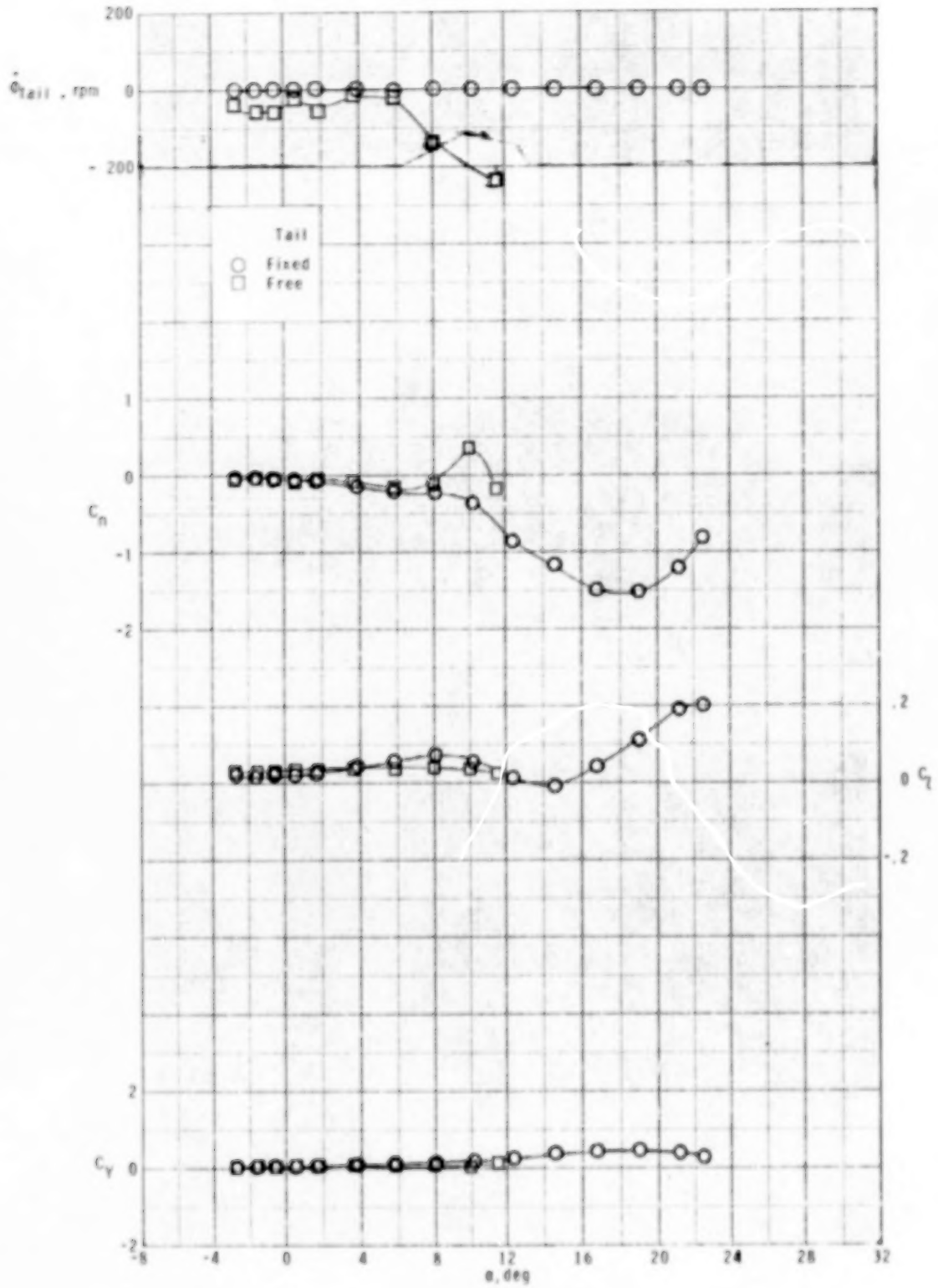

(d) M = 2.86.

Figure 8.- Concluded.

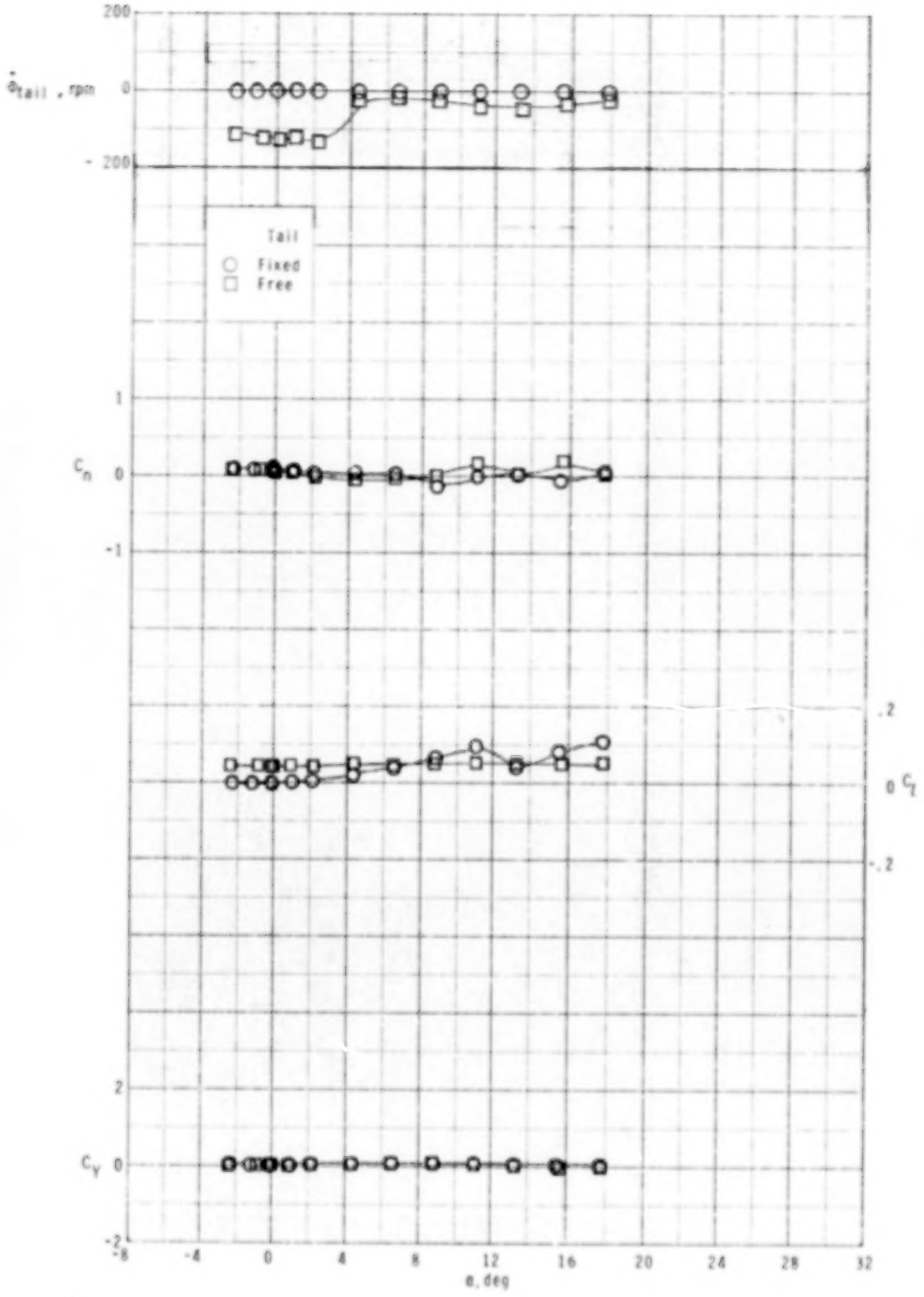

(a) M = 1.70.

Figure 9.- Effect of free-rolling tail on lateral aerodynamic characteristics of model with zero control deflection at $\phi_c = 45^o$.

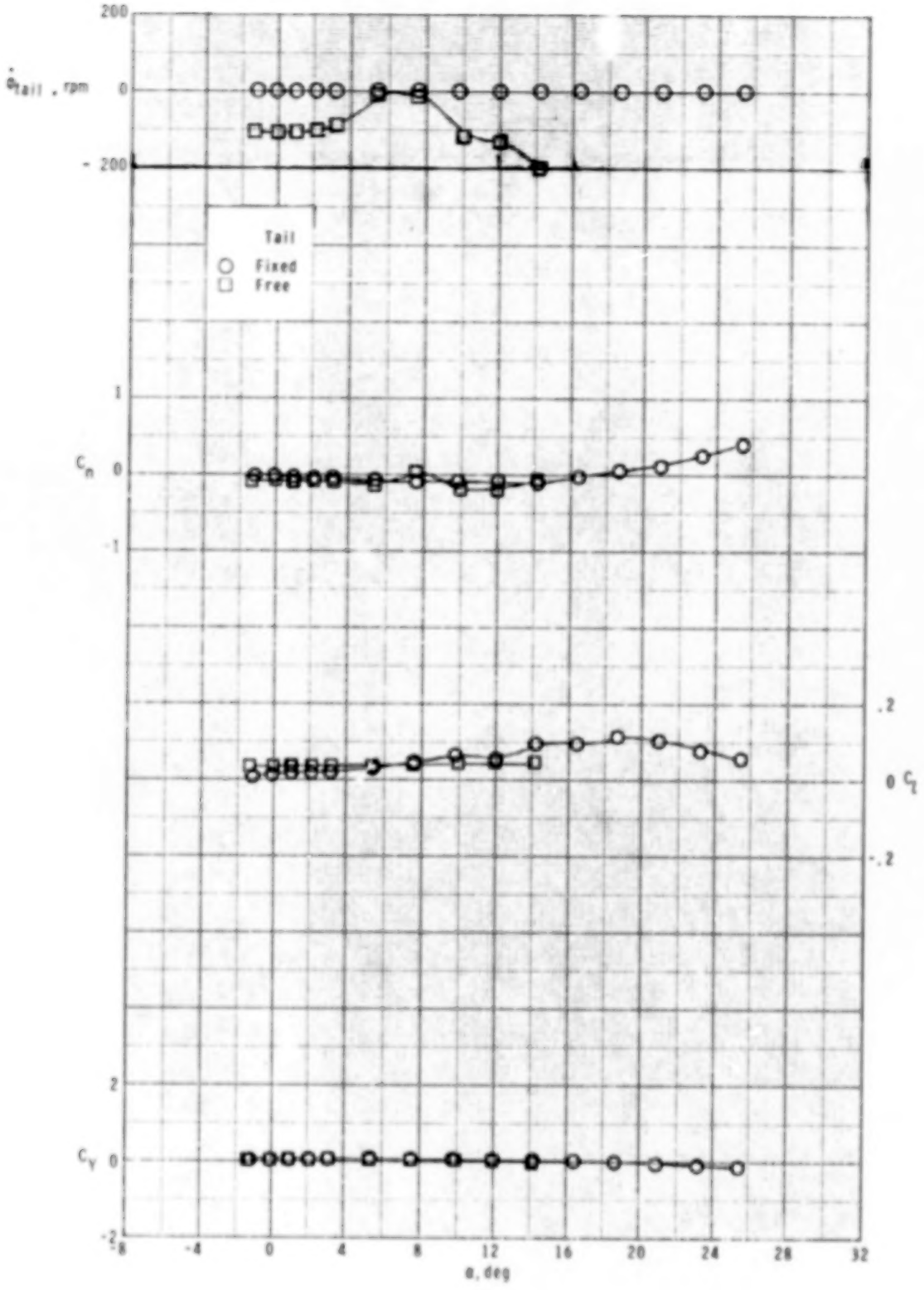

(b) M = 2.16.

Figure 9.- Continued.

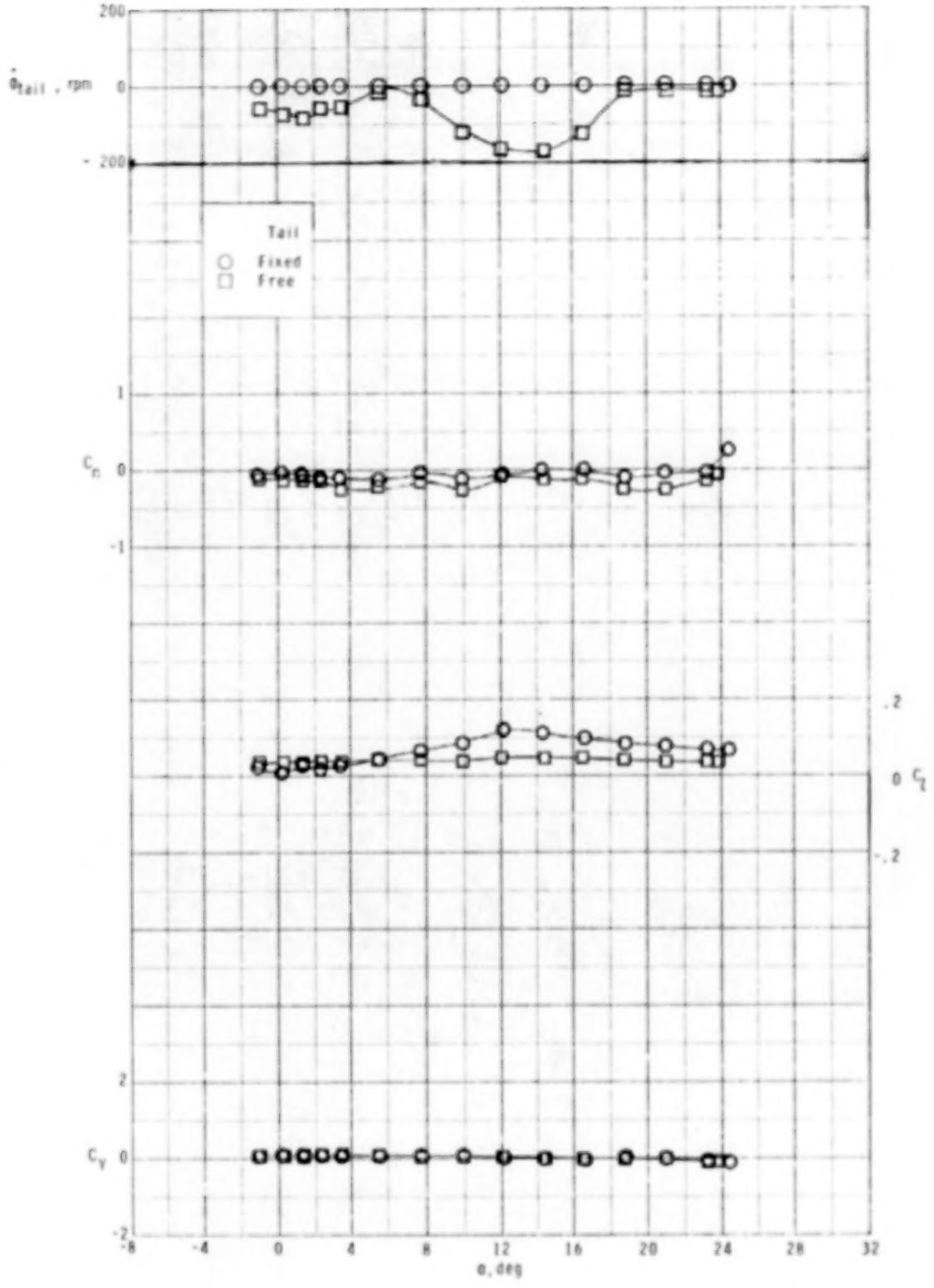

(c) M = 2.36.

Figure 9.- Continued.

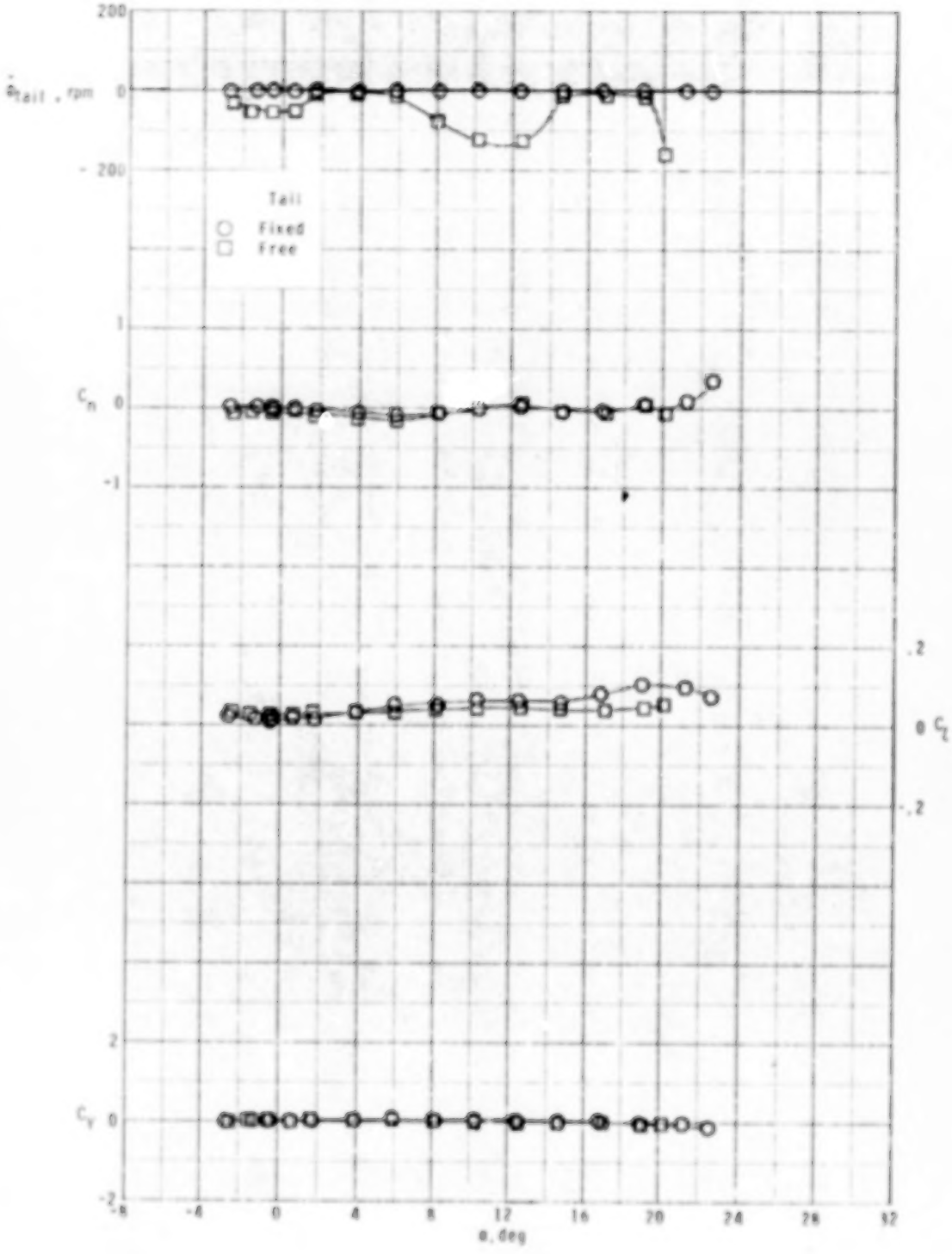

(d) M = 2.86.

Figure 9.- Concluded.

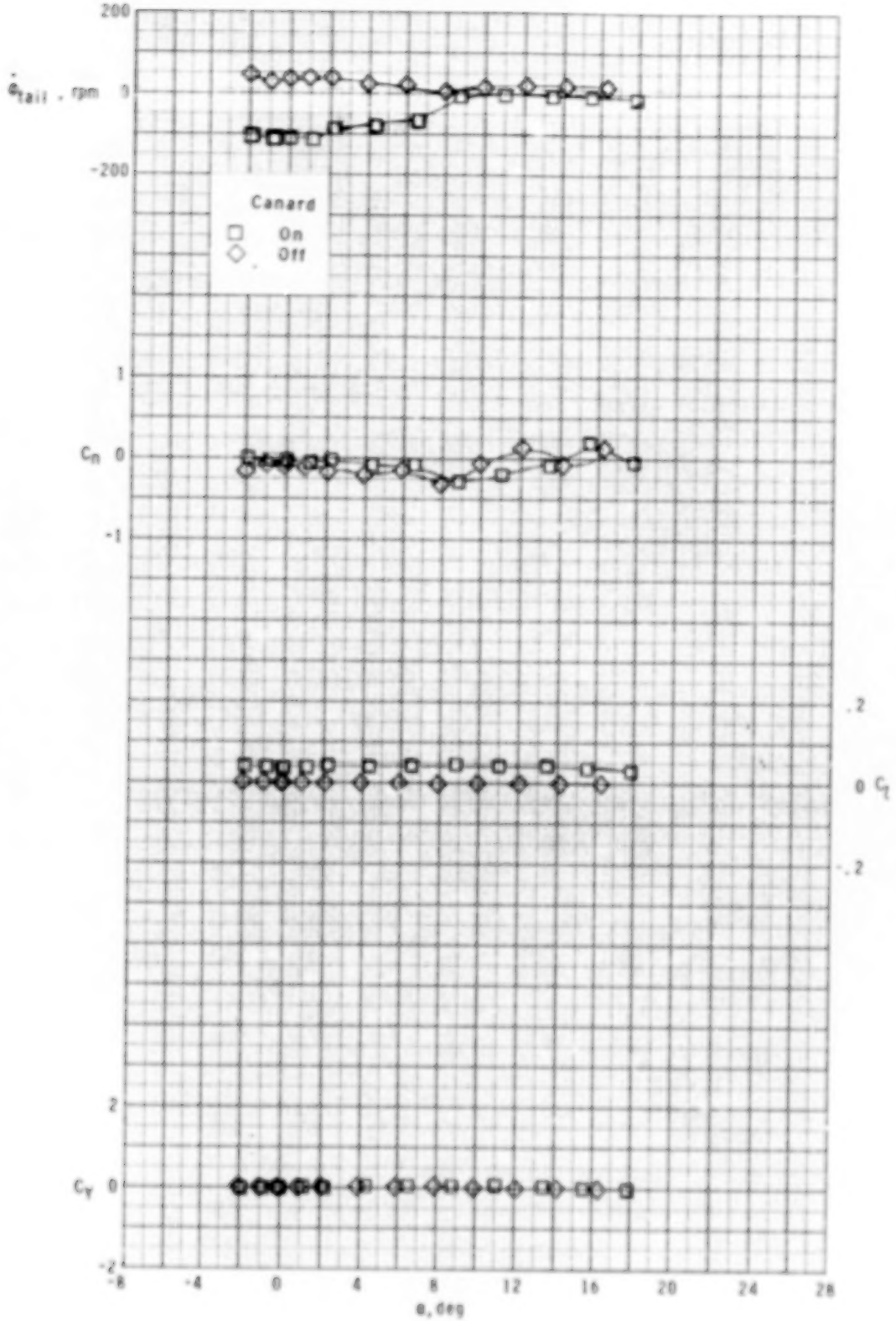

(a) M = 1.70.

Figure 10.- Effect of canards on lateral aerodynamic characteristics of model with a free-rolling tail at $\phi_c = 0^o$.

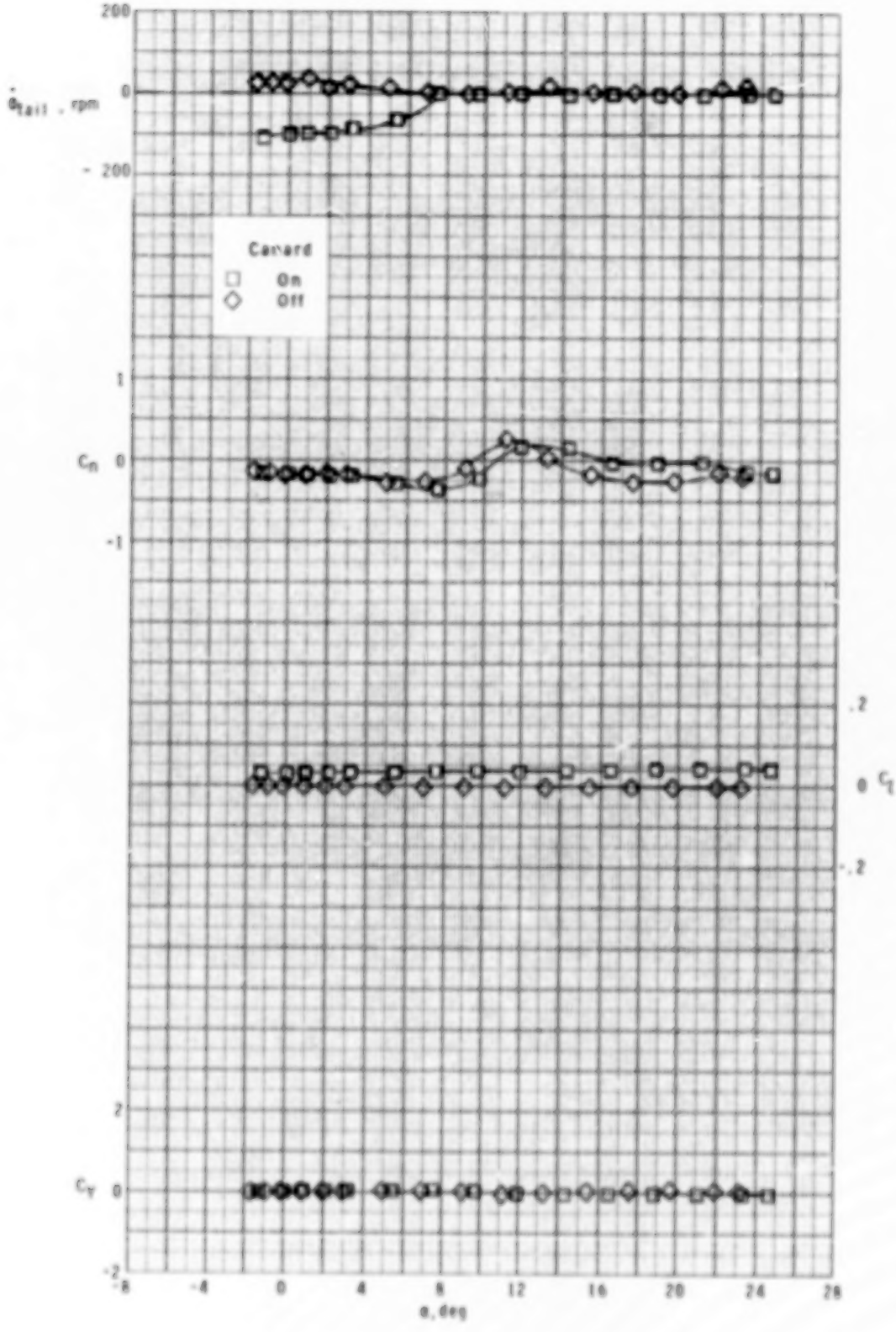

(b) M = 2.16.

Figure 10.- Continued.

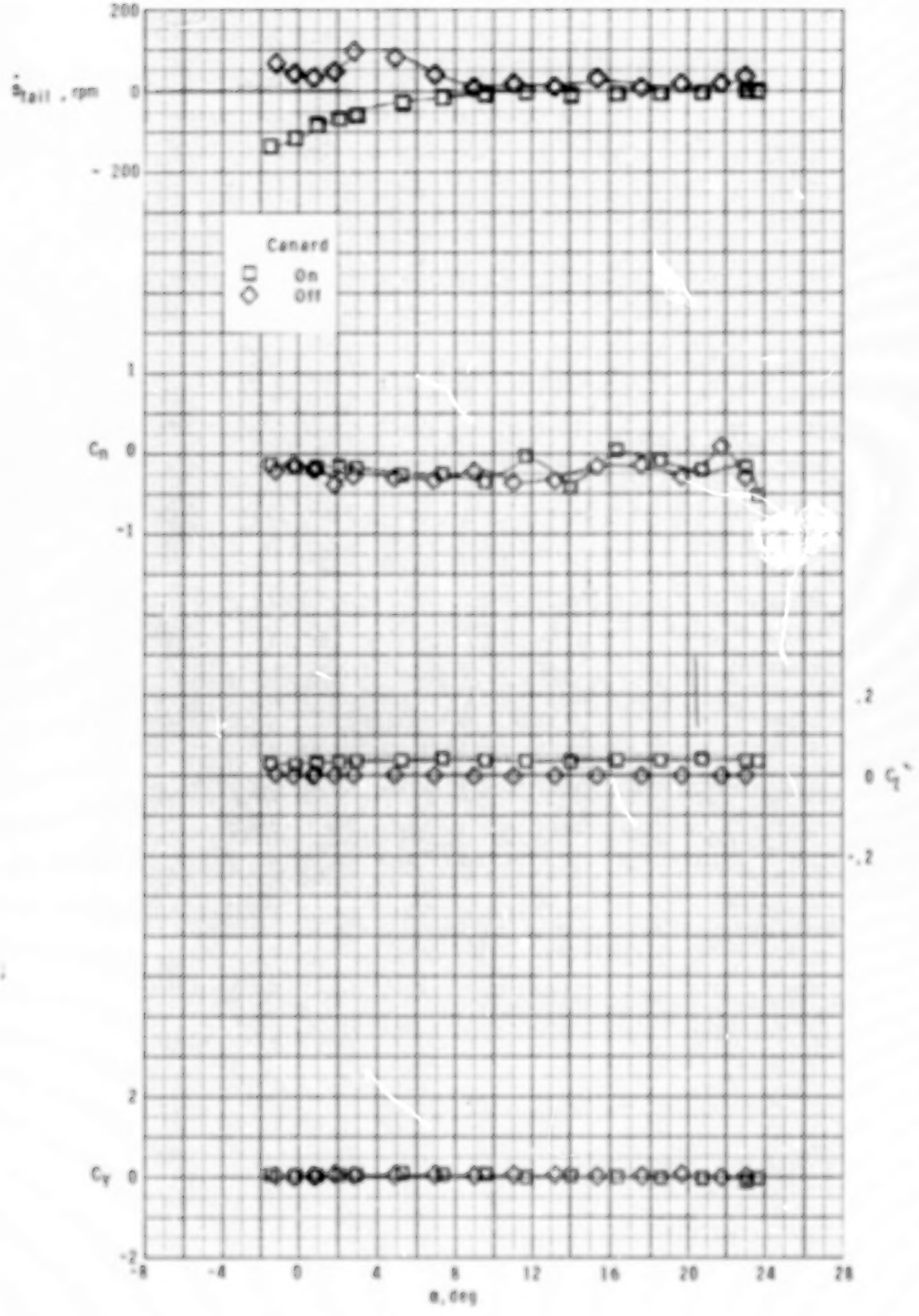

(c) M = 2.36.

Figure 10.- Continued.

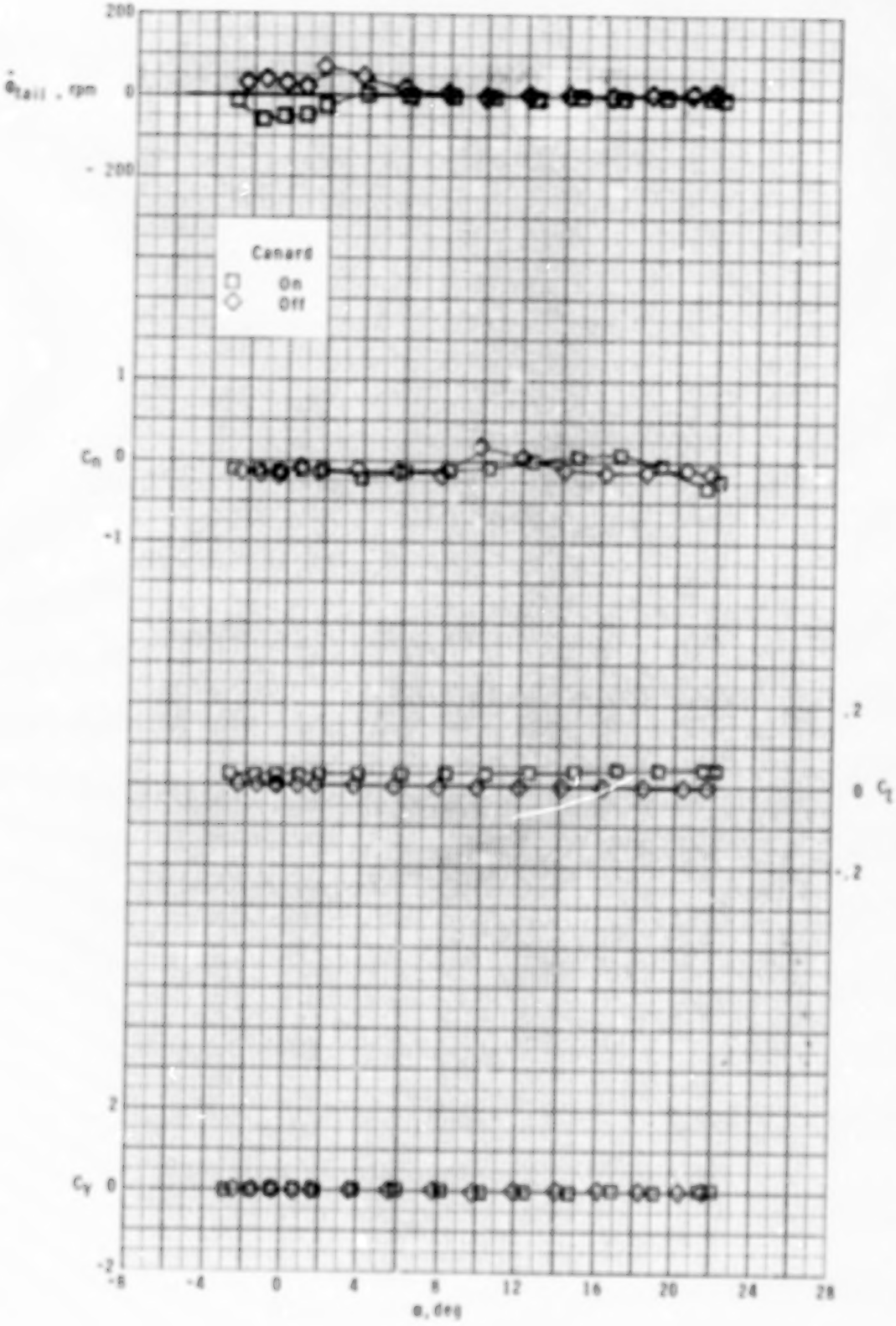

(d) M = 2.86.

Figure 10.- Concluded.

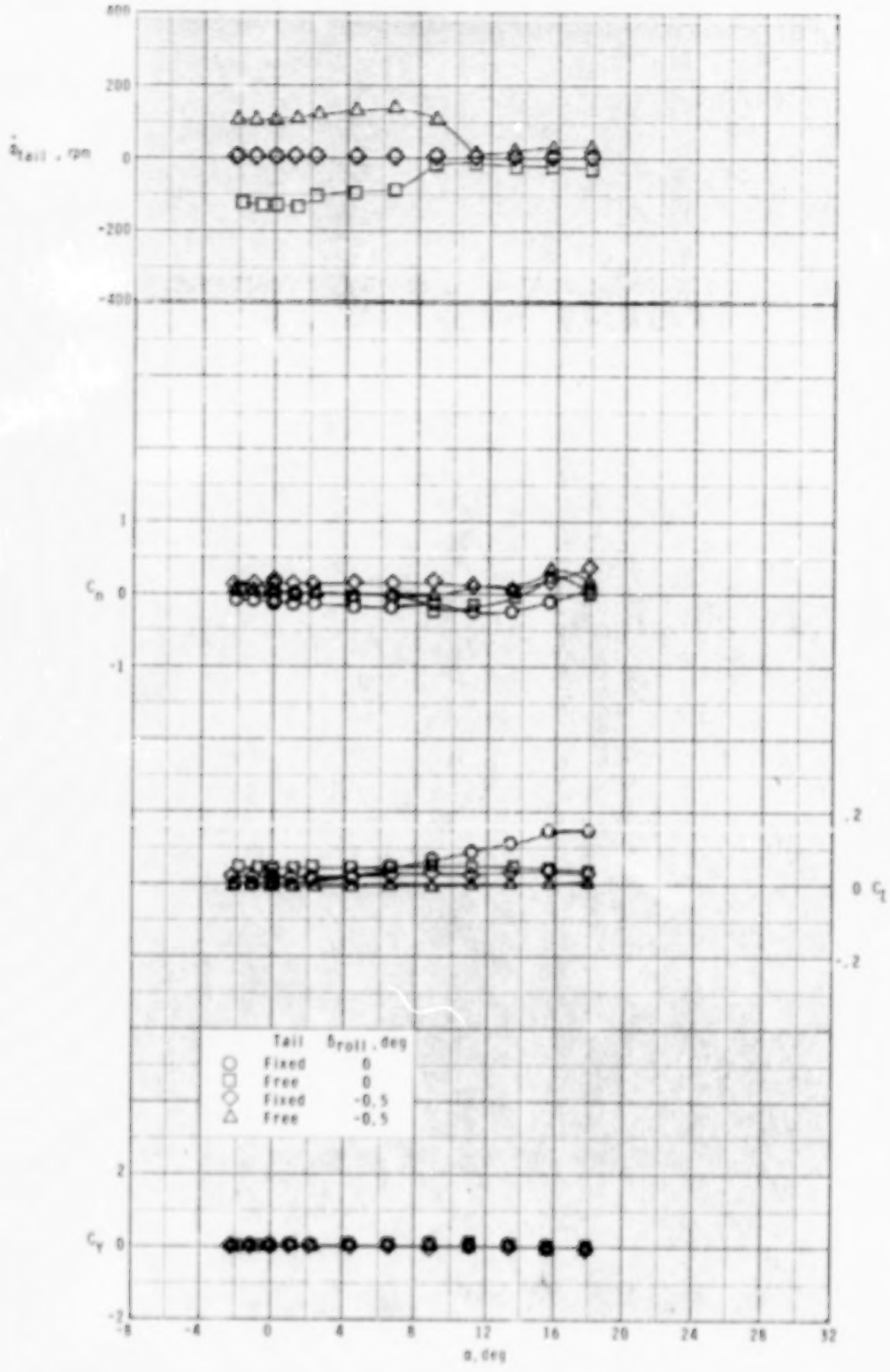

(a) M = 1.70.

Figure 11.- Roll-control characteristics of model with fixed and free-rolling tail at $\phi_c = 0^o$. Two canards deflected.

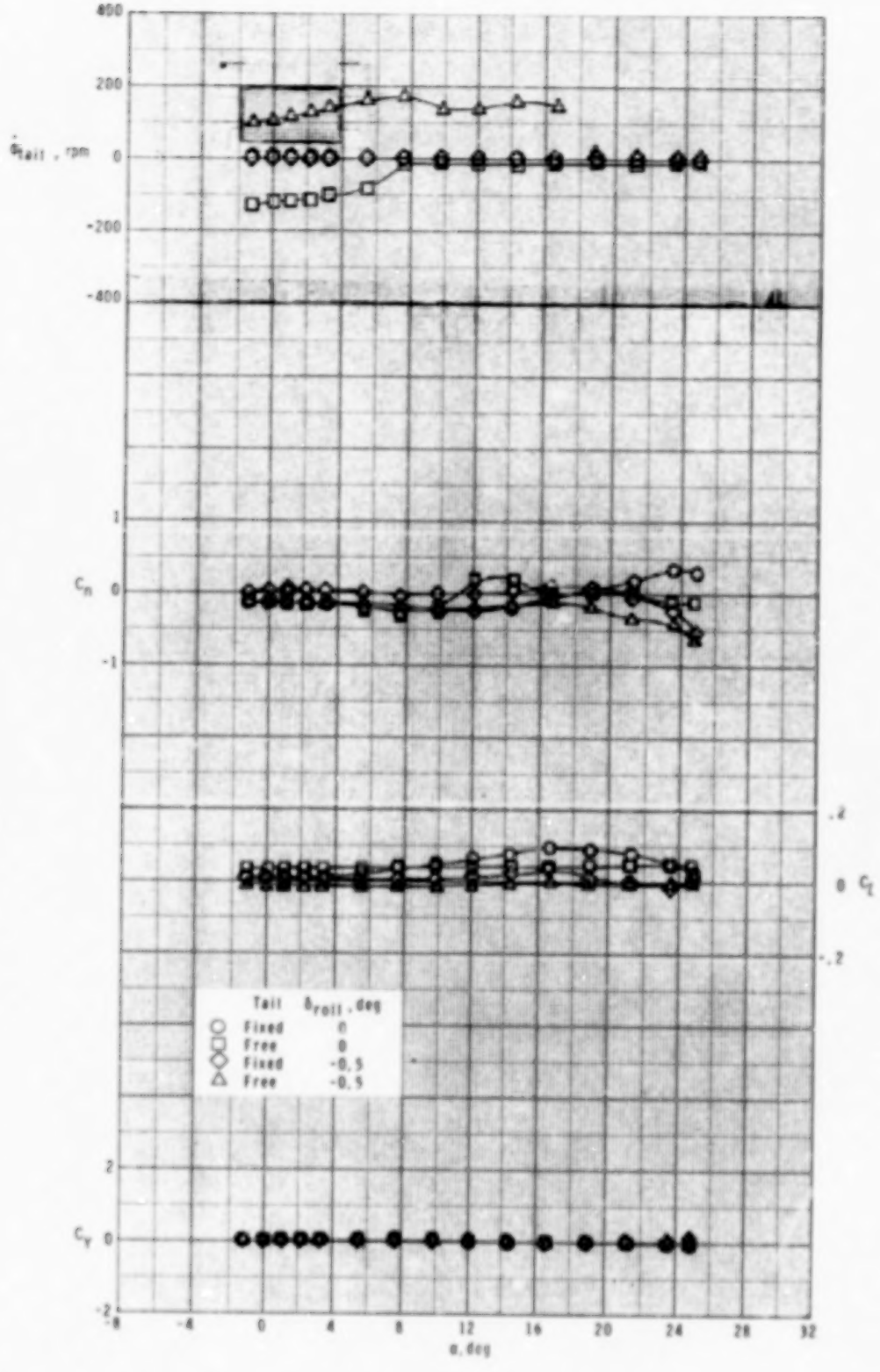

(b) M = 2.16.

Figure 11.- Continued.

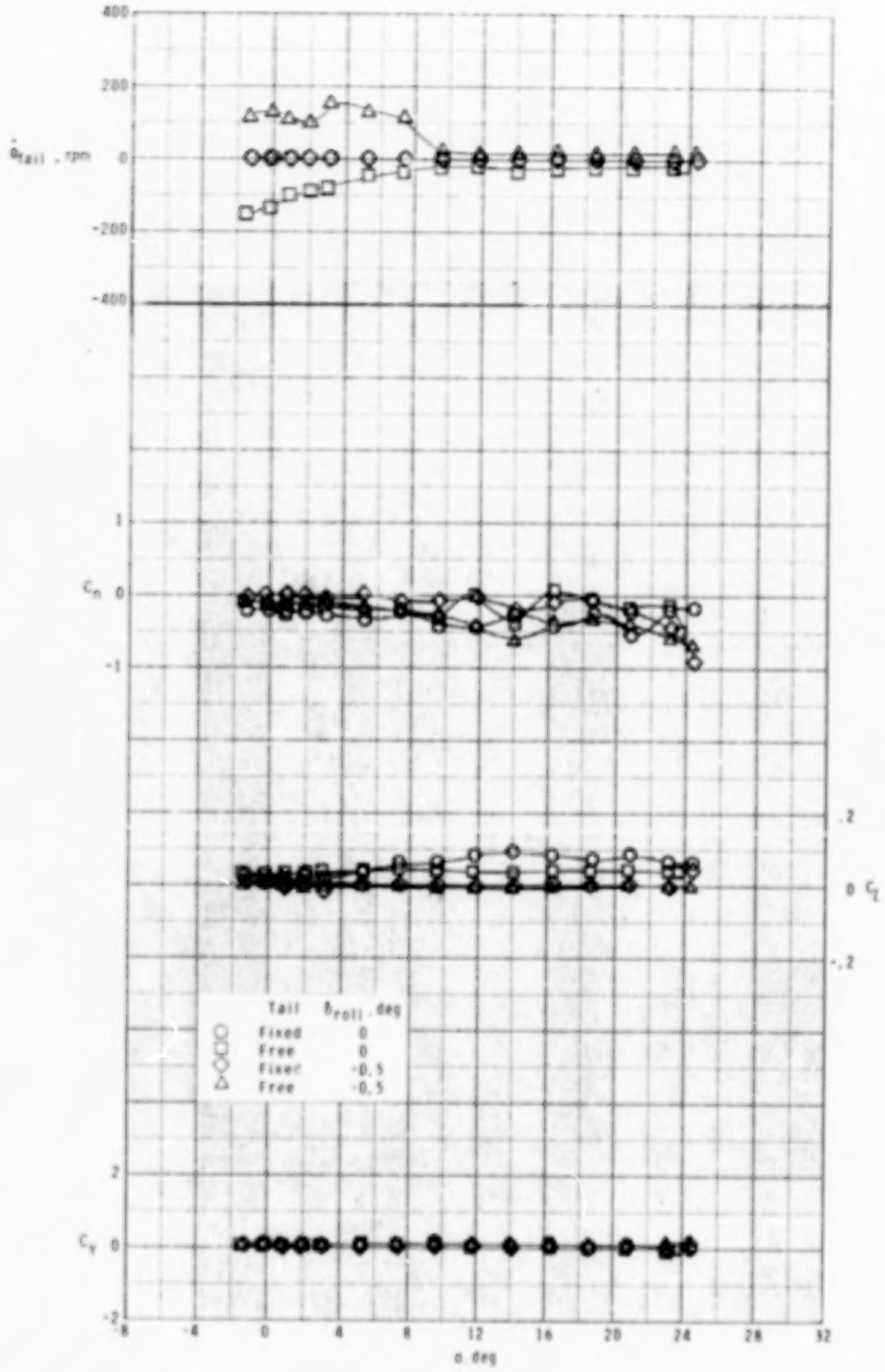

(c) M = 2.36.

Figure 11.- Continued.

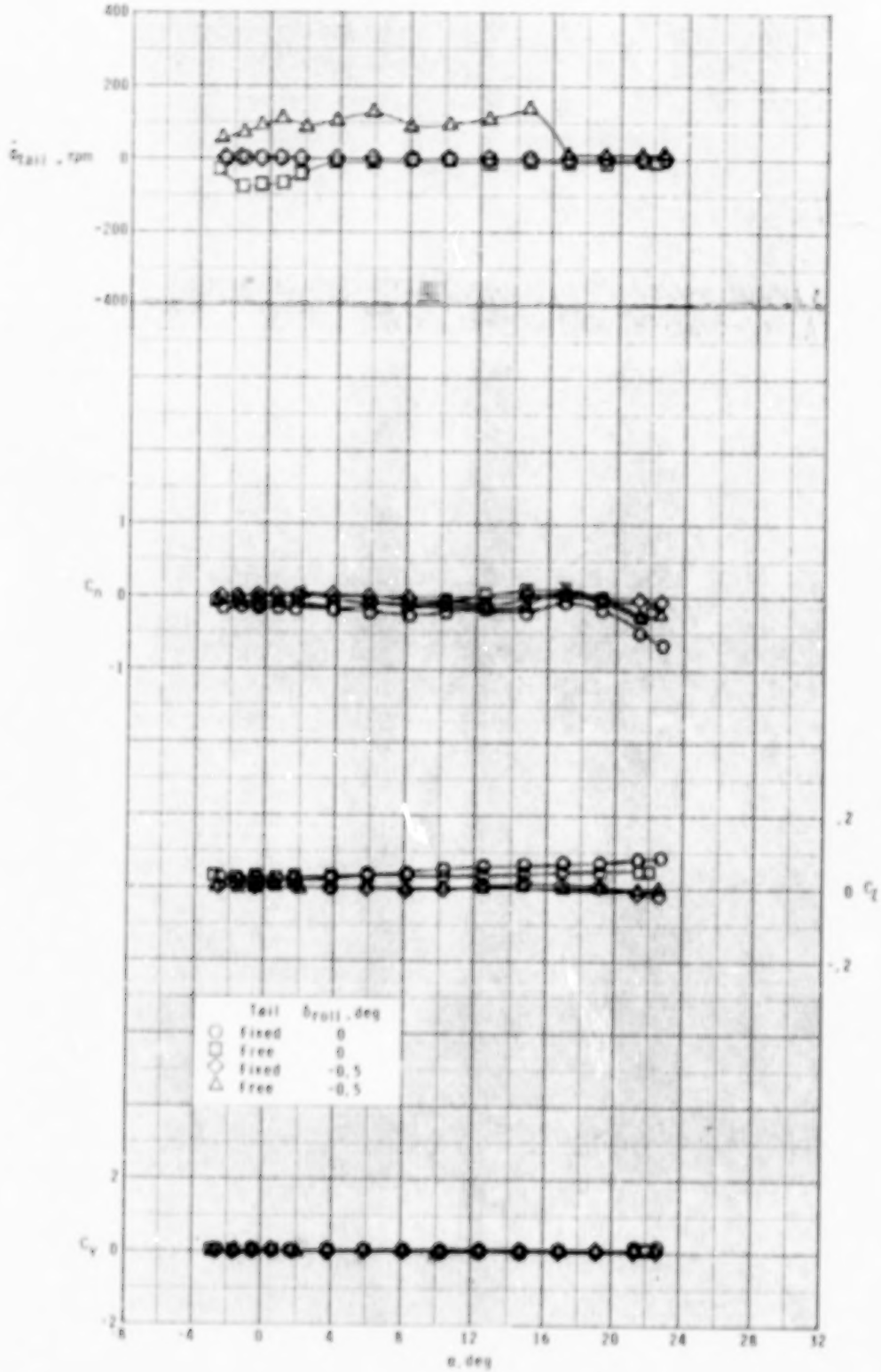

(d) M = 2.86.

Figure 11.- Concluded.

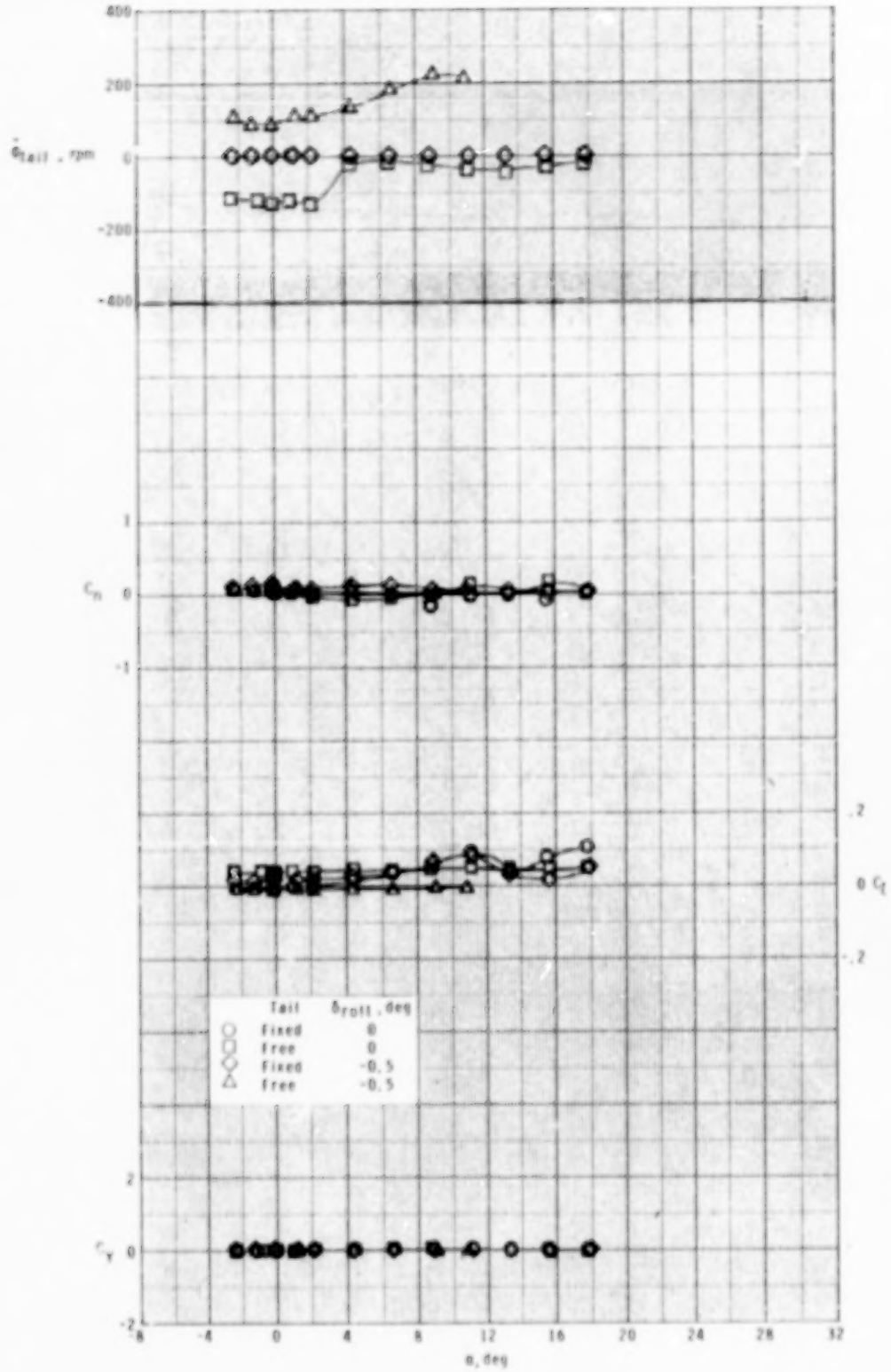

(a) M = 1.70.

Figure 12.- Roll-control characteristics of model with fixed and free-rolling tail at $\phi_c = 45^o$. Two canards deflected.

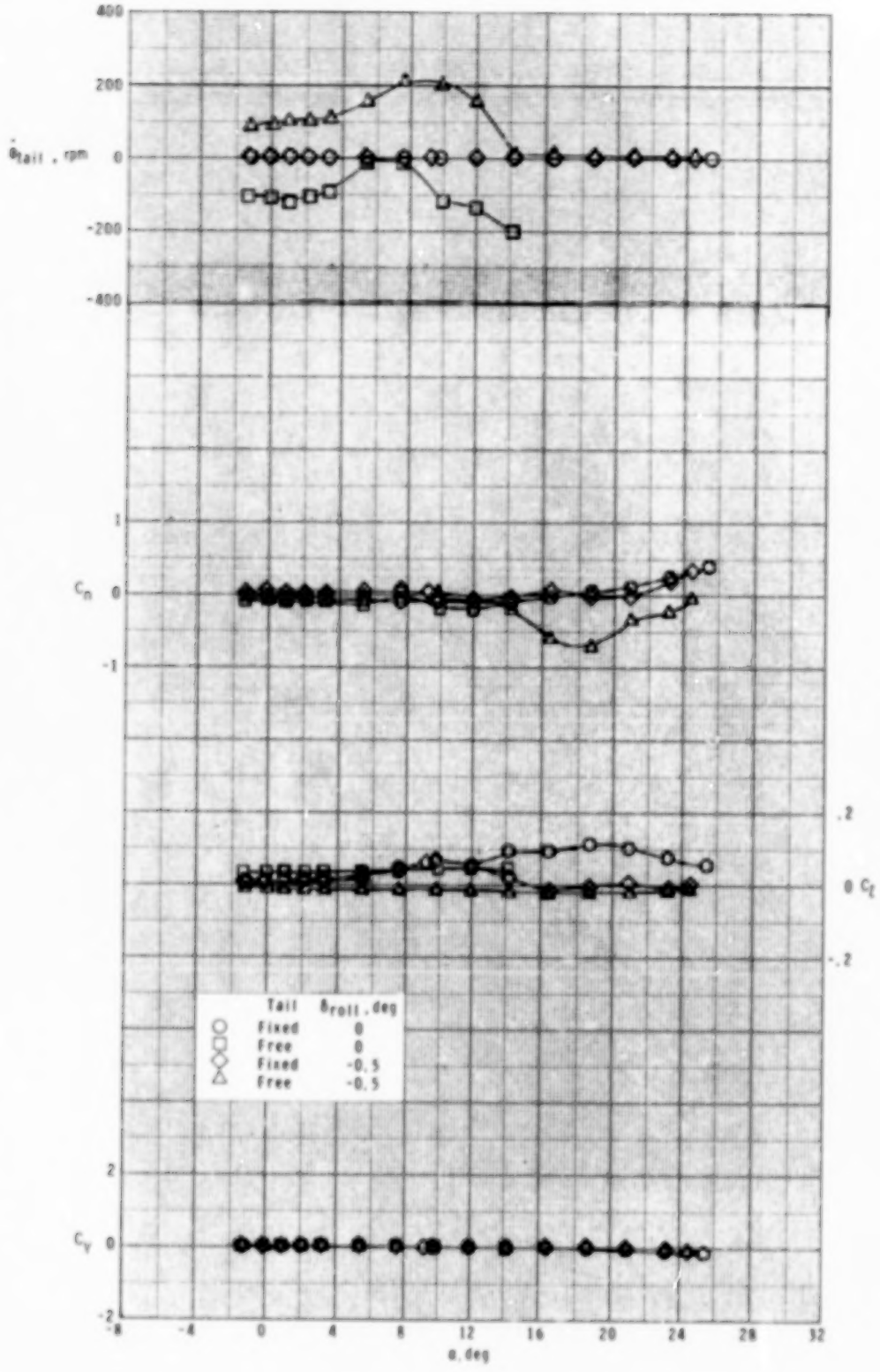

(b) M = 2.16.

Figure 12.- Continued.

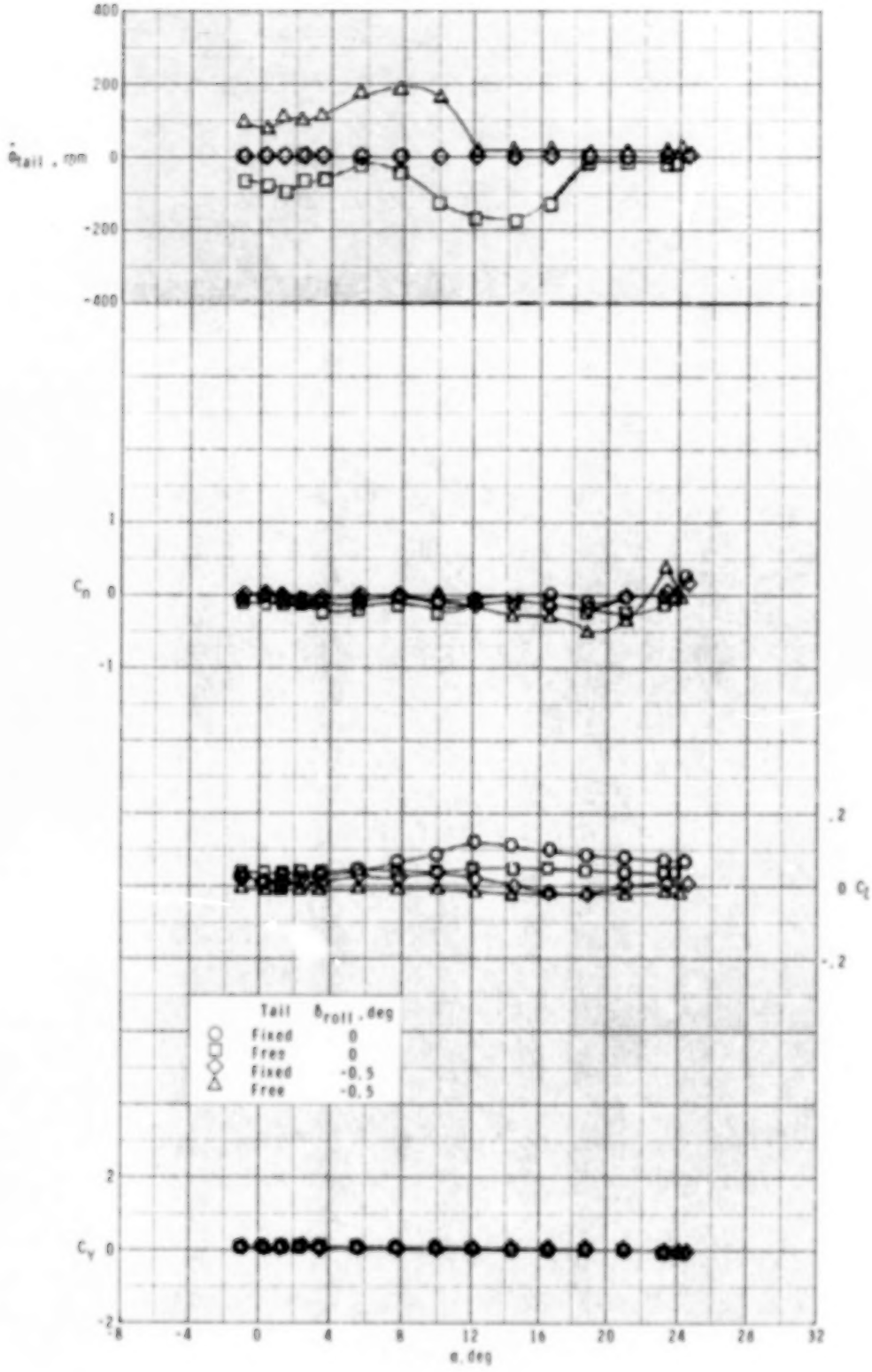

(c) M = 2.36.

Figure 12.- Continued.

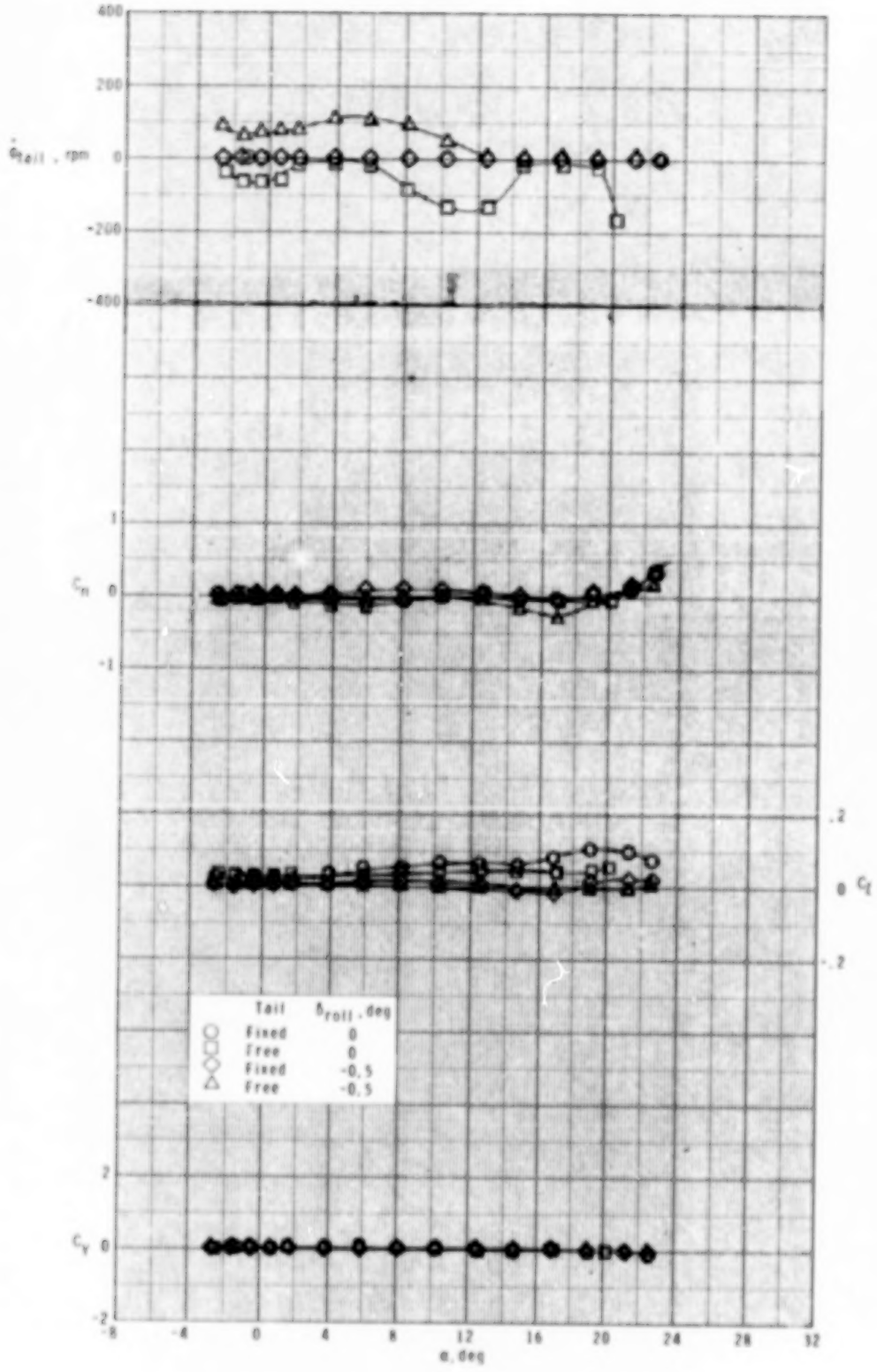

(d) M = 2.86.

Figure 12.- Concluded.

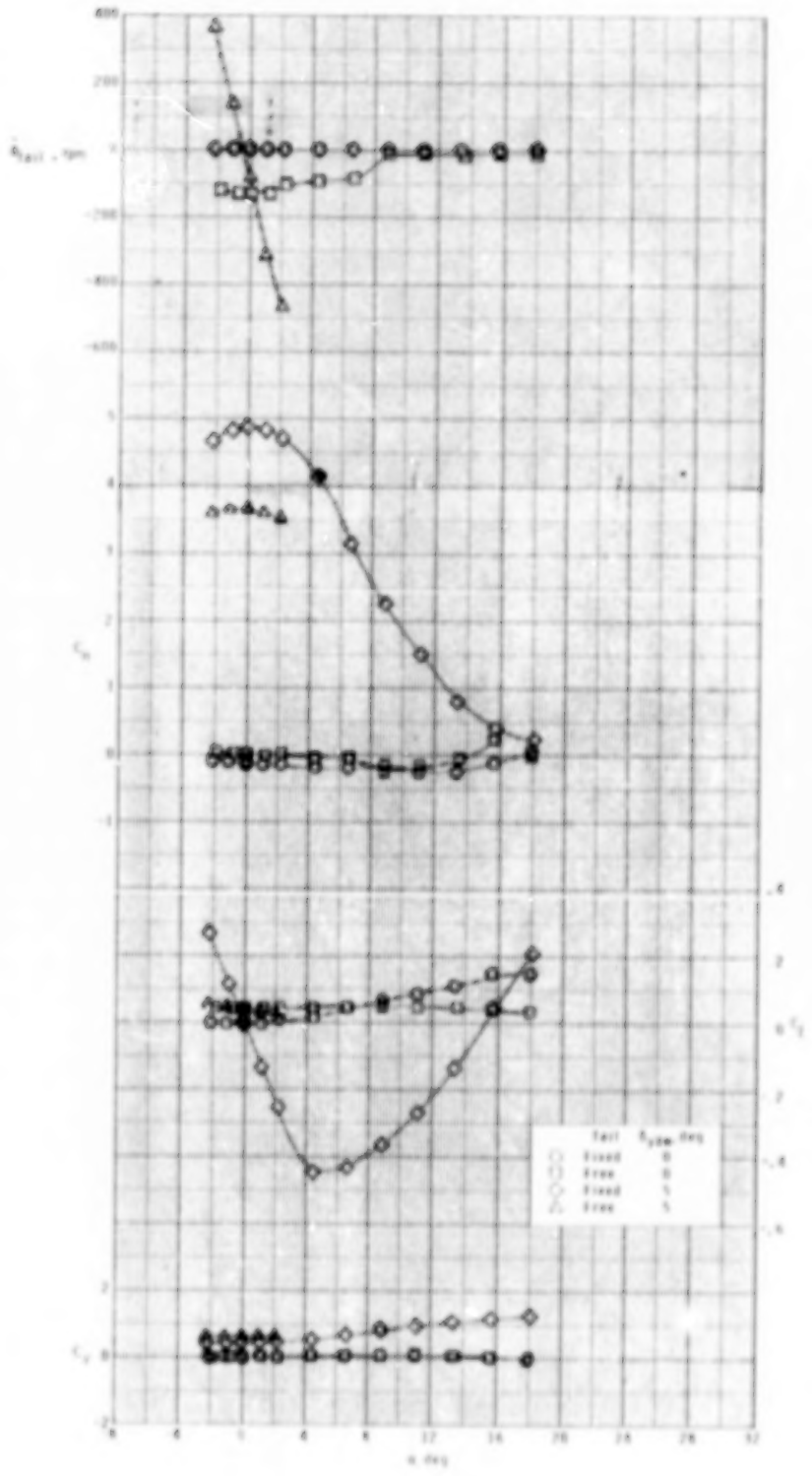

(a) M = 1.70.

Figure 13.- Yaw-control characteristics of model with fixed and free-rolling tail at $\phi_c = 0^{\circ}$. Vertical canards deflected.

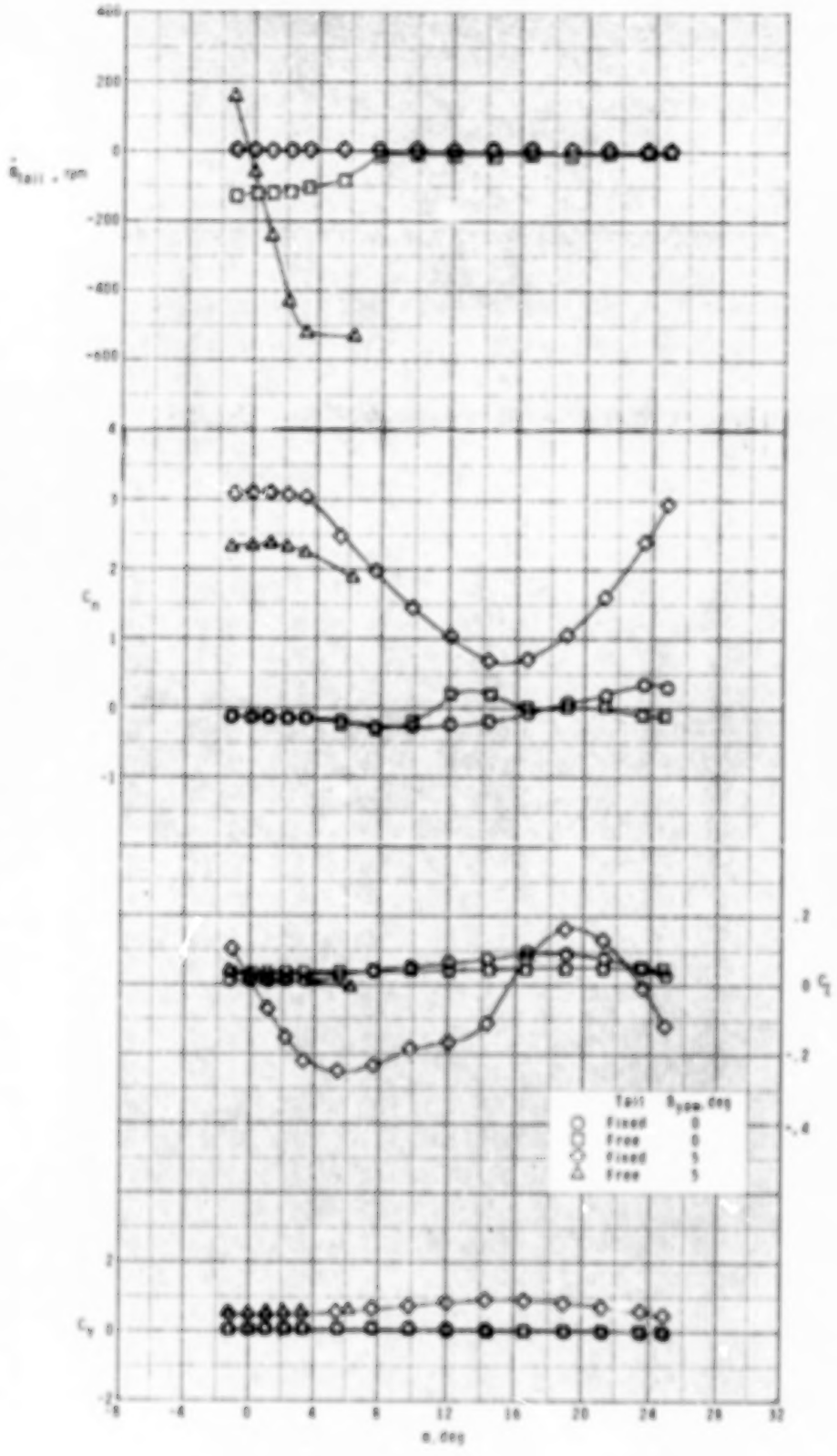

(b) M = 2.16.

Figure 13.- Continued.

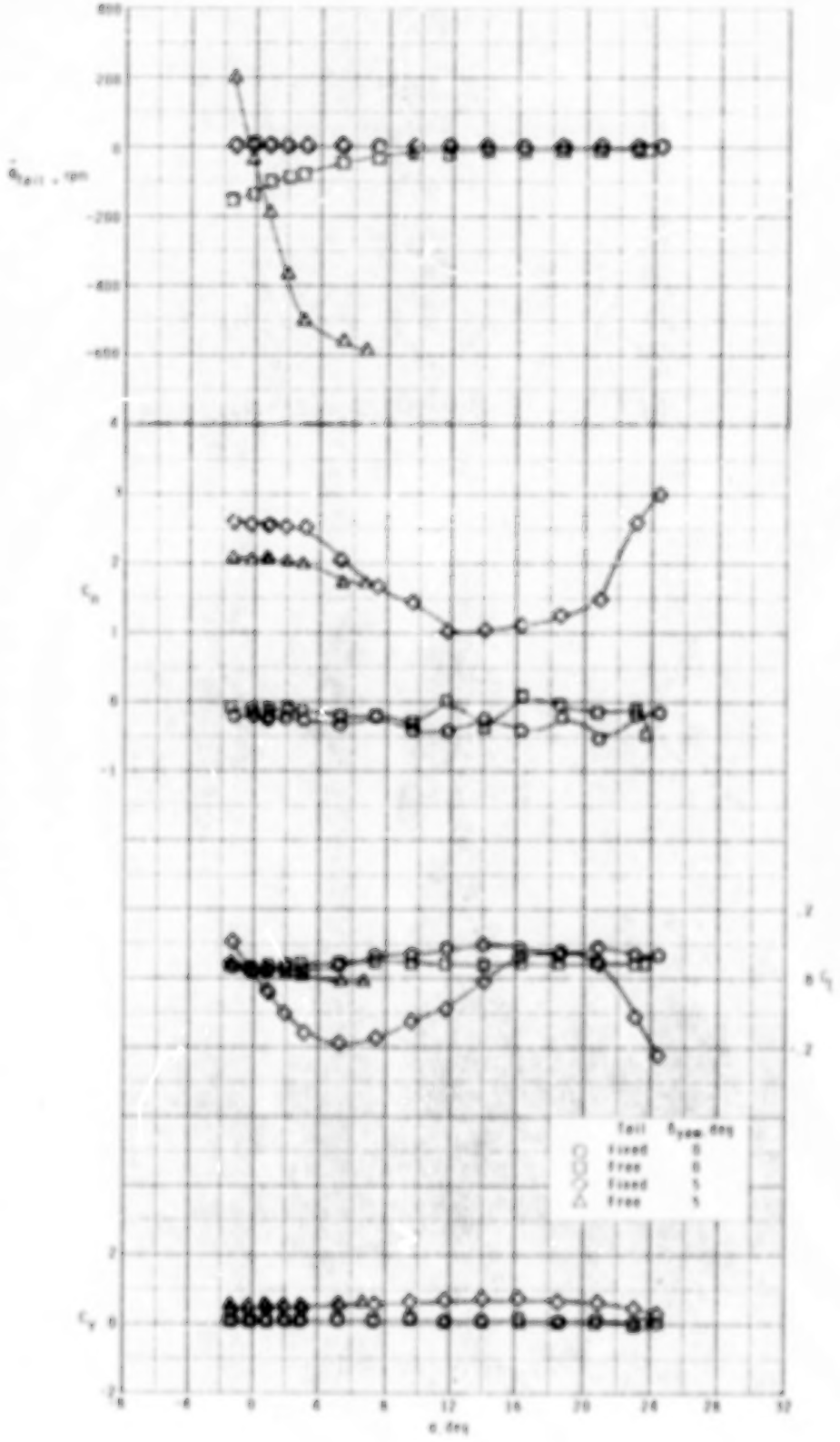

(c) M = 2.36.

Figure 13.- Continued.

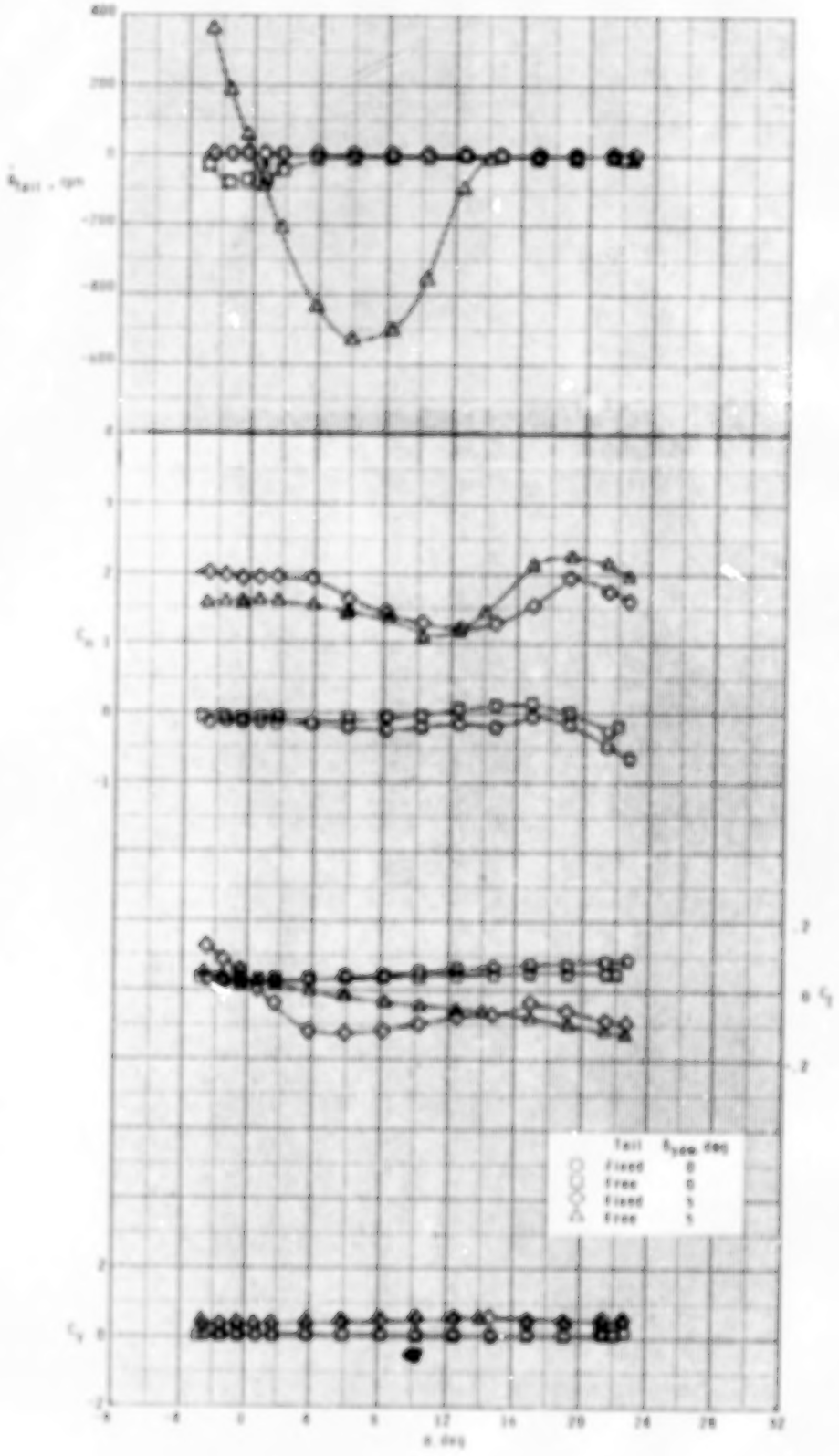

(d) M = 2.86.

Figure 13.- Concluded.

1. Report No.	2. Government Accession No.	3. Recipient's Catalog No.
NASA TP-1316		

4. Title and Subtitle	5. Report Date
WIND-TUNNEL INVESTIGATION AT SUPERSONIC SPEEDS OF A CANARD-CONTROLLED MISSILE WITH FIXED AND FREE-ROLLING TAIL FINS	September 1978
	6. Performing Organization Code

7. Author(s)	8. Performing Organization Report No.
A. B. Blair, Jr.	L-12297
	10. Work Unit No. 505-11-23-03

9. Performing Organization Name and Address	11. Contract or Grant No.
NASA Langley Research Center Hampton, VA 23665	

12. Sponsoring Agency Name and Address	13. Type of Report and Period Covered
National Aeronautics and Space Administration Washington, DC 20546	Technical Paper
	14. Sponsoring Agency Code

15. Supplementary Notes

16. Abstract

A wind-tunnel investigation was made at free-stream Mach numbers from 1.70 to 2.86 to determine the effects of fixed and free-rolling tail-fin afterbodies on the static longitudinal and lateral aerodynamic characteristics of a cruciform canard-controlled missile model. The effect of small canard roll- and yaw-control deflections was also investigated. The results indicate that the fixed and free-rolling tail configurations have about the same lift-curve slope and longitudinal stability level at low angles of attack. For the free-rolling tail configuration, the canards provide conventional roll control with no roll-control reversal at low angles of attack. The free-rolling tail configuration reduced induced roll due to model roll angle and canard yaw control.

17. Key Words (Suggested by Author(s))	18. Distribution Statement
Cruciform missile Canard control Free-rolling tail	Unclassified - Unlimited Subject Category 02

19. Security Classif. (of this report)	20. Security Classif. (of this page)	21. No. of Pages	22. Price*
Unclassified	Unclassified	76	$6.00

*For sale by the National Technical Information Service, Springfield, Virginia 22161

NASA-Langley, 1978

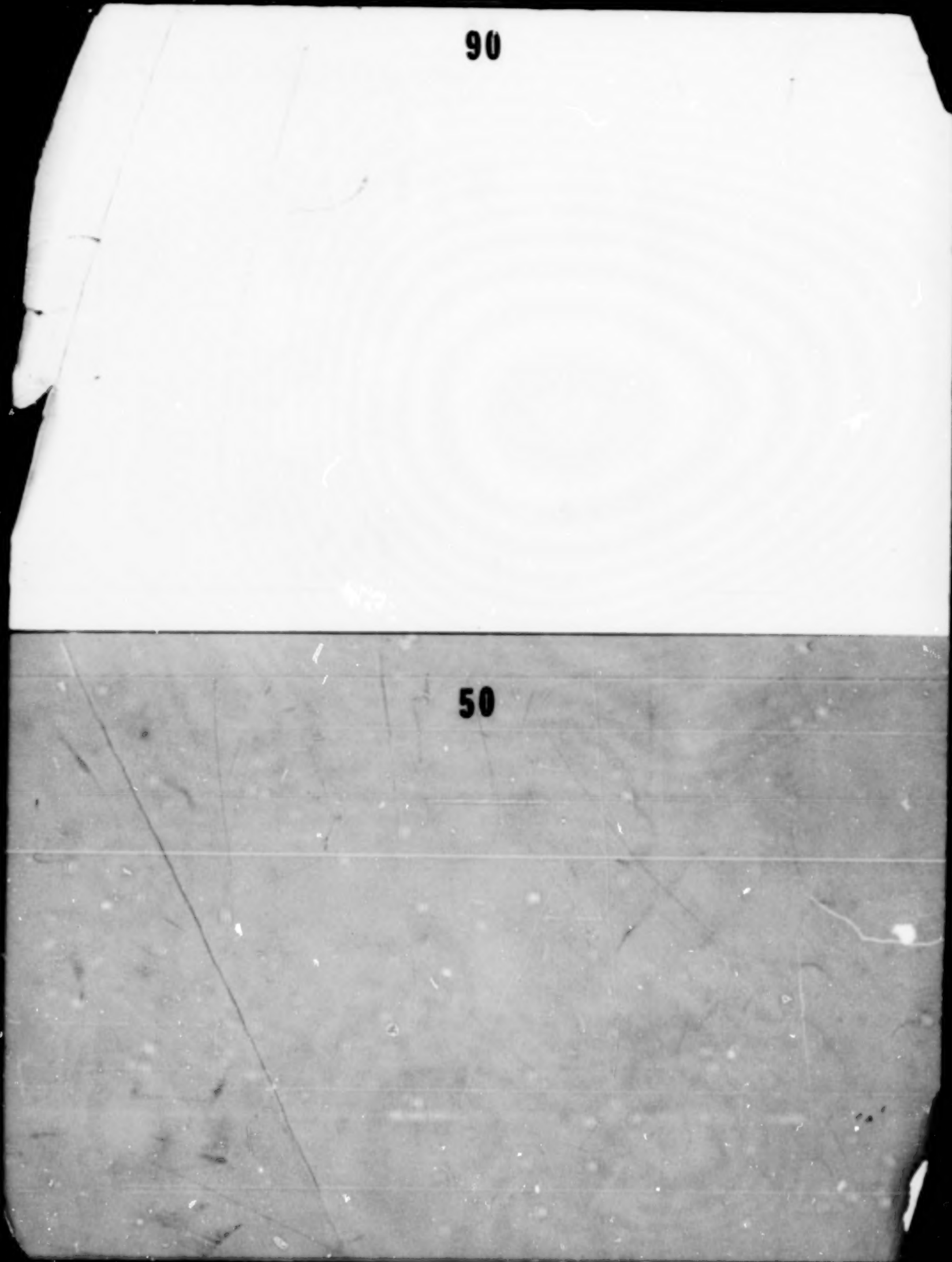
90
50

END

MAR 16 1979